Relativistic

Quantum Chemistry

Applied

Wibe Albert de Jong

Friese vertaling nederlandse samenvatting: Siegbert de Jong

Druk: Drukkerij de Jong, Aldeboarn

This work was sponsored by the Netherlands Foundation for Chemical Research (SON) and the Stichting Nationale Computerfaciliteiten (National Computing Facilities Foundation, NCF) for the use of supercomputer facilities both with financial support from the Nederlandse Organisatie voor Wetenschappelijk Onderzoek (Netherlands Organization for Scientific Research, NWO).

RIJKSUNIVERSITEIT GRONINGEN

Relativistic

Quantum Chemistry

Applied

PROEFSCHRIFT

ter verkrijging van het doctoraat in de
Wiskunde en Natuurwetenschappen
aan de Rijksuniversiteit Groningen
op gezag van de
Rector Magnificus Dr. F. van der Woude,
in het openbaar te verdedigen op
maandag 26 januari 1998
des namiddags te 4.15 uur

door

Wibe Albert de Jong

geboren op 13 mei 1969
te Assen

Promotor: Prof. Dr. W.C. Nieuwpoort

Referent: Dr. P.J.C. Aerts

Referent: Dr. L. Visscher

Mijn strijd is allereerst mijn eigen strijd
Mijn spijt is bovenal mijn eigen spijt
Mijn oordeel stoort zich niet aan hoe het hoort
Ik hou me liever aan mijn eigen woord

Mijn wet is wil ik ga mijn eigen gang
Ik ga mijn weg, ik ben voor niemand bang
Ik ken wel regels maar die zijn van mij
Als ik me aanpas ben ik nooit meer vrij

Laat me leven
Geen geregel
Stap voor stap
Red ik het heus wel !

uit "Nooit meer wetten", Angela Groothuizen

Voorwoord / Preface

Na enkele maanden hard zwoegen is mijn proefschrift dan eindelijk af en daarom is het tijd om een aantal mensen bedanken die, op verschillende manieren, hebben bijgedragen aan de vorm en inhoud van dit proefschrift.

Allereerst wil ik mijn promotor Wim Nieuwpoort bedanken voor de ruimte en vrijheid die hij mij gaf tijdens het onderzoek. Tevens dank ik hem voor het kritisch lezen en corrigeren van de door mij geschreven teksten voor artikelen, posters, sheets voor lezingen en natuurlijk mijn proefschrift. Ik heb veel gehad aan onze discussies die zich niet alleen beperkten tot de relativistische quantumchemie.

Een bijzonder woord van dank gaat uit naar Luuk Visscher, tevens één van mijn referenten. Ik dank hem voor de introductie in de relativistische quantumchemische wereld zoals die in MOLFDIR is geprogrammeerd. Daarnaast waardeer ik zijn bijdrage als discussiepartner, vraagbaak, co-auteur en kritisch lezer van eerste stadia van mijn proefschrift ten zeerste. Ik hoop dat onze samenwerking op het gebied van de relativistische quantumchemie nog wat langer voort zal duren.

Mijn andere referent, Patrick Aerts, dank ik voor het zorgvuldig lezen van de eerste en uiteindelijke versie van mijn proefschrift en zijn vele zinvolle op- en aanmerkingen betreffende de inhoud. Tevens dank ik hem voor de begeleiding die ik van hem heb gekregen.

I thank Knut Fægri and Bernd Heß for their careful reading of my manuscript as members of the quality assessment committee and their usefull comments. Dank ook aan Jaap Snijders voor het lezen en beoordelen van mijn manuscript als lid van de leescommissie.

Carmen Sousa, te agradesco mucho por tu agradable cooperación durante el trabajo en el proyecto "CuX", que nos produjo dos articulos muy bien. También aprecio mucho que has leido el capitulo tercero de mi tesis doctoral con esmero y detenimiento y mucha atención.

Jacek Styszynski, I think we have pleasantly worked together on the interhalogens project and I enjoyed your presence in our group. I hope that our work will be published soon.

Ik dank de mensen in onze werkgroep Theoretische Chemie, Ria Broer (ook voor het lezen van hoofdstuk 3), Coen de Graaf (veel succes met jou promotie op vrijdag 13 maart), Johan Heijnen, Bauke Kooistra, Alexxx de Vries en onze ex-studenten Michel "Great Dragon" Geleijns, Fokke Dijkstra en Gerrit-Jan Linker voor de prettige "werk"sfeer tijdens mijn vier jaren in deze groep. Ik heb veel gehad aan de (uitgebreide) discussies tijdens onze werkbesprekingen in het Ei. Mijn ex-kamergenoot Roger Erens en mijn, sinds kort, nieuwe kamergenoten Freddie Kootstra en Marcel Swart dank ik voor hun gezelschap.

I thank Jon Laerdahl, Trond Saue and Knut Fægri of the Theoretical Chemistry group at the University of Oslo (Norway) for a very rewarding visit and allowing me to use their DIRAC code. Also, I very much enjoyed the invitation of, and stay with, the groups of Wolfram Koch and Helmut Schwarz at the

Institut für Organische Chemie der Technischen Universität Berlin (Germany). I wish to acknowledge the financial support of the REHE programme of the European Science Foundation that allowed me to attend various conferences and workshops and for giving me the opportunity to visit other research groups in Europe.
Tevens wil ik het Material Science Center, onderzoeksschool van de Rijksuniversiteit Groningen, danken voor de financiële steun die het voor mij mogelijk maakte om twee conferenties in de Verenigde Staten te kunnen bezoeken.
Tenslotte wil ik mijn ouders bedanken voor hun ondersteuning en geloof in mijn kunnen. Ik hoop dat ik jullie op niet al te lange termijn eens mag begroeten in Richland (USA). Jeroen ik dank je dat je mij als paranimf tijdens de promotie wilt ondersteunen in een "apepakje".

Bert Oosterwolde, 1 December 1997

Contents

Chapter 1

General Introduction

Part of the phenomena in the chemistry and physics of atoms and molecules find their origin in the finite speed of light and need to be described in the framework of relativistic quantum mechanics. Relativity reveals itself for instance in the fine details of spectra of molecules and atoms and can nowadays be accessed by very accurate measurements, even for the elements in the upper region of the periodic system. If one wants to understand the chemistry and physics of substances containing heavy elements, for which the electrons close to the atomic nuclei acquire velocities approaching the speed of light, one needs a relativistic quantum mechanical description from the outset. In this chapter an introduction will be given on the importance of relativity in chemistry with a brief historical overview that puts my field of research, relativistic quantum chemistry, in perspective. Finally, the goals of this thesis and an outline of its contents are presented.

1.1 Relativity in chemistry

The *ab initio* study of molecules and crystals that contain heavy elements is a growing field of research. Most of the interesting chemical properties of light molecules can be satisfactorily explained on the basis of the Schrödinger equation or, in other words, in the framework of non-relativistic quantum mechanics. This was also the opinion of the founder of relativistic quantum mechanics, P.A.M. Dirac, as one can read in the first two lines of his paper[1] in 1929 on "Quantum Mechanics of Many-Electron Systems". However, if one wants to obtain very accurate results, even for systems as light as the H_2 molecule, one has to consider relativistic contributions. Properties that depend on electron spin such as the well-known yellow ^{2}D emission line in the spectrum of the sodium atom, can in fact only be properly explained by extending the Schrödinger equation with relativistic terms.

Relativity has a considerable and sometimes dominating influence on the properties of molecules or crystals containing heavy elements. Theoretically, relativity can be accounted for either by introducing

relativistic corrections into non-relativistic models or, more fundamentally, by the use of a relativistic quantum mechanical model from the outset. The latter approach is used in this thesis.

In every day life there are several phenomena that are intimately connected to relativity. The difference in color between the noble metals gold and silver is a conspicuous example. The color arises from an optical transition in which electrons are excited from a filled d-band to the Fermi level of mainly s-character. In silver this transition lies in the ultraviolet, but in gold a relativistic shift to the optical region occurs leading to the observed yellowish color. We will return to the origin of this shift later in this section. The extent to which relativity determines the catalytic properties[2,3] of platinum, of interest to the chemical industry, is a subject of study. Another interesting example is the lead battery that would not work in a non-relativistic world. The so-called "6s inert pair effect" (see for references 3) inhibits the oxidation of Pb^{2+} to Pb^{4+} which profoundly effects the redox reactions that drive the battery.

In addition to these general examples there are many more special scientific phenomena that require relativity for their explanation. Spectra showing "forbidden" transitions or spin-orbit induced avoided crossings of potential energy curves are well-known examples. As said before, these features are not restricted to molecules containing heavy atoms but also occur in systems with only light atoms. A recent example of the importance of relativity for the properties of light systems is the study of the chemical bonding in AlH_2[4]. Other aspects of relativity in chemistry are the preference of certain reaction paths and certain coordination numbers of heavy atoms in molecules and solids. For a further discussion of the influence of relativity in chemistry the reader is referred to the references at the end of this section.

Careful readers might have noticed that up to now the often used term "relativistic effects" has been avoided. Relativity is not something that causes effects that can be studied experimentally by switching it on and off. It is one of the fundaments of physics that is always present. Whenever the term "relativistic effects" is used, a difference is meant between the properties as they would appear in the non-relativistic Schrödinger world, in which the speed of light is implicitly assumed to be infinite, and in the (real) world, where the speed of light is finite. The latter is described to a very good approximation by Dirac's relativistic quantum mechanics[5], in agreement with Einstein's theory of special relativity[6], where the speed of light is a fundamental constant of nature.

In the study of atoms and molecules it is customary to separate these differences in "direct" and "indirect" effects. The best known direct effect arises from the coupling between the spin and orbital angular momenta of electrons. This so-called spin-orbit interaction leads to a breakdown of optical selection rules that follow from the *ad hoc* introduction of spin in the non-relativistic description. In a relativistic description for example, spin-forbidden singlet-triplet transitions[7] are allowed and also observed in spectra like the excitation spectra of the copper halides in chapter 3. Spin-orbit interaction not only affects spectroscopy but also has an effect on the chemical bonding properties of molecules. The interaction splits the shells with an angular momentum $\ell > 0$ into two subshells, which differ in energy, with a total angular momentum of $j = \ell - 1/2$ and $j = \ell + 1/2$. In valence shells both subshells are required to participate in bond formation. The $p_{1/2}$ and the $p_{3/2}$ subshells for example are a linear

combinations of p_x, p_y and p_z functions and in a linear molecule both subshells are required to form a σ-bond. For heavy elements the energy separation between the two subshells can be large so that the splitted orbitals may no longer be involved in bonding to the same extent with great effect on the bonding properties. An example is the ground state of the iodine molecule which is discussed in chapter 5.

A second direct effect is the contraction of the s and p shell orbitals which is a direct consequence of the fact that the mass of a particle increases with its velocity in the theory of special relativity. When electrons occupy the inner s orbitals they approach the atomic nuclei very closely and obtain higher average velocities than when they occupy the outer orbitals. Consequently their masses increase and their average distance from the nucleus decreases with respect to that expected from the non-relativistic description. Also the ionization potentials associated with these electrons are larger than one would obtain non-relativistically. All s orbitals have to be orthogonal to each other leading to an increase of the ionization potentials also for the outer (or valence) s-shells. The valence s and p orbitals also show a radial contraction which, however, is caused by direct as well as indirect effects (for a more detailed discussion see references 8 and 9). The origin of the color of gold mentioned before lies in the stabilization of the outer 6s shell (and to a lesser extent in the destabilization of the 5d shell).

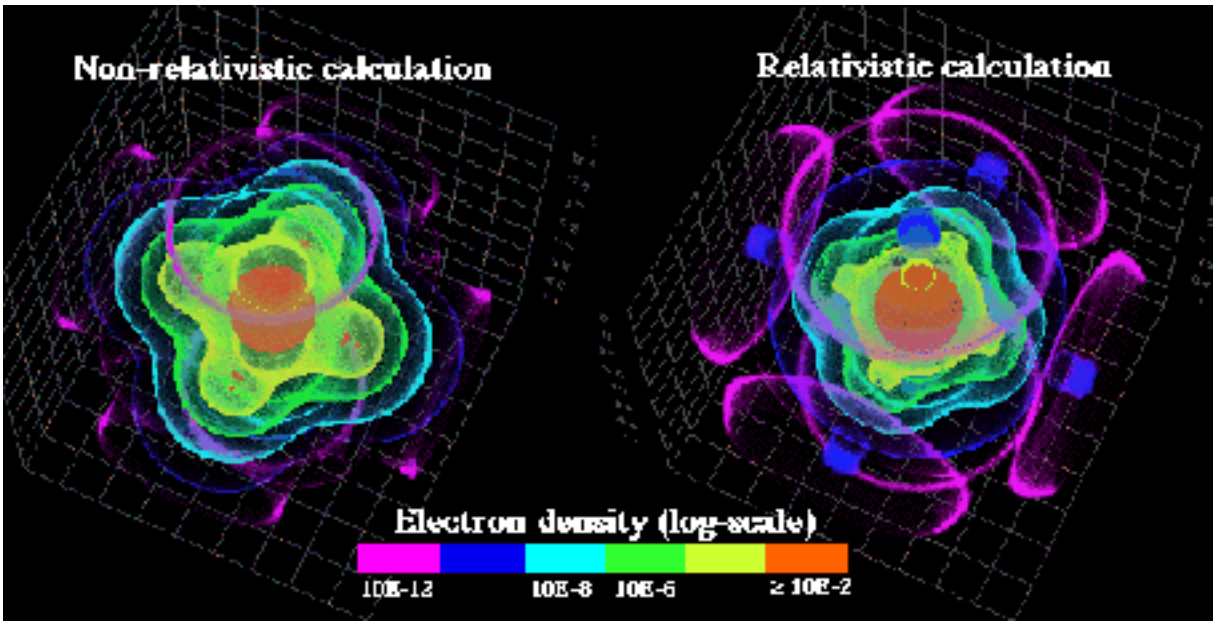

Figure 1.1. Non-relativistic and relativistic electron density plot[10] of the $7\gamma_{6g}$ spinor in UF_6.

The influence of this contraction on the bonding properties in a molecule is visualized for the uranium 6s in uranium hexafluoride (UF_6), a molecule that is discussed later in this thesis. In a non-relativistic calculation one finds a bond between the uranium 6s and the surrounding fluorine 2s orbitals. However, this bond practically disappears due to the relativistic contraction (see the yellow regions in figure 1.1).

For electrons in p shells a similar contraction is found but the effect is smaller. Besides this contraction there is also a spin-orbit effect for the p shells leading to the two subshells $p_{1/2}$ and $p_{3/2}$. Combining spin-orbit coupling and radial contraction leads for the $p_{3/2}$ subshell to a near cancellation of the relativistic effects whereas the two effects reinforce each other for the $p_{1/2}$, leading to a contraction and an increase of the ionization potential comparable to the s-shell with the same principle quantum number. The indirect effect is caused by the relativistic contraction of the s and p shells. As a result of this contraction a better screening of the nuclear charge occurs leading to radial expansion and smaller binding energies of the d- and f-shells.

It can be concluded that relativistic effects can have a considerable influence on the properties of atoms and molecules which explains the interest in the development and applications of relativistic quantum chemistry. More extensive reviews dealing with the influence of relativity on chemistry can be found in the literature[3,7,11-13].

1.2 Relativistic quantum chemistry

Chemistry is concerned with the formation and breaking of chemical bonds between atoms. These bonds arise from relatively subtle changes that can occur in the behaviour of electrons when atoms or molecular fragments approach each other. Since the behaviour of electrons is governed by quantum mechanics, the study of the chemical bond or, more generally, the study of the electronic states of molecules as a function of the positions of the constituting atoms is called quantum chemistry. The basis for the quantum mechanical treatment of electrons is the Schrödinger equation including the spin in the electronic degrees of freedom and imposing the Pauli principle on the wave function. Yet, because it is not based on relativistic mechanics this equation has fundamental flaws and fails for instance in describing spectroscopic phenomena, like for example the so-called "duplexity phenomenon", and the chemical bonding properties of heavy atoms. Relativistic quantum chemistry is based on the Dirac equation that correctly describes the quantized relativistic motion of one-electron systems. Dirac[5,14] linearized the relativistic free-particle energy expression ($E^2 = m^2c^4 + c^2p^2$), exploring the relation $(\sigma.\mathbf{p})(\sigma.\mathbf{p}) = p^2$, and came with his relativistic analogue of the Schrödinger equation. His equation was able to explain from first principles phenomena like the duplexity problem and the anomalous Zeeman effect. When analyzing his Hamiltonian in the presence of an arbitrary electromagnetic field, Dirac found that its properties could indeed be interpreted as describing an electron with a spin 1/2 as a degree of freedom and carrying a magnetic spin moment.

In chemistry one rarely works with one-electron systems which means that the one-electron Dirac equation is not sufficient. A generalization to the many-electron equation can be made starting from the Quantum Electro Dynamics (QED) framework. The two-electron interaction, obtained from QED, consists of a series expansion of the interaction where the zeroth-order and largest term is the Coulomb repulsion, similar to the non-relativistic electron-electron interaction. Of the remaining terms one generally includes the Breit interaction[15], which Breit already derived in 1929 from classical relativistic

mechanics. At this point it is convenient to separate the nuclear and electronic motion by the Born-Oppenheimer[16] approximation. This gives a many-electron Dirac-Coulomb equation where the electrons move in a fixed frame of nuclei. The general method to solve this electronic equation is to use a relativistic analogue of the Hartree-Fock approximation which turns the many-electron equation into an effective one-electron equation. In 1935 Swirles[17] was the first to derive the Dirac-Hartree-Fock (DHF) equations for an atom. Nowadays there are very good and fast computer programs[18,19] for atomic systems that go beyond the Hartree-Fock level and even include higher order Quantum Electro Dynamic effects like the Breit interaction[15], electron self-energy and vacuum polarization (the last two make up what one calls the Lamb-shift[20]).

If one wants to study molecules rather than atoms with the DHF approach one has to use approximate techniques similar to those employed in non-relativistic molecular quantum chemistry. The main methodology is to use a basis set expansion to approximate the one-electron orbitals. A relativistic analogue, however, is not quite straightforward and much effort has been put in solving the Dirac equation by basis set expansion, that can provide the proper balance between the large and small component basis sets. The first DHF calculations were flawed because the necessary relations between the large and small component wave functions could not be realized in the basis set used for the expansion of the wave function. Analysis of the problem resulted in concepts as kinetic[21-26] and atomic balance[27-29] that are nowadays used to construct adequate basis sets. As a results also other more fundamental problems, like the so-called "Brown-Ravenhall disease"[30], are now better understood.

In the last 20 years a large number of molecular codes have been developed[31-37] within the relativistic framework. The program we will use to perform accurate relativistic *ab initio* quantum chemistry calculations is MOLFDIR (MOLecular Fock DIRac), developed in our group at the University of Groningen. Patrick Aerts[26] started the development of this molecular Dirac-Hartree-Fock program in 1981 after attending a NATO Advanced Study Institute on "Relativistic Effects in Atoms, Molecules and Solids". The first closed shell version was ready in 1984. To overcome the restrictions of closed shell systems and to be able to handle more complex open-shell systems Olivier Visser[38] adapted the closed shell DHF to include one open shell, based on Roothaan's average of configuration energy expression. He also constructed a configuration interaction (CI) program to obtain the individual states of the averaged open-shell manifold. To further improve accuracy one needs to include electron correlation effects. Luuk Visscher[39] therefore implemented a general multi-reference CI (MRCI) and a singles and doubles Coupled Cluster (CCSD) method[40]. A very recent development is the addition of codes to calculate various properties and to study the response of properties[41] to external perturbations within the Random Phase Approximation (RPA).

Computer programs based on the Dirac equation are more expensive, in terms of required computer resources, then their non-relativistic counterparts. Various levels of fundamental[42-51] and numerical approximations have been developed over the years. At the end of chapter 2 we will discuss an

important numerical approximation in the evaluation of the electron-electron interaction of the small component wave functions.

1.3 Aim and structure of this thesis

In the past 15 years relativistic quantum chemistry theory and computer codes have evolved to a high level of physical accuracy. The current MOLFDIR code enables us to study the properties of various chemical systems and to address the influence and importance of relativity in chemistry. Except for some further developments and fine tuning of the MOLFDIR program package, discussed in chapter 2, this research and thesis are devoted to the calculation of chemically and physically interesting properties of chemical compounds which are significantly influenced by relativity, and to try to understand these from theoretical analysis of the calculated wave functions.

There are two reasons to do these calculations. The first has to do with the fact that a large number of methods has been developed and applied that account for relativity in approximate ways. Calculations that are performed within a fully relativistic framework can serve as a benchmark for these methods. However, benchmark calculations are just a small part of the work that can be done with a fully relativistic approach. There are many phenomena, as core-hole spectroscopy, indirect spin-spin coupling (NMR) and electric field gradients (EFG), that can be studied with approximate computational methods but can (or need to) be improved upon in order to get an accurate description of the relativistic effects. We will see for example for the interhalogen compounds that even for rather light systems it is difficult to include relativistic effects in approximate methods for the calculation of electric dipole and quadrupole moments. The chapters 3 to 7 discuss a variety of chemical systems and also a variety of chemical properties that have been studied within the fully relativistic framework. These chapters are based on previously published articles (see the list of publications at the end of this thesis). Finally, we will end with a summary in chapter 8.

Chapter 2

Theory and Methodology

The calculations presented in this thesis are performed within a relativistic framework. The starting point is the one-electron Dirac Hamiltonian. First we will go into the basic theory of the Dirac Hamiltonian and its extension to many electrons. Then, by gradually introducing more and more well defined standard quantum chemistry approximations, we will arrive at the relativistic quantum chemistry model that is implemented in the MOLFDIR program package. We will go in some detail into the methodology that is used in the program package. Finally an overview of the MOLFDIR program package is given.

2.1 Basic theory

In 1928 Dirac proposed[5,14] a one-electron equation that was in accordance with both quantum mechanics and the laws of special relativity. The time-dependent equation (2.1) represents an electron (with charge -|e|) moving in an arbitrary electromagnetic field described by the scalar potential ϕ and the vector potential (A_x, A_y, A_z).

$$\left[c\, a_x \left(p_x + \frac{e}{c} A_x\right) + c\, a_y \left(p_y + \frac{e}{c} A_y\right) + c\, a_z \left(p_z + \frac{e}{c} A_z\right) + \left(- e\phi + \beta\, mc^2\right) .\ 1_4 \right] \psi = i\hbar \frac{\partial}{\partial t} \psi \qquad (2.1)$$

where 1_4 is a 4x4 identity matrix and the matrices a and b are given as

$$a_x = \begin{pmatrix} 0&0&0&1\\ 0&0&1&0\\ 0&1&0&0\\ 1&0&0&0 \end{pmatrix} \quad a_y = \begin{pmatrix} 0&0&0&-i\\ 0&0&i&0\\ 0&-i&0&0\\ i&0&0&0 \end{pmatrix} \quad a_z = \begin{pmatrix} 0&0&1&0\\ 0&0&0&-1\\ 1&0&0&0\\ 0&-1&0&0 \end{pmatrix} \quad b = \begin{pmatrix} 1&0&0&0\\ 0&1&0&0\\ 0&0&-1&0\\ 0&0&0&-1 \end{pmatrix} \qquad (2.2)$$

The Dirac equation is a 4-component set of coupled first order differential equations with 4-component solutions ψ

$$\psi = \begin{pmatrix} \psi_\alpha^L \\ \psi_\beta^L \\ \psi_\alpha^S \\ \psi_\beta^S \end{pmatrix} \tag{2.3}$$

The labels L, S, α and β, not to be confused with the α and β matrices of (2.2), that are used here will be discussed in section 2.1.1.

The 4-component equation can also be written as a 2-component equation of 2-component spin-orbitals or spinors with the a and b matrices written as

$$a_x = \begin{pmatrix} 0_2 & s_x \\ s_x & 0_2 \end{pmatrix} \quad a_y = \begin{pmatrix} 0_2 & s_y \\ s_y & 0_2 \end{pmatrix} \quad a_z = \begin{pmatrix} 0_2 & s_z \\ s_z & 0_2 \end{pmatrix} \quad b = \begin{pmatrix} 1_2 & 0_2 \\ 0_2 & 1_2 \end{pmatrix} \tag{2.4}$$

in terms of the Pauli[52] spin matrices

$$s_x = \begin{pmatrix} 0 & 1 \\ 1 & 0 \end{pmatrix} \quad s_y = \begin{pmatrix} 0 & -i \\ i & 0 \end{pmatrix} \quad s_x = \begin{pmatrix} 1 & 0 \\ 0 & -1 \end{pmatrix} \tag{2.5}$$

and 1_2 and 0_2 are the two dimensional identity and null matrix respectively.

We will use time independent potentials so that the time dependent part can be split of and we are left with the time-independent equation

$$\begin{bmatrix} (mc^2 - e\phi) \cdot 1_2 & c\,\sigma\cdot\mathbf{p} + e\,\sigma\cdot\mathbf{A} \\ c\,\sigma\cdot\mathbf{p} + e\,\sigma\cdot\mathbf{A} & (-mc^2 - e\phi) \cdot 1_2 \end{bmatrix} \begin{pmatrix} \psi^L \\ \psi^S \end{pmatrix} = \varepsilon \begin{pmatrix} \psi^L \\ \psi^S \end{pmatrix} \tag{2.6}$$

Here $\sigma.\mathbf{p}$ and $\sigma.\mathbf{A}$ represent the inner product of a vector of three Pauli spin matrices (s_x, s_y, s_z) with the vector of the momentum operator (p_x, p_y, p_z) and the vector of the vector potential (A_x, A_y, A_z) respectively. This form of the time-independent Dirac Hamiltonian is most widely used for computational purposes. We will first discuss some aspects of the one-electron Dirac Hamiltonian.

2.1.1 The Dirac equation

The Dirac equation for a free particle in the two-component notation reduces to

$$\begin{pmatrix} mc^2 \cdot 1_2 & c\,\sigma.\mathbf{p} \\ c\,\sigma.\mathbf{p} & -mc^2 \cdot 1_2 \end{pmatrix} \begin{pmatrix} \psi^L \\ \psi^S \end{pmatrix} = \varepsilon \begin{pmatrix} \psi^L \\ \psi^S \end{pmatrix} \qquad (2.7)$$

Solving equation (2.7) yields two separate sets of solutions, the positive energy solutions with $\varepsilon \geq mc^2$ and the negative energy solutions with $\varepsilon \leq -mc^2$. So the positive and negative energy solutions are separated by a $2mc^2$ gap.

In the Born-Oppenheimer[16] approximation the field that the electron moves in is represented by a static potential ϕ of the nuclear framework

$$\begin{pmatrix} (mc^2 - e\phi) \cdot 1_2 & c\,\sigma.\mathbf{p} \\ c\,\sigma.\mathbf{p} & (-mc^2 - e\phi) \cdot 1_2 \end{pmatrix} \begin{pmatrix} \psi^L \\ \psi^S \end{pmatrix} = \varepsilon \begin{pmatrix} \psi^L \\ \psi^S \end{pmatrix} \qquad (2.8)$$

Solving equation (2.8) gives us, besides positive and the negative energy solutions outside the $2mc^2$ gap, bound energy solutions which lie inside the gap. Our main interest is in the positive energy solutions where the amplitude of the lower component (ψ^S) is much smaller than the amplitude of the upper component (ψ^L), while for the negative energy solutions it is the other way around. Therefore, the upper component of ψ is labelled L for "large amplitude" and the lower component by S for "small amplitude".

The inclusion of relativity in (2.8) is limited to the electrons of this Hamiltonian. In principle one should treat the nuclei as relativistic particles as well, to obtain a consistent treatment of all particles in the molecular system. However, it has been shown[53] that the relativistic effect is small enough to neglect in our calculations. In our approach we also neglect the nuclear spins and thereby neglect all hyperfine effects.

For an easier comparison with non-relativistic energies, and for technical reasons, we shift the spectrum downwards with the rest mass energy of the electron (mc^2). Herewith the bound electron like solutions lie roughly in the same energy domain as one would find using a non-relativistic Hamiltonian

$$\begin{pmatrix} (-e\phi) \cdot 1_2 & c\,\sigma.\mathbf{p} \\ c\,\sigma.\mathbf{p} & (-2mc^2 - e\phi) \cdot 1_2 \end{pmatrix} \begin{pmatrix} \psi^L \\ \psi^S \end{pmatrix} = \varepsilon \begin{pmatrix} \psi^L \\ \psi^S \end{pmatrix} \qquad (2.9)$$

where the new ε now is the difference with the rest mass energy.

Let us now consider the solution of the Dirac equation in (2.9). As a potential we consider a hydrogen like system where an electron is moving in an attractive Coulombic potential of a point charge Z ($\phi = eZ/r$). A graphical representation of the spectrum of solutions from this equation is given in figure 2.1.

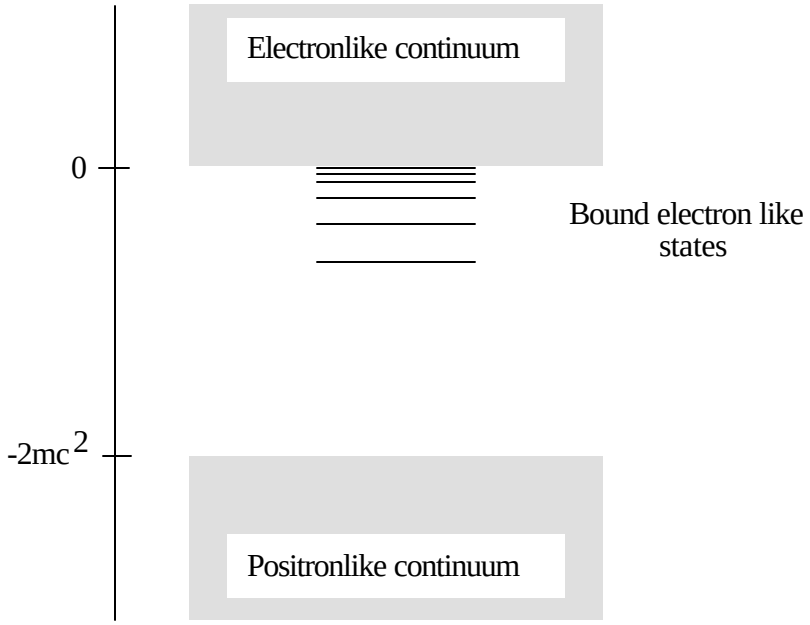

Figure 2.1. Graphical representation of the spectrum of a hydrogen like atomic system.

One can see from figure 2.1 that the spectrum is not bounded from below. The continuum states lie below $-2mc^2$ and above 0, whereas the bound electron like states lie close to the upper continuum. If we take a repulsive instead of an attractive Coulombic potential than the bound states lie close to the lower continuum.

The positive continuum and the bound electron like states are analogous to those that would be found when the Schrödinger equation was solved. There is however a fundamental problem with the occurrence of the negative continuum. One cannot discard these negative energy solutions, because this would violate the completeness assumption of the solution space of the Schrödinger theory. On the other hand not discarding them results in an unstable lowest positive energy state, because it is no longer the ground state. Dirac proposed a solution for this problem by postulating a new vacuum where all negative eigenvalues are already occupied. The Pauli exclusion principle now forbids additional occupation of the negative eigenvalues, hence the electron will now occupy a bound electron like state. Dirac's postulate has even further implications. One can excite an electron from the negative continuum which leaves a positively charged hole in the vacuum, which is generally called a positron. This means that one can create an electron-positron pair but for this an energy of approximately $2mc^2$ is required,

far above the energies that are involved in ordinary chemistry. Another problem connected with the filled negative continuum is that the vacuum is infinitely charged and that even the hydrogen problem becomes an infinitely many-body problem. This problem can be approached by adopting the Quantum Electron Dynamics (QED) picture. QED also introduces additional interactions like vacuum polarization (electron-vacuum interaction) and self energy (an electron interacting with itself). For this work it is sufficient to know that the Dirac equation can be embedded in a proper fundamental framework (QED). This framework is, however, not necessary for our practical purposes.

We will now show that there is a relation between the Dirac and Schrödinger equation. In this process we will also establish a relation between large and small component part of the wave function. This relation will be used in the discussion about solutions of the Dirac equation using a basis set expansion. We can write the matrix form as two coupled 2-component equations where we have used the second equation to express ψ^S in terms of ψ^L

$$\left(- e\phi \cdot 1_2\right) \psi^L + c\, \boldsymbol{\sigma}.\mathbf{p}\ \psi^S = \varepsilon\, \psi^L \qquad (2.10.a)$$

$$\psi^S = \left[\left(2mc^2 + e\phi + \varepsilon\right)^{-1} .\ 1_2\right] c\, \boldsymbol{\sigma}.\mathbf{p}\ \psi^L \qquad (2.10.b)$$

If we combine (2.10.a) and (2.10.b) one can eliminate ψ^S.

$$\left(- e\phi \cdot 1_2 + c\, \boldsymbol{\sigma}.\mathbf{p} \left[\left(2mc^2 + e\phi + \varepsilon\right)^{-1} \cdot 1_2\right] c\, \boldsymbol{\sigma}.\mathbf{p}\right) \psi^L = \varepsilon\, \psi^L \qquad (2.11)$$

We rewrite as

$$\left(- e\phi \cdot 1_2 + \boldsymbol{\sigma}.\mathbf{p} \left[\left(2m\left(1 + \frac{e\phi + \varepsilon}{2mc^2}\right)\right)^{-1} .\ 1_2\right] \boldsymbol{\sigma}.\mathbf{p}\right) \psi^L = \varepsilon\, \psi^L \qquad (2.12)$$

and expand the denominator. To zeroth order this yields the expression

$$\left(- e\phi \cdot 1_2 + \frac{1}{2m} (\boldsymbol{\sigma}.\mathbf{p})^2\right) \psi^L = \varepsilon\, \psi^L \qquad (2.13)$$

The operator $(\boldsymbol{\sigma}.\mathbf{p})^2$ is equal to $p^2 \cdot 1_2$ which gives us the Schrödinger equation in 2-component form where each of the two components represents one of the two possible spin states α and β. This now also explains the α and β notation of the 4-component wave function that was given in (2.3). Similarly we can express ψ^S in terms of ψ^L and from this derivation we will find an equation for a positron, an electron with opposite charge. So, in the non-relativistic limit the electron and positron space are again completely separated.

2.1.2 The many-electron approach

In this thesis we consider mainly systems that contain more than one electron. So we have to take the interaction between the electrons into account. The Hamiltonian for the complete electron-electron interaction can be obtained from QED[15,22,54]. This complete interaction can, however, not be written in closed form and can only be obtained from time-dependent perturbation theory[22]. Restricting the expansion to the lowest order of electron-electron interaction yields, in the so-called low-frequency limit, the Coulomb term and the Breit[15] term. The many-electron Hamiltonian is given by

$$\hat{H} = \sum_{i}^{N} \hat{h}_i + \frac{1}{2} \sum_{i \neq j}^{N} \left[\frac{1}{r_{ij}} - \left(\frac{(a_i \cdot a_j)}{r_{ij}} + \frac{(a_i \times \mathbf{r}_{ij}) \cdot (a_j \times \mathbf{r}_{ij})}{2 r_{ij}^3} \right) \right] \tag{2.14}$$

$\hat{h}_i$ is the one-electron Hamiltonian for electron i which is given in (2.9). The Hamiltonian presented in (2.14) is called the Dirac-Coulomb-Breit Hamiltonian. In a first approximation we can neglect the Breit interaction and only include the Coulomb term which is the dominant part of the electron-electron interaction. This gives the Dirac-Coulomb Hamiltonian

$$\hat{H} = \sum_{i}^{N} \hat{h}_i + \frac{1}{2} \sum_{i \neq j}^{N} \frac{1}{r_{ij}} \tag{2.15}$$

The last two terms in (2.14) together, already derived in 1929, form the Breit[15] term. We have included the first term of the Breit interaction, the Gaunt[55] term, in our Hamiltonian

$$\hat{H} = \sum_{i}^{N} \hat{h}_i + \frac{1}{2} \sum_{i \neq j}^{N} \left[\frac{1}{r_{ij}} - \frac{(a_i \cdot a_j)}{r_{ij}} \right] \tag{2.16}$$

The Dirac-Coulomb-Gaunt Hamiltonian obtained in this way will be used as a starting point of our calculations.

There has been a discussion about the validity of the Dirac-Coulomb Hamiltonian which we derived above. Brown and Ravenhall[30] argued that one cannot find stable stationary states for this Hamiltonian. If electron-electron interaction is turned on as a perturbation, one can construct an infinite number of degenerate states which consist of electrons as well as positrons. The final states will therefore be completely delocalized. This "problem" is referred to as the "Brown-Ravenhall disease" or "Continuum Dissolution". However, from QED one can derive a many-electron relativistic Hamiltonian that has bound states[56-58]. Brown and Ravenhall proposed to restrict the Hamiltonian to positive energy states (electron like solutions) by surrounding it with projection operators, i.e. we will have a fixed number of

electrons. There are a number of ways to construct the projection operators[56,57,59,60] but we will make use of the projection method of Mittleman[58], sometimes called the "fuzzy" picture[56]. We will come back to this projection method in section 2.2.3 where we will deal with the generation of one-electron wave functions.

The Hamiltonian of the molecular system in the Born-Oppenheimer approximation consists of the electronic Hamiltonian (2.14 - 2.16) and the nuclear Hamiltonian, where the latter reduces to a simple addition to the total energy.

2.1.3 Symmetry aspects

The inclusion of molecular point group symmetry into the calculations reduces the computational costs considerably and helps the interpretation of the results. Non-relativistically we only have to deal with the point group symmetry operations which act on the spatial coordinates of the molecule. Whereas the Schrödinger Hamiltonian is invariant under these symmetry operations the Dirac Hamiltonian (2.16) is not. In fact the symmetry operations which leave the Dirac Hamiltonian invariant are a product of spatial and spin operations. The inclusion of this extra operations on top of the symmetry operations for the spatial coordinates doubles the number of operations in the symmetry group and hence these groups are therefore called double groups. The theory of double group symmetry was first derived by Bethe[61]. Besides the boson irreducible representations (irreps), that are used in non-relativistic theory, one now also gets fermion irreps which describe the one-electron functions of the Dirac Hamiltonian.

The point double groups that will be used by us are those of O_h^* (where the asterix denotes the double group) and its subgroups. A part of these double groups are Abelian, giving only one-dimensional representations that allow for a unique labelling of one-electron spinors. However we also work on chemical systems with non-Abelian point double groups which have also degenerate representations. In the additional correlation calculations we will restrict ourselves to Abelian point double group symmetry. To use the Abelian symmetry one requires an additional transformation of the one-electron spinor basis. We have chosen to use a group chain[26] to decompose the higher group into a group of Abelian symmetry. For this chain we define a series of groups $G_1 > G_2 > ..$ where the second group will be a subgroup of the first group, etc. The last group in the chain will be an Abelian group. If we now choose the one-electron spinor such that it transforms according to all the groups in the chain then one can assign a unique label to this spinor. This decomposition now defines the rows of the degenerate representations in the higher group. This approach allows us to exploit the full point double group symmetry for the generation of one-electron spinors whereas we can use Abelian symmetry in the subsequent correlation calculations, without transformation of the spinor basis. The symmetry notation that we use is defined by Bradley and Cracknell[62].

The inclusion of point double group symmetry will block diagonalize the Dirac matrix and hence reduce the computational effort. However the elements in the matrices and the integrals are still complex

numbers and we can also not use spin α and β to further reduce the calculations, as is done in non-relativistic theory. However, there is another symmetry operation that can be used to block diagonalize the matrices even further and to make matrices real in certain cases. This symmetry operation is called time-reversal (TR) operator and it is defined as

$$\hat{T} = -i \begin{pmatrix} s_y & 0 \\ 0 & s_y \end{pmatrix} \hat{K} \qquad (2.17)$$

where s_y is one of the Pauli spin matrices, defined before, and $\hat{K}$ is the complex conjugation operator. This operator is not contained in the point double groups but it can be shown that the Dirac Hamiltonian, as it is defined in (2.16), commutes with this anti-unitary operator leaving double degenerate one-electron functions, called Kramers[63] pairs. This degeneracy disappears, however, if we want to study molecules in external magnetic fields, i.e. when a vector potential is introduced.
The combination of time-reversal symmetry and double group symmetry, in an effort to further reduce the computational effort, gives us three different cases depending on the distribution of the Kramers pairs over the fermion irreps:

Case 1. The components of a Kramers pair belong to different rows of a doubly degenerate irrep.
Case 2. The components of a Kramers pair belong to different one-dimensional irreps which together form a doubly degenerate reducible representation.
Case 3. The components of a Kramers pair belong to the same singly degenerate irrep.

Saue[34] uses quaternion algebra, on the so-called binary double groups (D_{2h}^* and it's subgroups), to include both point double group and time-reversal symmetry. They showed for the Dirac Hamiltonian defined in (2.16) that the spinor matrix elements are real for Case 1 and that the one-electron matrices are block diagonal in the Kramers components. The binary double groups belonging to this case are D_{2h}^*, D_2^* and C_{2v}^*. For Case 2, which includes the double groups C_{2h}^*, C_2 and Cs, the spinor matrix elements are complex but the one-electron matrices are still block diagonal. In Case 3, to which the double groups C_1^* and C_i^* belong, the spinor matrix elements are complex and the one-electron matrices are not block diagonal anymore. It is, however, possible to make the one-electron matrices block diagonal by a quaternionic transformation[34].
In our program package we only take advantage of the complex to real reduction in Case 1 using an approach developed by Visscher[64]. The one-electron spinors are constructed as Kramers pairs by introducing appropriate phase factors. This leads to real one- and two-electron integrals for double groups belonging to Case 1 and allows us to get computational savings.

2.2 Methodology

In section 2.1.2 we derived the Hamiltonian which we want to use to solve a N-electron wave-equation

$$\hat{H}\,\Psi(r_1, r_2, \ldots r_N) = E\,\Psi(r_1, r_2, \ldots r_N) \tag{2.18}$$

From this point on we will follow the same route that is used in the non-relativistic approach to arrive at expressions that can be solved by more or less the standard quantum chemistry techniques.

The N-electron wave function Ψ can be expanded in all possible Slater determinants Φ that can be generated from the complete set of one-electron wave functions ψ corresponding to the solutions of the Hamiltonian

$$?\,(r_1, r_2, \ldots r_N) = \sum_{\mu} C_{\mu} F_{\mu} \tag{2.19}$$

$$\Phi_{\mu}(r_1, r_2, \ldots r_N) = \frac{1}{\sqrt{N!}}\,\mathrm{Det}\left|\psi_{\mu 1}(r_1)\psi_{\mu 2}(r_2)\ldots \psi_{\mu N}(r_N)\right| \tag{2.20}$$

The simplest way to approximate the N-electron wave function is by restricting the expansion of Slater determinants to just one determinant which we will denote with Φ_0.

We now want to find a set of one-electron wave functions, or spinors, $\{\psi_i\}$ such that the determinant Φ_0 formed from these spinors is the best possible approximation to the solution of the N-electron system described by the Hamiltonian $\hat{H}$. The approach that we use to solve this equation is the relativistic analogue of the Hartree-Fock approximation or the Dirac-Hartree-Fock (DHF) approximation. A closed shell DHF formalism was first proposed by Malli[65]. The basic assumption of the Hartree-Fock approximation is that any one of the electrons moves in a static potential generated by the nuclei and an average potential of all other electrons. In this way the many-electron equation can be replaced by a set of one-electron equations (one for each electron that is described). The average potential in this one-electron equation, generated by all other electrons, depends on the one-electron wave functions of the other electrons, i.e. each one-electron equation depends on the results of the other one-electron equations. This means that the Hartree-Fock equations are non-linear and need to be solved iteratively. In every iteration one uses the new one-electron wave functions to obtain new average potentials until self-consistency is obtained in which the average potentials, and thereby the spinors, do not change anymore. This procedure to solve the Hartree-Fock equations is hence called the self-consistent-field or SCF method.

The variational *theorem* for Hamiltonian operators that are bounded from below, on which the procedure above is based, does not apply to our Dirac Hamiltonian because the states of interest, the electron like states, are excited states in the spectrum of the Hamiltonian. However, variational theory

also applies to stationary states and hence is still applicable in Dirac-Hartre-Fock theory. In particular LaJohn and Talman[66] pointed out that one can find the electron like spinors by using the so-called minimax principle where the energy is minimized with respect to rotations into the virtual electron-like spinor space, the optimization process used in the non-relativistic approach, and maximized with respect to rotations in the positron spinor space. The optimization procedure we use is in fact a process searching for a stationary value instead of a minimalization process.

2.2.1 Basis set considerations

So far we have discussed the Dirac-Hartree-Fock approach in terms of a general set of spinors. We have to define the form of these spinors in order to do the actual calculations. A standard way to approximate the 4-component spinors ψ is by expanding them into a finite basis set. Due to the nuclear framework one can also introduce point group symmetry by adapting the basis to the appropriate double group symmetry. We will use separate double group symmetry adapted basis sets for the upper two (Large) and for the lower two components (Small) of the 4-component wave function

$$\psi_a^L = \begin{pmatrix} \psi_a^{L\alpha} \\ \psi_a^{L\beta} \\ 0 \\ 0 \end{pmatrix} \quad \text{and} \quad \psi_b^S = \begin{pmatrix} 0 \\ 0 \\ \psi_b^{S\alpha} \\ \psi_b^{S\beta} \end{pmatrix} \tag{2.21}$$

where each of the four components is a linear combination of scalar basis functions χ (atomic basis functions) with the transformation coefficients d_{ia}^{LX} and d_{ib}^{SX} (which generally are complex)

$$?_a^{LX} = \sum_i d_{ia}^{LX} ?_i^L \quad \text{and} \quad ?_b^{SX} = \sum_j d_{jb}^{SX} ?_j^L \quad (\text{with } X = a \text{ or } ß) \tag{2.22}$$

The set of Large and Small scalar basis functions consists of two separate sets of primitive Cartesian Gaussian basis functions, usually centered on each of the nuclear positions

$$\chi_i^L = g_i^L = N_i^L x^{u_i^L} y^{v_i^L} z^{w_i^L} e^{-\alpha_i^L r^2} \quad \text{and} \quad \chi_j^S = g_j^S = N_j^S x^{u_j^S} y^{v_j^S} z^{w_j^S} e^{-\alpha_j^S r^2} \tag{2.23}$$

or as contracted sets of scalar basis functions with different exponents α

$$?^{L}_{i} = \sum_{p} c^{L}_{ip} g^{L}_{p} \quad \text{and} \quad ?^{S}_{j} = \sum_{q} c^{S}_{jq} g^{S}_{q} \tag{2.24}$$

In the contraction defined above all the primitive functions defined in (2.23) can contribute to all contracted scalar functions. This scheme is called the general contraction scheme[67]. The contraction leads to a significant reduction of the basis set size while keeping high quality.

In (2.21) - (2.24) we have defined two separate basis sets, one for the large component and one for the small component, but they should not be chosen independently. The differential equation (2.10.b) links the large and small component part of the wave function for each solution. This relation must be expressible by the basis set, at least for the solutions one wants to find. Neglecting this relationship can cause the so-called "variational collapse"[68] or "basis set disease"[69]. In our many-electron Dirac-Hartree-Fock calculations the potential ϕ and the energy ε are not known on forehand and therefore we have to use an approximate form of the operator in (2.10.b) to define our basis set. The simplest approximation is the kinetic balance[21-26] relation

$$\psi^{S} \approx \frac{1}{2mc} \boldsymbol{\sigma}.\mathbf{p}\ \psi^{L} \tag{2.25}$$

In this kinetic balance relation the potential ϕ and the energy ε are assumed to be much smaller than $2mc^2$. The generation of small component basis functions from large component basis functions by this relation is nowadays used as concept for the construction of uncontracted basis sets. In practise, we will use a Gaussian basis function $r^{\ell}\, e^{-\alpha r^2}$ in the large component and we use the kinetically balanced Gaussian basis functions $r^{\ell-1}\, e^{-\alpha r^2}$ (if $\ell > 0$) and $r^{\ell+1}\, e^{-\alpha r^2}$ in the small component. This means that for a p-type large component function a s-type and a d-type function will be included in the small component basis.

The uncontracted basis sets will become large if one wants to describe the interactions in molecules with a high level of accuracy, similar to non-relativistic basis sets. To reduce the computational effort one can make use of contracted basis sets. We use the same primitive set for both spin-orbit split components which generally have a different radial behaviour. A consequence of this approach is that the number of large component contracted functions is doubled compared to a non-relativistically contracted function. Erroneous results are obtained if one constructs a contracted small component basis directly from the contracted large component basis using the kinetic balance relation (2.25). These errors are caused by the singular character of the large component in the innermost atomic orbitals[25-28] $1s_{1/2}$ and $2p_{1/2}$. The exact hydrogen-like solution of the large component $1s_{1/2}$ function has the form

$$D(r) = r^{\gamma-1} e^{-\lambda r} \quad \text{with} \quad \gamma = \sqrt{1 - \frac{Z^2}{r^2}} \tag{2.26}$$

The kinetically balanced small component function diverges then as $r^{\gamma-2}$ which, when numerically approximated by a basis set, necessary leads to a diverging proces. One can try to overcome the error made in applying (2.25) by decontracting functions in the core-region[25-28,70], increasing the variational freedom of the innermost spinors, or by not contracting after all (the latter option is common practice in atomic calculations). However, for molecules an alternative approach is to obtain a better approximation of the exact relation between the large and small component (2.10.b) in the first place. Already in 1991 our group developed the so-called atomic balance[27,28] procedure that is applied in general contracted basis sets. It should be noted that Watanabe and Matsuoka[29] proposed a similar procedure more recently.

The atomic balance procedure consists of two steps:

1. An atomic calculation is performed using uncontracted basis functions where the small component is generated from the large component using the kinetic balance relation.
2. A new set of large and small component contracted basis functions is constructed from the uncontracted basis combined with the expansion coefficients from this atomic calculation.

A good description of the exact relation (2.10.b) is obtained although our results will depend on the potential ϕ and the energy ε. This is not a real problem because the atomic potential and the molecular potential in the core-region will be very similar.

We have talked about the contraction but we did not yet define the exponents needed for the primitive basis functions in (2.20). To a first approximation one could use non-relativistic primitives to define the large component basis functions, deriving the small component functions using the kinetic balance procedure. This will lead to a reasonable basis for the lighter atoms but will lead to poor sets for the heavier elements. As already discussed in chapter 1 the s and p functions have in general smaller radii whereas for example the d and f functions have larger radii compared to the radii one would find using a non-relativistic framework. This difference in radial behaviour, but also in nodal behaviour, is the strongest for functions close to the nuclei. For most heavy elements it is sufficient to add a few extra functions with high exponents to the large component basis, consisting of non-relativistically optimized s and p basis functions, to describe the inner part of the $1s_{1/2}$ and $2p_{1/2}$ radial functions. However, in superheavy elements the addition of some extra functions is often insufficient and one should use relativistically optimized basis sets instead. To obtain relativistically optimized exponents for our calculations we need to optimize the exponents using the Dirac-Coulomb Hamiltonian. A numerical

program that can handle this optimization is the GRASP[19] program. It was recently adapted[71] to generate (general) contracted, atomically balanced, basis sets.

To reduce the computational effort we introduce the use of common subsets of functions, also called "family" basis sets. In the large component basis set the exponents for the (ℓ+2) functions are chosen as a subset of the exponents for the ℓ functions, for example the exponents of the d function are a subset of the s exponents. This gives us, for the large component, two interleaving families of exponents for even and odd ℓ functions each where the (ℓ+2) and ℓ large component functions have a common set of small component basis functions of type (ℓ+1). The subset strategy leads to smaller basis sets for the small component basis functions but also leads to a lower flexibility in the exponents of the large component basis.

Dyall and Fægri[72] suggest an alternative definition of the exponents for the large component basis functions. They group the functions on the basis of their j quantum number instead of the angular quantum number ℓ. In this case one uses one set of exponents to describe the $s_{1/2}$ and $p_{1/2}$ functions and another set to describe the $p_{3/2}$ and $d_{3/2}$, etc. This approach is favorable for superheavy elements where the $p_{1/2}$ and the $p_{3/2}$ function have a considerably different radial behaviour.

2.2.2 Nuclear model

Another problem that should be addressed is related to the weak singularity (2.26) at the nucleus. This weak singularity arises from a fractional power of r, as a result of the finite speed of light, in the radial solution from the $1s_{1/2}$ (and the $2p_{1/2}$) wave function. The weak singularity can be described by a Gaussian basis set but there are a large number of steep functions required to obtain a good description. Another and better approach, which is now commonly used in calculations, is to make use of a finite nucleus. A nucleus with a finite dimension is a better physical description than the point charge model anyway and only slightly more complicated to work with. The most widely used model to describe the interaction between a nucleus and an electron is a Gaussian distribution

$$f(\mathbf{r}) = \sum_{M=1}^{\#nuc} \int N_M \frac{Z_M e^{-?_M (\mathbf{r}-\mathbf{R}_M)^2}}{(\mathbf{r}-\mathbf{R}_M)} d\mathbf{R}_M \qquad (2.27)$$

$$\text{with} \quad N_M = \left(\frac{\xi_M}{\pi}\right)^{3/2} \qquad (2.28)$$

This potential form is used in the one-electron part of the Dirac-Coulomb Hamiltonian defined in (2.16). One has to find a way to relate the Gaussian exponent ξ to the measured properties of the atomic nucleus. In this thesis two definitions are used for the Gaussian exponent using the charge Z_M and the

nuclear mass W_M or atomic mass number A_M as parameters. The first definition makes use of the expression

$$\xi_M = 3.88 * 10^{-9} (W_M)^{-2/3} \qquad (2.29)$$

whereas the second uses

$$\xi_M = \frac{3}{2\, r_{nuc}^2} \quad \text{with} \quad r_{nuc}^2 = \left[0.836\ A_M^{1/3} + 0.570\right] / 52917.7249 \qquad (2.30)$$

to generate the exponent. The exponent that is derived with the model in expression (2.29) is an older model[73] that is used in chapter 6. In 1995 on a REHE meeting in "Il Ciocco" (near Pisa in Italy) Visscher and Dyall[74] suggested a standardization of the model used to obtain the Gaussian exponent. This is the model presented in formula (2.30). The standardization makes it possible to compare the results of different program packages. Visscher and Dyall therefore calculated the atomic properties for all the elements up to 109 which can be used as a reference. More about this model can also be found on the WWW pages of Visscher[75]. The second model is used for all calculations except those in chapter 6, as mentioned before.

2.2.3 The Dirac-Hartree-Fock-Roothaan approach

In section 2.2.1 we have shown that one can approximate the one-electron wave functions by expanding them in a finite set of (spatial) basis functions (2.21-2.24). When we combine this expansion with the Dirac-Hartree-Fock (DHF) approach, sketched at the beginning of section 2.2, matrix eigenvalue equations for the expansion coefficients are obtained. These equations are generally called the Roothaan equations. We use the so-called open-shell Hartree-Fock-Roothaan equations[76] to obtain the one-electrons spinors. With these equations one can handle molecules with open and closed shells (denoted with O and C respectively). The relativistic analogue[77] for the corresponding energy expression, for an average of configurations[78], is defined as

$$E = \left\langle ? \left| \hat{H} \right| ? \right\rangle = \sum_i^C h_i + \frac{1}{2}\sum_{i,j}^C Q_{ij} + f\left[\sum_k^O h_k + \frac{1}{2} af \sum_{k,l}^O Q_{kl} + \sum_{i,k}^{C,O} Q_{ik}\right] \qquad (2.31.a)$$

$$\text{with } f = \frac{n}{d} \qquad a = \frac{d\,(n-1)}{n\,(d-1)} \qquad Q_{ij} = J_{ij} - K_{ij} \qquad (2.31.b)$$

h_i is the diagonal matrix element of the one-electron Dirac operator (2.9) and J_{ij} and K_{ij} are the Coulomb and Exchange integrals. The indices i and j denote spinors with occupation one and the indices

k and l are used to label the open-shell spinors with a fractional occupation. The variables n and d denote the number of electrons and the number of spinors respectively. We can derive the DHF equations by putting

$$\frac{\partial E}{\partial ?_i} = 0 \qquad (2.32)$$

under the constraint that the spinors ψ_i, that make up the determinantal wave function Ψ, form an orthonormal set. The derivation, and the exact form of the working formulas used can be found in various articles[37-39,77,79] and will not be repeated here. Nowadays a number of computer codes, based on the DHF approach, are available[33-36,80,81].

The electron and positron like solutions are well separated and easily identifiable and one can easily select the electron like solutions. This selection of electron like solutions corresponds to the iterative projection method proposed by Mittleman[58], as was discussed at the end of section 2.1.2.

2.2.4 The correlated approach

The spinors obtained with the DHF approximation, defined in 2.2.3, are generated in an average field of all the other electrons. In reality the motion of the electrons will depend on the instantaneous positions of all the other †electrons in the system, hence the motion of the electrons is "correlated". This lack of correlation in the DHF method is the reason why the error in the energy is called the correlation energy. First, it is convenient to describe the Hamiltonian in a second quantized formalism based on spin-orbitals

$$\hat{H} = \sum_{i,j} \langle i|h|j\rangle a_i^\dagger a_j + \frac{1}{2}\sum_{i,j,k,l} \langle ij|g|kl\rangle a_i^\dagger a_k^\dagger a_j a_l \qquad (2.33)$$

where h is the Dirac one-electron Hamiltonian and g represents the electron-electron interaction (Coulomb and Gaunt). The operators $a_i^\dagger$ and a_i are creation and annihilation operators of one-particle spinors obtained by solving the DHF equations. Here the creation of electron-positron pairs will be neglected, so the sums of i, j, k and l will run over electron like spinors only, and therefore this second quantized Hamiltonian has a similar form as the non-relativistic Hamiltonian for spin orbitals, i.e. we are using the no-pair approximation[57].

Various methods have been developed to include electron correlation effects. Two of these methods are implemented and used in our calculations, (Multi-Reference) Configuration Interaction (MRCI) and Coupled Cluster Singles Doubles (CCSD).

The correlation methods mentioned deal with dynamical correlation which is due to short range electron-electron interaction. Non-dynamical correlation, which is mainly due to near-degeneracies and

can generally be described with a few determinants requires an relativistic analogue of the MCSCF method[82]. We include non-dynamical correlation using the average of configuration DHF approach. This method, which gives us one set of spinors for the whole manifold of states in the open-shell system, is expected to show a balanced, global picture of the manifold with not too much emphasis on a particular state. After the Dirac-Hartree-Fock (DHF) calculation a CI can be performed in the open-shell spinor space in order to project out the different states that arise from the open-shell manifold if these are required. The combination of an DHF calculation and a full CI within the open-shell manifold will be called a COSCI calculation.

For the (Multi-Reference) CI approach we consider first a general expansion of the many-electron wave function into a basis of determinants, as defined in (2.19). Combining this expansion with the Hamiltonian gives us a matrix representation of the Hamiltonian which is a sum of one- and two-electron molecular integrals multiplied with one- and two-electron coupling constants

$$H_{\mu?} = \sum_{ij} h_{ij} A_{ij}^{\mu?} + \frac{1}{2} \sum_{ijkl} (ij|kl) B_{ijkl}^{\mu?} \qquad (2.34)$$

where the different terms are defined as

$$h_{ij} = \langle i | \hat{h} | j \rangle \qquad (ij \mid kl) = (ij \mid g \mid kl) \qquad (2.35.a)$$

$$A_{ij}^{\mu\nu} = \langle \mu | e_{ij} | \nu \rangle \qquad B_{ijkl}^{\mu\nu} = \langle \mu | e_{ij}\, e_{kl} - e_{il}\, \delta_{jk} | \nu \rangle \qquad (2.35.b)$$

A and B are the one-electron and two-electron coupling coefficients written in term of generators of the unitary group ($e_{ij} = a_i^\dagger a_j$). The size of this matrix, which is defined by the number of determinants in the expansion, is generally too large to store all the matrix elements. To circumvent this problem we make use of the direct diagonalization technique of Davidson[83] to find the eigensolution of the many-electron wave function. In this method a subspace of m trail (or basis) functions is constructed that spans the space of the required eigensolutions. This subspace is than extended, in an iterative procedure, with new expansion functions to improve the wave function expansion C_μ and its eigenvalue

$$C_\mu^{m+1} = C_\mu^m + \frac{1}{E^m - H_{\mu\mu}} (\sigma_\mu - E^m C_\mu^m) \qquad (2.36)$$

where E^m is the energy evaluated using vector C^m. We will not derive the final expressions because this is already done in several articles about the MOLFDIR program package[37,39,79]. However, we will

stand still at the most difficult and time-consuming step in the construction process, the evaluation of the so-called sigma vector, the first term in the summation in (2.36)

$$\sigma_\mu = \sum_\nu H_{\mu\nu} C_\nu^M = \sum_\nu \left[\sum_{ij} h_{ij} A_{ij}^{\mu\nu} + \frac{1}{2} \sum_{ijkl} (ij|kl) B_{ijkl}^{\mu\nu} \right] C_\nu^M \tag{2.37}$$

It is possible to write the two-electron coupling coefficient B in terms of one-electron coupling coefficients by including the resolution of the identity where we can restrict the sum of this resolution to the N determinants in the CI space we are considering

$$B_{ijkl}^{\mu\nu} = \sum_\nu^N A_{ij}^{\mu\nu} A_{kl}^{\nu\nu} - \delta_{jk} A_{il}^{\mu\nu} \tag{2.38}$$

This restriction is valid exactly because we use the RAS type expansion of the CI wave function[84]. We will come back to this expansion after deriving the final expression for the sigma vector

$$\sigma_\mu = \sum_\nu^N \sum_{ij} \tilde{h}_{ij} A_{ij}^{\mu\nu} C_\nu + \sum_{\nu,\nu}^N \sum_{ij} \sum_{kl \le ij} \frac{(ij|kl)}{1+\delta_{ij,kl}} A_{ij}^{\mu\nu} A_{kl}^{\nu\nu} C_\nu \tag{2.39.a}$$

$$i \ge j : \tilde{h}_{ij} = h_{ij} - \frac{(ii|jj)}{1+\delta_{ij}} - \sum_{k<i} (ik|kj) \tag{2.39.b}$$

$$i < j : \tilde{h}_{ij} = h_{ij} - \sum_{k<i} (ik|kj) \tag{2.39.c}$$

It should be noted that the final formula for the sigma vector, as it was printed in previous papers[37,39,79], contains some small errors and that the expression given here is the correct formula.

We will now return to the RAS formalism used to define the reference wave function in the CI expansion space. In the Restricted Active Space formalism we divide the space of active spinors into three classes. The first class contains spinors that are occupied and is generally called RAS1. In the second class, RAS2, contains the spinors with a variable occupation. If we have an open-shell DHF wave function as a starting point for our calculations than these open-shell spinors, i.e. the COSCI wave function, can be defined as RAS2. The third class (RAS3) contains spinors that are unoccupied, or virtuals. The RAS CI expansion space is now defined by allowing a certain number of electrons to be excited from the occupied RAS1 spinors and by allowing a defined number of electrons to occupy the virtuals in RAS3.

One can define various CI expansions and we will take a closed shell molecule (where the RAS2 space contains no spinors) as an example, allowing a maximum of two electrons in the virtual space. This expansion is known as the single reference CISD wave function

$$\Psi_{CISD} = (1 + T_1 + T_2)\Phi_0 \qquad (2.40)$$

where Φ_0 is the closed shell reference wave function. The operators T_1 and T_2 are excitation operators defined as

$$T_1 = \sum_{i,a} t_i^a a_a^\dagger a_i \qquad T_2 = \sum_{i,j,a,b} t_{ij}^{ab} a_a^\dagger a_b^\dagger a_i a_j \qquad (2.41)$$

where the t's are called the cluster amplitudes or CI-coefficients depending on whether we are talking about CI or Coupled Cluster expansions. The indices i and j label the occupied spinors whereas the indices a and b label the spinors that are unoccupied in the reference wave function.
The example chosen in (2.40) is not an accidental choice. It allows us to compare the CI wave function expansion with the Coupled Cluster approach, the second correlation method that has been implemented. Whereas the CISD wave function is a linear expansion, for the Coupled Cluster approach the expansion of the closed shell reference wave function Φ_0 is written as an exponential expansion of the operators T

$$\Psi_{CCSD} = \mathrm{Exp}\,(T_1 + T_2)\,\Phi_0 \qquad (2.42)$$

One can include higher order excitation operators T but here we have restricted the expansion to the single and double excitations, hence this expansion is called the Coupled Cluster Singles Doubles wave function. Whereas we can use a multi-reference wave function as a start in the CI calculation a single determinantal wave function is required in a CCSD calculation. Although CCSD theory has its restrictions concerning the reference wave function it has the advantage of being a size-extensive theory[85], i.e. the correlation energy scales linearly with the number of atoms or molecules in the system, this in contrast to CI theory.
The Coupled Cluster program[86] in our package can be used to perform closed shell[40] CCSD. In the derivation of the CCSD equations we end up with an energy expression that contains the amplitudes t_i^a and t_{ij}^{ab}. The expressions required for the evaluation are more demanding and are therefore not written down in this thesis. The reader is referred to the literature[40,87] given in this section for the explicit form of the expressions. The latest version can handle open-shell[87] systems, as long as they are single reference, and also includes the next higher corrections, the (perturbative) triple excitations[88-90]. With

the implementation used we can also derive the MP2 energy. MP2 is the highest level of correlation currently implemented in other four-component codes[81,91]. Both the CCSD program and the (MR)CI code do not exploit the Kramers symmetry.

2.2.5 Property calculations

The advantage of optimizing the wave function explicitly and also the combination with an analytic approach is the ease of obtaining virtually any electronic property, not just the energies. From the calculated energies one can obtain spectroscopic properties, like the equilibrium bond length, the harmonic frequency and dissociation energy, which can be compared with, or used to explain, experimental data.

Recently an even larger variety of properties, other than the spectroscopic properties mentioned before, is calculated. A large group of these properties can be evaluated as expectation values using the corresponding (relativistically formulated) operator and the calculated wave function.

Another group of properties that can be studied is the response of a wave function (state), or properties from this wave function, to an external perturbation. One general approach to calculate these response properties is by using propagator theory[92]. It allows us to study the response of the molecule to a static or an oscillatory perturbation (the latter with a certain frequency ω). We will limit ourselves to the linear response which, in the so-called superoperator formalism, can be written as

$$\langle\langle A;B \rangle\rangle_\omega = \left\langle A \left| (\omega \hat{1} - \hat{H})^{-1} \right| B \right\rangle \qquad (2.43)$$

where A and B are property operators and $\hat{H}$ and $\hat{1}$ are the Hamiltonian (2.16) and the identity matrices respectively. The linear response function describes the change in the expectation value of operator A if a perturbation operator B, with a frequency ω, is applied to the molecule in a reference state and is correct to first order in the perturbation B. We introduce the resolution of identity (twice) by inserting a complete excitation operator manifold. In our calculations we will work in the random phase approximation (RPA) where we take a closed-shell Hartree-Fock determinant as the reference state and restrict the operator manifold, introduced by the resolution of identity, to single excitations. This RPA approximation is also known as time-dependent Hartree-Fock (TDHF). The final expression[93], in matrix representation, can be written as

$$\langle\langle A;B \rangle\rangle_\omega = \begin{pmatrix} \mathbf{A} & -\mathbf{A}^d \end{pmatrix} \begin{pmatrix} \omega \hat{1} - \mathbf{C} & -\mathbf{D}^\dagger \\ -\mathbf{D} & -\omega \hat{1} - \mathbf{C}^\dagger \end{pmatrix} \begin{pmatrix} \mathbf{B} \\ -\mathbf{B}^d \end{pmatrix} \qquad (2.44.a)$$

with

$$A_{ai} = \langle i | A | a \rangle \quad A^d_{ia} = \langle a | A | i \rangle \quad B_{ai} = \langle i | B | a \rangle \quad B^d_{ia} = \langle a | B | i \rangle \qquad (2.44.b)$$

$$A_{ai,bj} = \langle aj||ib\rangle + (\varepsilon_a - \varepsilon_i)\,\delta_{ab}\delta_{ij} \qquad B_{ia,bj} = \langle ji||ab\rangle \tag{2.44.c}$$

where the indices {i, j} refer to occupied and {a, b} to unoccupied DHF molecular spinors. The final expression is an eigenvalue problem, with in general large matrices, that can be solved in the same iterative approach[83] used for large CI problems[94]. Visscher[41] has implemented the RPA equations in a modified version of RELCCSD. This implementation allows us to calculate the response property for certain frequencies and to find the lowest eigenvalues of the matrix eigenvalue problem.

We require property integrals for the calculation of response functions and expectation values. The necessary property integrals are obtained from the HERMIT[95] integral code via the DIRAC[91] program and subsequently used by our property codes.

2.3 The MOLFDIR program package

The methodology described in section 2.2 has been implemented in MOLFDIR over the last twelve years. The MOLFDIR program package[96] consists of 14 separate modules that communicate by means of data files. There is only one input file required because the modules use NAMELIST type input. The modules are written in about 60,000 lines of Fortran 77 code and (a few) C-routines. Figure 2.2 gives an graphical overview of the organisation of the program package.

The package can be divided in four major sections. The first section, consisting of four modules, solves the DHF equations and generates a wave function that can be used in subsequent calculations. The DHF wave function can be analyzed or we can improve the wave function by subsequent correlation calculations. In the case of atomic calculations, one can also use the generated wave function to construct general contracted basis sets. Table 2.1 gives a very brief description of the functionality of the modules in our program package.

The program package can be used to do non-relativistic calculations (using a two-component formalism) though one still has to work in the double group symmetry.

The required property integrals, needed for the calculation of response functions and expectation values, are obtained from the HERMIT[95] integral code via the DIRAC[91] program and subsequently used by our property codes. Basis set generation is nowadays done with an adapted version[71] of the numerical GRASP[19] program.

More information about the MOLFDIR program package can be found in various articles[26,37-39,41,77,79,80,87,98]. The references to these articles and also various other articles, including chemical applications, can be found on the WWW pages[99].

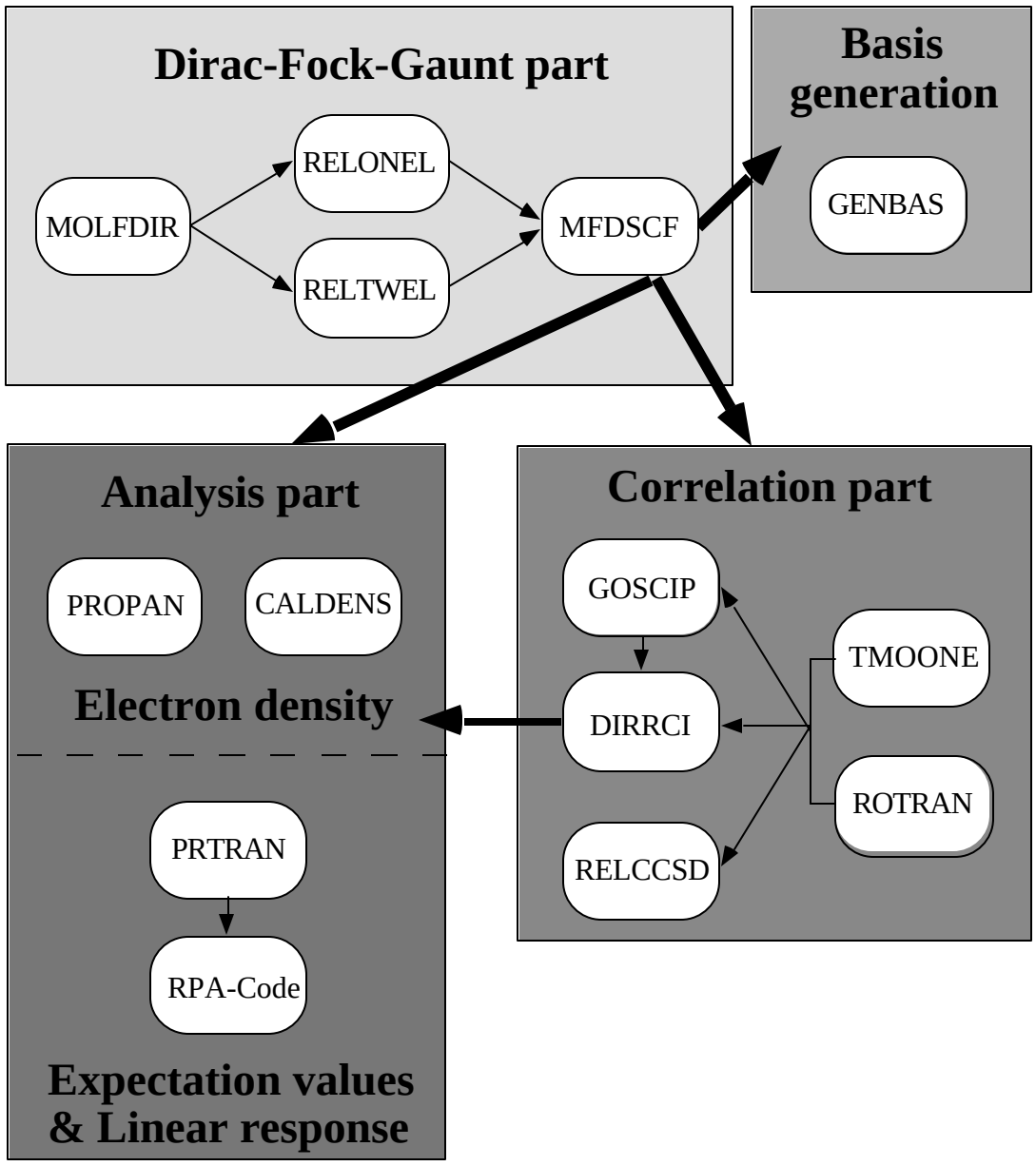

Figure 2.2. Graphical overview of the MOLFDIR program package

Table 2.1. Overview functionality modules in MOLFDIR.

Program section	Module	Function
Dirac-Fock-Gaunt	MOLFDIR	Generation of double group symmetry adapted basis functions
	RELONEL	Generation of all required 1-electron integrals
	RELTWEL	Generation of all required 2-electron integrals
	MFDSCF	Solves open or closed shell DHF equations
Correlation	TMOONE	Generates effective 1-electron molecular integrals
	ROTRAN	Generates 2-electron molecular integrals
	GOSCIP	Solves full CI equation for a small set of spinors
	DIRRCI	Solves RASCI type equations
	RELCCSD[86]	Solves CCSD -T/+T/(T) equations
Analysis	PROPAN	Spinor analysis using the Mulliken[97] scheme
	CALDENS	Generates for a set of spinors the electron density on grid
	PRTRAN	Calculates expectation values and generates molecular property integrals
	RPA-code	Solves linear response equations within RPA
Basis set generation	GENBAS	Generates general contracted basis sets using the atomic and/or kinetic balance procedure

2.4 Approximations within the 4-component approach

In the four-component Dirac-Hartree-Fock-Gaunt formalism there are four classes of integrals labelled with L for a large and S for a small component basis function. The (LL|LL), (LL|SS) and (SS|SS) classes are used for the description of the Coulomb interaction whereas the (SL|SL) class occurs in the Gaunt term. For most molecular systems the Gaunt term will have a small effect on molecular valence properties, like bond lengths and excitation energies, and therefore it is often neglected.

Of the three classes that are left the number of (SS|SS) integrals is around 70% of the total amount of integrals that has to be calculated. A large speed-up of the DHF calculations would be found if we could perform our calculations without this large set of integrals. The (SS|SS) class of integrals arises from the small component part of the wave function and contributes formally to order α^4 to the electronic energy. Although the contribution of these integrals is formally small they still have a significant effect on the molecular properties like the bond length, vibrational frequency and dissociation energy if they are just left out of the calculation. The reason for this is that we neglect electronic repulsion energy

between the small component densities which are build up from the (SS|SS) class of integrals. We can try to define a correction procedure for the missing (SS|SS) class of integrals by analyzing the one-center and a multi-center contribution of these integrals to the electronic energy[100,101]. The one-center contribution has a large energy contribution but is essentially the same as in an atom and will not influence the shape of the potential energy surface. This contribution, which is not distance dependent, can therefore easily be obtained as the difference between an atomic calculation with or without the (SS|SS) class of integrals. The multi-center contribution consists of a Coulomb and Exchange contribution. However, the small component densities are highly localized close to their respective nuclei and will have an almost zero overlap. Therefore we can neglect the Exchange contribution and approximate the multi-center contribution by a Coulombic repulsion between the small component densities. We have chosen to represent this contribution as a Coulomb repulsion between the small component charges on the respective nuclei

$$E_{Corrected} = E_{without(SS|SS)} + \sum_{A<B} \frac{q_{sA} q_{sB}}{r_{AB}} \qquad (2.45)$$

where q_{sA} the total charge associated with the small components of the spinors of atom A. The approximation is called "Simple Coulomb Correction" or SCC.
The values for q_{sA} can be obtained from atomic DHF or numerical atomic calculations. As an example we will present some results of calculations on the iodine molecule. For the iodine atom a charge of 0.1895 electrons is found in an atomic DHF calculation. We have checked this approach by calculating the charge associated with the small components of the molecular spinors obtained at the end of the DHF process.

Table 2.2. Comparison of full calculation with a calculations with (SS|SS) integrals omitted and a SCC corrected calculation.

Method	DHF		MP2		CCSD(T)	
	r_e (Å)	ω_e (cm^{-1})	r_e (Å)	ω_e (cm^{-1})	r_e (Å)	ω_e (cm^{-1})
Full with 5s, 5p	2.682	228.6	2.688	221.1	2.717	205.8
Without (SS|SS)	2.676	230.7	2.682	223.5	2.710	208.4
SCC	2.682	228.5	2.688	221.1	2.717	205.7
Full with 4d, 5s, 5p	---	---	2.667	227.0	2.699	210.5
Without (SS|SS)	---	---	2.661	229.3	2.692	213.4
SCC	---	---	2.667	227.0	2.699	210.8

This charge was indeed found to be equal to the atomic value of 0.1895 electrons confirming the locality of the small component density. Numerical data, from calculations on the iodine molecule, substantiating the above are displayed in table 2.2.

For the ground state of iodine eight points of the potential energy curve are calculated. In the SCC calculations the (SS|SS) class of integrals is neglected. This leads to a 74% reduction in the number of integrals that need to be calculated, handled and stored to disk. An overall CPU-time reduction of 67% is found for correlated calculations. The largest reductions are found for the DHF step, which now only has to handle 26% of the integrals per iteration (compared to the calculation with the (SS|SS) class of integrals), and the four-index integral transformation. Correlation is introduced using the MP2, the CCSD and the CCSD(T) method. Two different sets of correlation calculations are performed, the first includes the 5s, 5p and the full virtual space and the second also contains the 4d spinors. The SCC results and the calculations with a full set of integrals are in close agreement.

A more extensive discussion of the SCC approximation including a larger series of test calculations can be found in reference 101.

Chapter 3

Copper Halides

In this chapter the excited states of the copper halides CuCl, CuBr and CuI are investigated within the presented relativistic framework. The so-called ionic excited states are best described by starting from the states arising from a $Cu^+(3d^9 4s^1)$ $X^-(ns^2np^6)$ configuration. In particular the spin-orbit splittings that arise from the $Cu^+(3d^9 4s^1)$ configuration can clearly be recognized throughout the whole copper halide series, although a considerable mixing occurs due to spin-orbit interaction. Spin-orbit splittings in the so-called neutral states, arising from the $Cu(3d^{10} 4s^1)$ $X(ns^2np^5)$ configuration, are caused by the splitting in the halide atoms $X(np^5)$ and lead to a reordering of certain states going from CuCl to CuI. The neutral states, however, are found well above the ionic states. These findings are in contrast with allocations in CuI from previous theoretical work.

3.1 Introduction

Our interest concerns the properties of CuCl, CuBr and CuI in the solid state. Changes in the ionization spectra along the series CuCl, CuBr to CuI have been ascribed to a substantial increase of covalency in these compounds[102]. If such an increase in covalency occurs, one would expect to find a similar increase already in the diatomic molecules. Ramírez-Solís[103] performed calculations, in which relativistic effects were included, on the CuF, CuCl and the CuI molecule and they found a small increase in covalency. Extensive non-relativistic calculations performed by Sousa *et al.* [104,105], however, reveal a slight increase in covalency as might be expected, but not nearly enough to explain the trends in the ionization spectra. We therefore performed fully relativistic calculations to examine the influence of relativity on the relative positions of the neutral and ionic states.

There are many experimental spectra available for the ionic states of the copper halides. The spectra of the lightest halide, CuF, can be fully understood on basis of experimental[106-109] and theoretical work[110-114]. And although some of the bands in the spectra of the heavier halides could be assigned to particular

excitations, there is no consensus on the interpretation of these spectra. In more recent work Delaval *et al.* [107,115,116] measured, from fluorescence decay, radiative lifetimes of the excited states of CuCl, CuBr and CuI thus allowing insight in the singlet and triplet character of the states. The measured transitions are between the ground state X $^1\Sigma^+$, coming from the configuration $Cu^+(3d^{10})$ $X^-(ns^2np^6)$, and the ionic excited states from the configuration $Cu^+(3d^94s^1)$ $X^-(ns^2np^6)$. Here X is the respective halide and n the principle quantum number of the valence shell, i.e. 3 for Cl, 4 for Br and 5 for I.

Some theoretical work has been done for the excited states of the CuCl molecule but there is hardly any theoretical data available on the excited states of CuBr and CuI. Nguyen *et al.* [112] studied the ground state and low-lying excited states of CuCl using SCF calculations and subsequent Møller-Plesset perturbation theory. Ramírez-Solís *et al.* [117] performed MCSCF calculations and subsequent MRCI calculations on CuCl and included scalar relativistic effects. Winter and Huestis[118] performed SCF calculations on the CuCl molecule and included spin-orbit interaction semi-empirically using an atoms-in-molecules technique. Ramírez-Solís *et al.* [119] also performed MCSCF calculations and MRCI calculations on the CuI molecule and including scalar relativistic and spin-orbit effects. In these calculations the neutral states, arising form the $Cu(3d^{10}4s^1)$ $X(ns^2np^5)$ configuration, appear in the same energy region as the ionic states, even without the inclusion of spin-orbit interaction. Our calculations on the ionic states will be used to discuss the assignment of the measured bands.

3.2 Computational model

In the calculation of the excitation spectra the experimental equilibrium distances[120] are used of the respective molecules, 3.878 Bohr for CuCl, 4.107 Bohr for CuBr and 4.419 Bohr for CuI. A standard Gaussian distribution (see chapter 2.2.2) is used to represent the spatial extent of the nuclei in both the relativistic and non-relativistic calculations. C_{4v}^* double group symmetry is used in the calculations.

To start the relativistic calculations we optimized the primitive basis set exponents of Cu within the Dirac-Hartree-Fock formalism using GRASP[19]. The small component basis is related to the large component by kinetic balance. Subsequently an atomic balance procedure is used to generate a contracted basis set for use in the molecule.

Table 3.1. Basis set size for copper.

	Large Component		Small Component	
	Uncontracted	Contracted	Uncontracted	Contracted
Non-relativistic	21s16p10d3f	7s6p5d3f	--	--
Relativistic	21s16p10d3f	7s9p6d3f	16s31p16d10f3g	7s12p9d6f3g

The size of the basis set for Cu is described in table 3.1 and its primitive exponents are listed in appendix I. The basis sets of Cl, Br and I are described in chapter 4 where we present results of calculations on interhalogens.

For the ionic excited states, arising from a $Cu^+(3d^9 4s^1)$ $X^-(ns^2np^6)$ configuration, the basis of spinors is optimized for the weighted average of all states[121] derived from the basic configuration $Cu^{2+}(3d^9)$ $X^-(np^6)$ of the CuX^+ ionized systems. Subsequently, a CI is performed in which all states arising from a $Cu^+(3d^9 4s^1)$ $X^-(ns^2np^6)$ configuration are included. For the neutral states, coming from a $Cu(3d^{10}4s^1)$ $X(ns^2np^5)$ configuration, the basis of spinors is optimized for the $Cu^+(3d^{10})$ $X(np^5)$ configuration and followed by a CI calculation including all states based on the $Cu(3d^{10}4s^1)$ $X(ns^2np^5)$ configuration. In both cases the spinors are optimized without including the $Cu(4s^1)$. Including the 4s introduces two open shells of the same symmetry. This cannot be handled yet in the present version of the MOLFDIR program package. However, in our calculations the Cu 4s virtual is rather localized and we expected the spinors to give a reasonable description of the relative energies of the ionic and neutral excited states.

In non-relativistic calculations we can assign the molecular states using Λ–Σ coupling. In our relativistic calculations we work with intermediate coupling so only the ω and Ω quantum numbers apply. To connect to previous discussions on the assignment of states we have analyzed the calculated states in terms of Ω components of Λ–Σ states. This analysis is facilitated by comparing with a non-relativistic calculation in a two-component spinor basis (using the non-relativistic option of MOLFDIR). We analyze which Ω components of the Λ–Σ states contribute to a particular relativistic state by comparing the determinantal compositions of the (non-relativistic) Λ–Σ states, which are also calculated in double group symmetry, with those of the relativistic Ω states. The molecular states are then labelled on the basis of the dominant Λ–Σ state.

3.3 Ionic states

The ionic states we consider are those that arise from the $Cu^+(3d^9 4s^1)$ $X^-(ns^2np^6)$ configuration. For these states the halogen is closed shell and spin-orbit coupling will arise basically from the atomic $Cu^+(3d^9 4s^1)$ splitting (into $^3D_3$, $^3D_2$ and $^3D_1$) which is about 2000 cm^{-1}. This effect, however, is expected to be the same for all three species. However, besides the splitting of the d-orbitals there is also an spin-orbit interaction between states of the same Ω symmetry which allows them to mix. Both spin-orbit effects are implicitly included in our calculations.

In order to get a correct offset for comparison with previous, non-relativistic calculations by Sousa *et al.* [104] we performed a non-relativistic calculation with MOLFDIR. Our non-relativistic results, denoted with HF / CI, presented in table 3.2 are in reasonable agreement with the CASSCF results of Sousa *et al.* The width of the calculated spectrum is somewhat smaller than what is found in CASSCF calculations and there is a small deviation in the relative positions of the Δ states relative to the Σ and Π states, but the singlet-triplet splittings show a close agreement with those of a CASSCF. We find the singlet-triplet splitting of the Σ state to be slightly smaller. The differences can be explained by the

following factors. Firstly, the Cu 4s is not included in our HF calculation which will have some effect on the form of the generated orbitals. Secondly, we use orbitals averaged over all states whereas the orbitals in a CASSCF are state optimized. Also in the CASSCF a larger orbital space, two sets of d-orbitals plus the 4s orbital are included, is used. A smaller CASSCF space gives a singlet-triplet splitting which is comparable to our results[122]. So the discrepancies between the two non-relativistic methods can be accounted for, and as long as singlet-triplet splittings are concerned the non-relativistic starting point is accurate enough for later comparisons.

Table 3.2. Relative energies (in cm^{-1}) of the lowest ionic excited states obtained from a non-relativistic calculation. The CI expansions include all states derived from $Cu^{+}(3d^{9}4s^{1})$ $X^{-}(np^{6})$. The singlet-triplet splitting is given in parenthesis.

Molecule	State	HF / CI		CASSCF[104]	
CuCl	$^3\Sigma^+$	0		0	
	$^3\Pi$	1187		1580	
	$^3\Delta$	3098		3777	
	$^1\Sigma^+$	3623	(3623)	4020	(4020)
	$^1\Pi$	3897	(2710)	4305	(2725)
	$^1\Delta$	5013	(1915)	5849	(2072)
CuBr	$^3\Sigma^+$	0		0	
	$^3\Pi$	815		1212	
	$^3\Delta$	2310		3058	
	$^1\Sigma^+$	3402	(3402)	3733	(3733)
	$^1\Pi$	3447	(2632)	3902	(2690)
	$^1\Delta$	4127	(1817)	5066	(2008)
CuI	$^3\Sigma^+$	0		0	
	$^3\Pi$	508		872	
	$^3\Delta$	1525		2279	
	$^1\Sigma^+$	3060	(3060)	3395	(3395)
	$^1\Pi$	3113	(2605)	3504	(2632)
	$^1\Delta$	3213	(1688)	4175	(1896)

We will now turn to the relativistic results and compare them with experimental results. In table 3.3 the results of the relativistic calculations, denoted with DHF / CI, are presented and compared with experimental and other theoretical work. In table 3.4 the spin-orbit induced mixing of the states is given.

Table 3.3. Relative energies (in cm^{-1}) of the lowest ionic excited states obtained from a relativistic calculation compared with experiment. The CI expansions include all states derived from $Cu^{+}(3d^{9}4s^{1})$ $X^{-}(np^{6})$. The triplet and singlet components of Π_1 and of Δ_2 are mixed and denoted with ^{3,1} or ^{1,3}. Experimental values in parenthesis have not been assigned. The assignment of Lefebvre *et al.* [116] and Delaval *et al.* [115] is given instead. The experimental error bounds are smaller than 25 cm^{-1}.

Molecule	State	DHF / CI	Experiment[107,115,116,123]
CuCl	$^{3}\Sigma_{0^-}^{+}$	0	
	$^{3}\Sigma_{1}^{+}$	97	0
	$^{3}\Pi_2$	943	
	$^{3,1}\Pi_1$	1575	1451
	$^{3}\Pi_{0^+}$	1616	1613
	$^{3}\Pi_{0^-}$	2514	
	$^{3}\Delta_3$	2579	
	$^{3,1}\Delta_2$	3180	
	$^{3}\Delta_1$	4085	(6291)
	$^{1}\Sigma_{0^+}^{+}$	4823	4032
	$^{1,3}\Pi_1$	5035	(3952)
	$^{1,3}\Delta_2$	5880	
CuBr	$^{3}\Sigma_{0^-}^{+}$	0	
	$^{3}\Sigma_{1}^{+}$	94	0
	$^{3}\Pi_2$	649	
	$^{3,1}\Pi_1$	1344	669
	$^{3}\Pi_{0^+}$	1338	
	$^{3}\Pi_{0^-}$	2362	3209
	$^{3}\Delta_3$	1915	
	$^{3,1}\Delta_2$	2510	
	$^{3}\Delta_1$	3556	3632
	$^{1}\Sigma_{0^+}^{+}$	4687	
	$^{1,3}\Pi_1$	4599	5087
	$^{1,3}\Delta_2$	5127	

Table 3.3. Continued

Molecule	State	DHF / CI	Experiment[107,115,116,123]
CuI	$^3\Sigma_{0^-}^+$	0	
	$^3\Sigma_1^+$	76	0
	$^3\Pi_2$	386	
	$^{3,1}\Pi_1$	1152	
	$^3\Pi_{0^+}$	1087	2133
	$^3\Pi_{0^-}$	2283	
	$^3\Delta_3$	1232	
	$^{3,1}\Delta_2$	1812	
	$^3\Delta_1$	3002	
	$^1\Sigma_{0^+}^+$	4501	4266
	$^{1,3}\Pi_1$	4196	(3223)
	$^{1,3}\Delta_2$	4300	

Table 3.4. Mixing of the ionic states as a result of spin-orbit coupling. The triplet and singlet component of Π_1 and of Δ_2 are mixed and denoted with ^{3,1} or ^{1,3}.

State	CuCl	CuBr	CuI
$^3\Sigma_{0^-}^+$	6% $^3\Pi_{0^-}$	10% $^3\Pi_{0^-}$	15% $^3\Pi_{0^-}$
$^3\Sigma_1^+$	9% $^{3,1}\Pi_1$	16% $^{3,1}\Pi_1$	27% $^{3,1}\Pi_1$
$^3\Pi_2$	1% $^{3,1}\Delta_2$	2% $^{3,1}\Delta_2$	3% $^{3,1}\Delta_2$
$^{3,1}\Pi_1$	9% $^3\Sigma_1$+1% $^{3,1}\Delta_1$	15% $^3\Sigma_1$+2% $^{3,1}\Delta_1$	25% $^3\Sigma_1$+5% $^{3,1}\Delta_1$
$^3\Pi_{0^+}$	29% $^1\Sigma_{0^+}^+$	30% $^1\Sigma_{0^+}^+$	32% $^1\Sigma_{0^+}^+$
$^3\Pi_{0^-}$	6% $^3\Sigma_{0^-}^+$	10% $^3\Sigma_{0^-}^+$	15% $^3\Sigma_{0^-}^+$
$^3\Delta_3$	--	--	--
$^{3,1}\Delta_2$	1% $^3\Pi_2$	2% $^3\Pi_2$	3% $^3\Pi_2$
$^3\Delta_1$	48% $^{1,3}\Pi_1$	35% $^{1,3}\Pi_1$+1% $^3\Sigma_1^+$	26% $^{1,3}\Pi_1$+1% $^3\Sigma_1^+$
$^1\Sigma_{0^+}^+$	29% $^3\Pi_{0^+}$	30% $^3\Pi_{0^+}$	32% $^3\Pi_{0^+}$
$^{1,3}\Pi_1$	47% $^3\Delta_1$	30% $^3\Delta_1$	23% $^3\Delta_1$
$^{1,3}\Delta_2$	--	--	--

Most of the states can still be directly related to the corresponding non-relativistic state. However, in relativistic theory the spin- and angular momenta are coupled and therefore we cannot distinguish between the singlet and triplet states of the Π_1 and the Δ_2 by mere labelling. Therefore ^{3,1} (and ^{1,3}) is used as a superscript for the spin.

In all three molecules a small spin-orbit splitting, of less than 100 cm^{-1}, is found for the $^3\Sigma^+$ states. The splitting in $^3\Pi$ increases slightly going from CuCl to CuI, being 1571 cm^{-1} for CuCl, 1713 cm^{-1} for CuBr and 1897 cm^{-1} for CuI. Non-relativistically the $^3\Pi$ and the $^3\Sigma^+$ states lie closer together going from CuCl to CuI and leads to an increased mixing of the $^3\Pi_{0^-}$ and the $^3\Sigma^+_{0^-}$ state shifting the $^3\Pi_{0^-}$ state up relative to the other $^3\Pi$ states. The relative position of the $^3\Pi_{0^+}$ state is affected by a mixing with the $^1\Sigma^+_{0^+}$ state. This mixing is similar in all three molecules. For the $^3\Delta$ splitting we also see an increase, from 1506 cm^{-1} for CuCl, 1641 cm^{-1} for CuBr to 1770 cm^{-1} for CuI. Here the $^3\Delta$ and $^1\Pi$ state, non-relativistically, have an increasing separation when going from CuCl to CuI leading to a smaller mixing between the $^3\Delta_1$ and the $^{1,3}\Pi_1$ state. In CuCl the $^3\Delta_1$ shifts towards the other $^3\Delta$ states whereas this shift becomes smaller in the CuI molecule. The mixing due to spin-orbit coupling will also affect the relative position of the $^1\Sigma^+_{0^+}$ and $^{1,3}\Pi_1$ states in the spectrum. The $^{1,3}\Pi_1$ state becomes around 1100 cm^{-1} higher for all molecules whereas the $^1\Sigma^+_{0^+}$ state shifts up between 1200 and 1450 cm^{-1}, relative to the non-relativistic results.

The transition energies and radiative lifetimes of the low-lying states in CuCl molecule have been measured and assigned by Delaval *et al.* [107,115]. A theoretical study was performed by Winter and Huestis[118] who suggest a different assignment of the measured states, compared to Delaval *et al*. The results of Winter *et al*. are in fact in close agreement with our results except for the $^1\Sigma^+_{0^+}$ state which lies 900 cm^{-1} higher in our case. They find, however, a reversed ordering of the two spin-orbit components of the $^3\Sigma^+$. A similar relativistic mixing of states is found in both calculations.

For the CuBr molecule we can compare our results with the experimental data of Lefebvre *et al.* [116] and Kowalczyk *et al.* [123]. The lowest state, on 19820 cm^{-1} relative to the ground state X $^1\Sigma^+_{0^+}$, was measured by Kowalczyk *et al.* and assigned to a $^3\Sigma^+_1$ which was later confirmed by rotational analysis[124]. Surprising is the short lifetime (12 μs) compared to the lifetime of this state in CuCl (60 μs). This is probably due to the increased mixing of the $^3\Sigma^+_1$ with the $^{3,1}\Pi_1$ compared to CuCl. Lefebvre *et al.* measured the transitions and lifetimes of four other bands. The bands at 20489 cm^{-1} and 23452 cm^{-1} are assigned to a $^{3,1}\Pi_1$ and a $^1\Sigma^+_{0^+}$ respectively, based on their lifetimes. Experimentally the $^{3,1}\Pi_1$ state lies 669 cm^{-1} above the $^3\Sigma^+_1$ whereas we find a splitting that is twice as large. Non-dynamical correlation effects due to charge transfer will reduce this calculated splitting[104].

A theoretical study on the CuI molecule was performed by Ramírez-Solís *et al.* [119] and experimental excitation energies and lifetimes of four bands were measured by Lefebvre *et al.* [116]. Lefebvre *et al.* did

not assign the lower two bands appearing at 19734 and 21867 cm^{-1} although they were able to determine the spin-orbit components of both which are Ω=1 and Ω=0 respectively, and the lifetimes 1.9 and 1.0 μs respectively. Ramírez-Solís *et al.* assigned these states to a mixture of singlet and triplet Π neutral states, arising from the Cu($3d^{10}4s^1$) X(ns^2np^5) configuration, and the second arises mainly from the Ω=0 component of the ionic $^3\Sigma^+$ state with a mixture of the $^1\Sigma^+$ state. The neutral states, however, lie much higher in energy as will be shown in section 3.4. We therefore assign the measured bands to states arising from the ionic configuration. We confirm the assignment of the $^1S^+_{0^+}$ at 24002 cm^{-1}. Assuming that the spin-orbit components of the two unidentified bands are indeed Ω=1 and Ω=0, the lower experimental band can be assigned to the Ω=1 component of the $^3\Sigma^+$ state. The second band, with spin-orbit component Ω=0, could be assigned to a $^3\Pi$ state which presents a mixture with a $^1\Sigma^+$ state and that can explain the low lifetime, 1.0 μs.

Up to now we have not discussed the assignment of the $^3\Delta_1$ and the $^{1,3}\Pi_1$ state. In CuCl the $^3\Delta$ states appear too low in energy in comparison with the assignment of the experimental results by Delaval et al[107,115]. Our calculations and those of Winter and Huestis[118] place these $^3\Delta$ states in the lower part of the spectrum. A strong mixing between the highest two Ω=1 states $^3\Delta_1$ and $^{1,3}\Pi_1$ is found in our relativistic calculations which can explain the large value of the transition dipole moment found for the pure $^1\Pi$ electronic state in comparison with experiment[104].

For the CuBr molecule Lefebvre *et al.* [116] find two Ω=1 states at 23029 cm^{-1} and 24907 cm^{-1} of which the lower was assigned to a $^1\Pi_1$ based on the short lifetime. The short lifetime also implies that this state has dominantly singlet character. Our calculations suggest that these two states are heavily mixed and that the lower Ω=1 state has mainly $^3\Delta_1$ character whereas the other is dominantly $^1\Pi_1$.

In CuI the band at 22957 cm^{-1} was assigned to a $^1\Pi_1$ by Lefebvre *et al.* [116]. Our calculations again would suggest this state to be dominantly $^3\Delta_1$.

In all our calculations we find the $^3\Delta_1$ below the $^1\Pi_1$ suggesting an opposite ordering compared to the experimental assignments. However, the relative positions of the final states strongly depends on the ordering and the magnitude of the energy differences between the two electronic states at the non-relativistic level. If the states lie close together a large mixing will be found whereas the dominant contribution to the character of the final states dependents on the relative ordering of the $^3\Delta$ and the $^1\Pi$. Extensive correlation calculations of Sousa *et al.* [104] show that charge-transfer effects can bring the $^1\Pi$ below the $^3\Delta$, which is the opposite of what is found by us and by Winter *et al.* [118]. We have not included these correlation effects in our calculations and therefore cannot give a definite conclusion on the ordering and mixing of these two states. In the future extensive electron correlation calculations should be performed to elucidate the influence of change-transfer effects on the ordering of the $^3\Delta$ and $^1\Pi$ states.

3.4 Neutral states

The neutral states come from the Cu($3d^{10}4s^1$) X(ns^2np^5) configuration. Here the halogen is formally an open shell, in contrast to the ionic excited states, hence the spin-orbit effects arise from the halogen. In the case of ionic excited states the spin-orbit effects are constant, arising

Table 3.5. Energies (in cm^{-1}), relative to the ionic $^3\Sigma^+$ (and $^3\Sigma^+_{0^-}$) state, of the lowest neutral states obtained from non-relativistic and relativistic calculations. The CI expansions include all states derived from Cu($3d^{10}4s^1$) X(np^5). The triplet and singlet components of the Π_1 are mixed and denoted with ^{3,1} or ^{1,3}.

Molecule	Non-relativistic			Relativistic	
	State	HF / CI	CASSCF[104]	State	DHF / CI
CuCl	$^3\Pi$	24645	25604	$^3\Pi_2$	27241
				$^{3,1}\Pi_1$	27482
				$^3\Pi_{0-}$	27941
				$^3\Pi_{0+}$	27950
	$^1\Pi$	25568	26790	$^{1,3}\Pi_1$	28700
	$^3\Sigma^+$	27380	30422	$_3\Sigma^+_{0^-}$	30313
				$_3\Sigma^+_1$	30318
	$^1\Sigma^+$	31585	36186	$_1\Sigma^+_{0^+}$	35008
CuBr	$^3\Pi$	20572	21822	$^3\Pi_2$	22266
				$^{3,1}\Pi_1$	22658
				$^3\Pi_{0-}$	24118
				$^3\Pi_{0+}$	24571
	$^1\Pi$	21515	23013	$^{1,3}\Pi_1$	24628
	$^3\Sigma^+$	24231	26123	$_3\Sigma^+_{0^-}$	27879
				$_3\Sigma^+_1$	27997
	$^1\Sigma^+$	28833	31975	$_1\Sigma^+_{0^+}$	32674
CuI	$^3\Pi$	16672	17677	$^3\Pi_2$	16103
				$^{3,1}\Pi_1$	16559
				$^3\Pi_{0-}$	18755
				$^3\Pi_{0+}$	20286
	$^1\Pi$	17685	18930	$^{1,3}\Pi_1$	19143
	$^3\Sigma^+$	21265	20889	$_3\Sigma^+_{0^-}$	25693
				$_3\Sigma^+_1$	25926
	$^1\Sigma^+$	25952	26684	$_1\Sigma^+_{0^+}$	30146

from the Cu atom, but here the spin-orbit effect rapidly increases with the atomic number of the halogen. The atomic spin-orbit splittings are 874, 3758 and 7603 cm^{-1} for Cl, Br and I respectively. Thus, in the neutral states the diagonal spin-orbit coupling can already have an important effect specially for the heaviest molecule CuI.

We will first compare our results with those of Sousa *et al.* [104]. A reasonable agreement is found for all the states except the $^1\Sigma^+$ states in CuCl, and in a lesser extent, in CuBr. These differences should be attributed to the different computational models used. The neutral excited states all lie far above the ionic excited states, presented in section 3.3 although a monotonic decrease of the neutral excitation energies is clearly seen. For CuI our results are in great contrast with those of Ramírez-Solís *et al.* [119] who placed the neutral Π states between the lower ionic states.

In the last two colums of table 3.5 we present the results of the relativistic calculations. The states can be related to the corresponding non-relativistic state except for the Π_1 state because we cannot distinguish between its singlet and triplet character. Just as for the ionic states we will use ^{3,1} (and ^{1,3}) as a superscript for the spin. It was found that the spin-orbit induced mixing between the Π and Σ states was small (less than 3% for all states).

The spin-orbit splitting for the $^3\Pi$ states turned out to be around 700 cm^{-1} for CuCl, 2300 cm^{-1} for CuBr and more than 4000 cm^{-1} for CuI. For CuI this leads to a reordering of the spin-orbit split Π states. If we now compare the relative energies of the neutral states to those of the ionic states then it is clear that even after inclusion of spin-orbit coupling these states lie far above in energy than the ionic states. In CuCl and CuBr the splitting between the highest ionic state and the lowest neutral state increases when relativity is included. For the CuI molecule a decrease is observed but the lowest neutral state still lies 12000 cm^{-1} above the highest ionic state. This is in contradiction with the results of calculations by Ramírez-Solís *et al.* [119]. More extensive theoretical work and experimental evidence is required to understand these discrepancies for the neutral states.

3.5 Conclusions

The lowest excited states of CuCl, CuBr and CuI have been studied by four-component calculations which account for spin-orbit coupling and scalar relativistic effects. For all molecules the lowest excited states are best described starting from the ionic $Cu^+(3d^94s^1)$ $X^-(ns^2np^6)$ configuration. The calculations show that for the ionic excited states spin-orbit coupling comes basically from the $Cu^+(3d^94s^1)$ atomic splitting. However, spin-orbit interactions do not affect the relative ordering of the low-lying ionic excited states of these molecules. The $^3\Delta_1$ and $^1\Pi_1$ state have a large spin-orbit induced mixing which is strongly dependent on the relative positions of these states. Sousa *et al.* [104] showed that charge-transfer correlation effects can lead to a reordering of these two states. This will also give an opposite assignment compared to what is found in the calculations presented here.

The neutral excited states, arising form the configuration $Cu(3d^{10}4s^1)$ $X(ns^2np^5)$, lie far above the ionic states. For these states spin-orbit coupling has been shown to be important, specially for CuI where the

spin-orbit splitting due to the $^3\Pi$ neutral states is around 4000 cm^{-1}. In the case of CuI it even leads to a different ordering of the states, compared to the ones of CuCl and CuBr. Nevertheless, even after inclusion of spin-orbit coupling these states appear much higher in energy than the ionic states. This result is in contradiction with previous theoretical results of Ramírez-Solís *et al.* [119]. Based on our calculations, the lowest two bands of the CuI spectrum can be assigned to the Ω=1 spin-orbit component of the $^3\Sigma^+$ state and to the Ω=0 component of the ionic $^3\Pi$ state respectively.

Chapter 4

Interhalogens

In this chapter the effect of relativity on the properties of the interhalogens ClF, BrF, BrCl, IF, IBr and IBr is studied by comparing relativistic and non-relativistic calculations. Bond lengths, harmonic frequencies and dissociation energies show that the bond is weakened in the relativistic formalism. Relativity increases the electric dipole moment whereas the electric quadrupole moment and dipole polarizability display an irregular behaviour. The relativistic contributions to the electric dipole and quadrupole moment of the iodine containing molecules are 10-20% of the total value whereas the contributions in the other molecules cannot be neglected. The value of the electric quadrupole moment is dominated by the relativistic contributions.

4.1 Introduction

In two previous papers[125,126], hereafter called paper I and paper II, the influence of relativity and correlation effects on spectroscopic constants in the series X_2 and HX (with X = F, Cl, Br, I, At) were studied. The methods used were Hartree-Fock (HF), second order Møller-Plesset perturbation theory (MP2), Configuration Interaction with Single and Double excitations (CISD), Coupled Cluster with Single and Double excitations (CCSD) and the latter method perturbatively corrected for the effect of triple excitations (CCSD(T)). This gives a range of correlation treatments, from no electron correlation in the HF method to a fairly high level of correlation in the CCSD(T) method.

In this paper we complete the previous work with a study on the spectroscopic properties of the interhalogen series XY (with X = F, Cl, Br, I). The influence of relativity and correlation on the spectroscopic properties are investigated at the correlated levels MP2, CCSD and CCSD(T). Hardly any previous theoretical work is available on the spectroscopic properties, but much theoretical work has been done on the electric dipole moments. In these calculations relativistic effects were disregarded or approximated neglecting the spin-orbit interaction. Here we study the relativistic effects on the

electric dipole and quadrupole moments and the dipole polarizability within a fully relativistic framework. Correlation effects for these properties are estimated by means of CISD calculations.

4.2 Computational model

All calculations on the spectroscopic properties are performed using MOLFDIR. The property integrals needed to calculate the expectation values of the electric properties are obtained from the HERMIT[95] part of the DIRAC[91] program. The dipole polarizibility is evaluated as a response property using the propagator method[92] within the Random Phase Approxima-tion[41,93]. A gaussian distribution is used to represent the spatial extent of the nucleus in both the relativistic and the non-relativistic calculations (for the exponents see Table I of paper II). The speed of light is taken to be 137.0359895 au. Basis sets for the halogens are described in paper II and will be denoted by apVDZ and apVTZ.

In the MP2, CC and CISD calculations the halogens are treated as 7 valence electron atoms, correlating only the valence s- and p-electrons. In the correlated calculations of the spectroscopic properties the highest virtuals (with energies above 10 atomic units) are left out. In the CISD calculations on the electric properties all virtuals are included.

All molecular calculations are performed using C_{4v} symmetry. The atomic calculations are carried out in O_h. To prevent spurious discrepancies between the non-relativistic and relativistic dissociation energies, we calculate both the non-relativistic and the relativistic atomic asymptotes in a basis of spinors optimized for the average energy of the $5p_{1/2})^2\ 5p_{3/2})^3$ configuration.

Spectroscopic constants are obtained by fitting the potential energy curves to a 4^{th} order polynomial in the internuclear distance. The electric properties are calculated at the experimental bond length. The quadrupole moment is computed relative to the center of mass of the molecule (considered for this purpose as two spherical symmetric atoms, separated by the equilibrium bond distance) using the masses 18.99840, 34.96885, 78.91834 and 126.90448 au. from Ref. 127 for F, Cl, Br and I, respectively.

We calculate the electric properties as an expectation value of the CISD wave function. Since the Hellmann-Feynman[128,129] theorem is not fullfilled[130,131] in a CISD calculation our results will differ from a more rigorous energy derivative formulation. Kucharski *et al.* [132] compared these two approaches and found only small differences for the dipole moment of IF calculated with the MBPT(4) method.

4.3 Spectroscopic properties

The calculated spectroscopic properties for the six interhalogen molecules ClF, BrF, BrCl, IF, ICl and IBr are presented in table 4.1-4.6 whereas the relativistic effects, defined as x(relativistic) - x(non-relativistic), on these properties are summarized in table 4.7.

The dissociation energy (D_e) shows a relativistic decrease for all interhalogen molecules. This decrease, arising from the spin-orbit coupling in the valence p-shell, is also seen in the homonuclear diatomic molecules (see paper I). In these molecules the molecular spin-orbit coupling is almost completely quenched for elements up to iodine, while the atomic asymptotes are lowered for each atom by 1/3 of

the ^2P atomic ground state splitting. Assuming complete quenching in the present series of molecules gives an estimated SO-effect (hereafter called ASO-only and given in table 4.7) on the D_e of 1/3 of the atomic spin-orbit splitting from both atoms.

Relativity destabilizes the molecular bond leading to a longer equilibrium bond length (r_e) and a decrease of the harmonic frequencies (ω_e). This destabilization can be understood by looking at the molecular orbital formation by the valence p orbitals. The six atomic valence p orbitals combine to anti-bonding and bonding or molecular spin orbitals which can be labelled as $\sigma_{1/2}$, $\pi_{1/2}$, $\pi_{3/2}$, $\pi_{1/2}^*$, $\pi_{3/2}^*$, $\sigma_{1/2}^*$. Spin-orbit coupling lifts the degeneracy of the π-orbitals introducing σ-character in the $\pi_{1/2}$ and $\pi_{1/2}^*$. The weakening of the chemical bond is caused by the introduction of anti-bonding character from the unoccupied $\sigma_{1/2}^*$ into the bonding $\pi_{1/2}$ orbital.

The size of the relativistic effects is similar to that in the homonuclear diatomics in paper I. The magnitude of the Gaunt interaction correction for the interhalogens is small which suggests that higher-order two-electron relativistic effects will be small as well.

We will now compare our results with experimental data after which a comparison will be made with the few available theoretical results. Our r_e are longer than the experimental values, varying from less then 0.01 Å for the lighter to 0.05 Å for the heaviest molecules. The errors in the ω_e are generally smaller than 10 cm^{-1}. The D_e values are systematically too low by 5 kcal/mol. However, for the iodine molecule we have shown[133] that extensive core-valence correlation and the addition of a g-type basis function reduces the r_e with around 0.04 Å and increases the ω_e and D_e with 10 cm^{-1} and 5.5 kcal/mol respectively.

There are hardly any theoretical results available for the spectroscopic properties of the interhalogens. Straub and McLean[134] performed a systematic study on these molecules at the Hartree-Fock level within the non-relativistic framework. Their findings are in close agreement with our non-relativistic NR-HF results, except for IBr where they had to use a basis set of lower quality due to the limited computational resources at the time.

For the ClF molecule we can compare our results with other theoretical work, the CISD+Q calculations of Pettersson *et al.* [135] and the CPF calculations of Scharf and Ahlrichs[136], both in a non-relativistic framework. The results in these papers agree very well with our non-relativistic correlated work. Balasubramanian[137] calculated the ICl molecule using averaged relativistic effective potentials (AREP), followed by CI calculations to include spin-orbit effects. We find large discrepancies between his results and the ones presented here.

Table 4.1. Properties of ClF calculated at various levels of theory.

	r_e (Å)		ω_e (cm^{-1})		D_e (kcal mol^{-1})	
Method	apVDZ	apVTZ	apVDZ	apVTZ	apVDZ	apVTZ
NR-HF	1.619	1.590	907	918	10.5	17.1
DC-HF	1.620	1.590	905	915	9.0	15.2
DC-HF+G		1.590		915		15.2
NR-MP2	1.676	1.637	780	809	57.3	68.1
DC-MP2	1.677	1.637	780	808	55.9	66.4
NR-CCSD	1.674	1.632	782	814	48.6	56.1
DC-CCSD	1.674	1.633	783	814	47.3	54.7
NR-CCSD(T)	1.685	1.645	751	781	52.3	61.1
DC-CCSD(T)	1.685	1.645	751	780	51.0	59.4
NR-HF[15]	1.585		912			
NR-CISD+Q[135]	1.653				49.6	
NR-CPF[136]	1.636				55.3	
Experiment[120]	1.628		786		66.3	

Table 4.2. Properties of BrF calculated at various levels of theory.

	r_e (Å)		ω_e (cm^{-1})		D_e (kcal mol^{-1})	
Method	apVDZ	apVTZ	apVDZ	apVTZ	apVDZ	apVTZ
NR-HF	1.744	1.716	772	777	14.3	20.1
DC-HF	1.746	1.718	765	771	9.9	14.9
DC-HF+G		1.719		771		15.0
NR-MP2	1.797	1.759	674	699	60.7	70.1
DC-MP2	1.799	1.762	668	693	57.0	66.3
NR-CCSD	1.793	1.754	679	705	52.1	59.1
DC-CCSD	1.795	1.757	673	699	48.3	54.5
NR-CCSD(T)	1.804	1.765	655	679	55.6	63.1
DC-CCSD(T)	1.806	1.769	649	673	51.8	59.1
NR-HF[134]	1.719		770			
Experiment[120]	1.759		671		64.7	

Table 4.3. Properties of ClBr calculated at various levels of theory.

	r_e (Å)		ω_e (cm^{-1})		D_e (kcal mol^{-1})	
Method	apVDZ	apVTZ	apVDZ	apVTZ	apVDZ	apVTZ
NR-HF	2.157	2.129	466	487	18.0	26.1
DC-HF	2.157	2.130	463	483	13.4	21.1
DC-HF+G		2.131		483		21.2
NR-MP2	2.188	2.143	427	458	44.4	55.1
DC-MP2	2.189	2.144	424	455	40.3	50.9
NR-CCSD	2.202	2.156	413	446	39.9	48.1
DC-CCSD	2.203	2.157	410	443	35.8	43.2
NR-CCSD(T)	2.212	2.165	399	433	42.7	51.2
DC-CCSD(T)	2.213	2.166	395	429	38.6	46.9
NR-HF[134]	2.137		482			
Experiment[120]	2.136		444		52.1	

Table 4.4. Properties of IF calculated at various levels of theory.

	r_e (Å)		ω_e (cm^{-1})		D_e (kcal mol^{-1})	
Method	apVDZ	apVTZ	apVDZ	apVTZ	apVDZ	apVTZ
NR-HF	1.904	1.876	698	703	24.6	30.1
DC-HF	1.914	1.886	675	680	16.3	20.7
DC-HF+G		1.887		680		20.9
NR-MP2	1.954	1.916	622	645	69.2	78.1
DC-MP2	1.965	1.928	601	624	62.4	70.5
NR-CCSD	1.947	1.910	631	654	60.9	66.1
DC-CCSD	1.959	1.921	610	632	53.8	58.8
NR-CCSD(T)	1.956	1.920	613	634	64.1	70.5
DC-CCSD(T)	1.969	1.932	590	611	57.1	63.1
NR-HF[134]	1.86		711			
Experiment[120]	1.910		610		67.3	

Table 4.5. Properties of ICl calculated at various levels of theory.

	r_e (Å)		ω_e (cm^{-1})		D_e (kcal mol^{-1})	
Method	apVDZ	apVTZ	apVDZ	apVTZ	apVDZ	apVTZ
NR-HF	2.355	2.319	408	424	21.5	29.1
DC-HF	2.362	2.326	395	411	13.9	20.9
DC-HF+G		2.327		411		21.0
NR-MP2	2.384	2.330	379	405	46.1	56.1
DC-MP2	2.392	2.338	366	392	39.4	49.1
NR-CCSD	2.397	2.341	368	395	42.0	49.1
DC-CCSD	2.406	2.349	355	383	35.3	41.7
NR-CCSD(T)	2.406	2.349	358	385	44.5	52.3
DC-CCSD(T)	2.416	2.359	344	372	38.0	45.2
NR-HF[134]	2.33		421			
RCI[137]	2.53		327			
Experiment[120]	2.321		384		50.2	

Table 4.6. Properties of IBr calculated at various levels of theory.

	r_e (Å)		ω_e (cm^{-1})		D_e (kcal mol^{-1})	
Method	apVDZ	apVTZ	apVDZ	apVTZ	apVDZ	apVTZ
NR-HF	2.508	2.472	284	295	18.4	25.7
DC-HF	2.510	2.475	276	287	8.0	14.5
DC-HF+G		2.476		287		14.6
NR-MP2	2.537	2.483	264	283	40.2	50.5
DC-MP2	2.541	2.486	256	275	30.9	40.4
NR-CCSD	2.552	2.497	255	275	37.2	44.0
DC-CCSD	2.557	2.501	246	266	28.0	34.1
NR-CCSD(T)	2.562	2.506	247	267	39.5	47.1
DC-CCSD(T)	2.568	2.511	237	258	30.4	37.4
NR-HF[134]	2.29		342			
Experiment[120]	2.469		269		42.3	

Table 4.7. Relativistic effects on the properties at different levels of theory.

		Δr_e (Å)		$\Delta \omega_e$ (cm^{-1})		ΔD_e (kcal mol^{-1})	
Molecule	Method	apVDZ	apVTZ	apVDZ	apVTZ	apVDZ	apVTZ
ClF	HF	0.001	0.000	-2	-2	-1.5	-1.5
	HF + G		0.000		-3		-1.5
	MP2	0.000	0.001	0	-1	-1.3	-1.4
	CCSD	0.000	0.001	0	-1	-1.3	-1.4
	CCSD(T)	0.000	0.001	0	-1	-1.3	-1.4
	ASO-only					-1.3	
BrF	HF	0.002	0.003	-7	-6	-4.3	-4.6
	HF + G		0.003		-6		-4.5
	MP2	0.002	0.003	-6	-6	-3.7	-4.0
	CCSD	0.002	0.003	-6	-6	-3.8	-4.1
	CCSD(T)	0.002	0.003	-6	-6	-3.7	-4.0
	ASO-only					-4.0	
BrCl	HF	0.000	0.001	-3	-3	-4.6	-4.9
	HF + G		0.001		-4		-4.8
	MP2	0.001	0.001	-3	-3	-4.1	-4.5
	CCSD	0.001	0.001	-3	-4	-4.1	-4.4
	CCSD(T)	0.001	0.001	-4	-4	-4.0	-4.3
	ASO-only					-4.5	
IF	HF	0.010	0.010	-23	-23	-8.3	-8.8
	HF + G		0.011		-23		-8.7
	MP2	0.012	0.011	-21	-21	-6.9	-7.4
	CCSD	0.011	0.011	-21	-21	-7.2	-7.6
	CCSD(T)	0.012	0.012	-23	-23	-7.0	-7.4
	ASO-only					-7.8	
ICl	HF	0.008	0.007	-13	-13	-7.6	-8.2
	HF + G		0.008		-13		-8.1
	MP2	0.009	0.008	-13	-12	-6.6	-7.4
	CCSD	0.009	0.009	-13	-13	-6.6	-7.2
	CCSD(T)	0.010	0.010	-14	-13	-6.5	-7.1
	ASO-only					-8.3	
IBr	HF	0.003	0.003	-8	-8	-10.5	-11.2
	HF + G		0.004		-8		-11.0
	MP2	0.004	0.004	-8	-8	-9.3	-10.1
	CCSD	0.005	0.004	-9	-8	-9.2	-9.8
	CCSD(T)	0.006	0.005	-10	-9	-9.1	-9.7
	ASO-only					-11.0	

4.4 Electric properties

In contrast to the spectroscopic properties much theoretical attention has been given to the electric properties, especially to the dipole moment μ_z. Most of the calculations are performed within a non-relativistic framework whereas in some calculations relativistic corrections are included either by the use of a Cowan-Griffin (CG) [138] or a Douglas-Kroll (DK) [43,44] Hamiltonian, both without spin-orbit coupling. In table 4.8-4.10 the results of the electric property calculations for respectively the dipole moment, quadrupole moment and static dipole polarizability, are given. We have summarized the relativistic effects, defined as x(relativistic) - x(non-relativistic), on these properties in table 4.11.

4.4.1 Electric dipole moment

The electric dipole moment, (μ_z) presented in table 4.8, shows a relativistic increase for all molecules. We find that the relativistic contribution becomes increasingly important when going to the heavier interhalogens. For the iodine containing molecules this contribution is 10-20% of the total value. The increase of the electric dipole moment can be understood by considering that relativistic effects reduce the ionization potential especially for the heaviest atom in the molecule which leads to a more ionic molecule[139]. Our relativistic correlated μ_z overestimates the experimental values by 0.020 to 0.044 au which is an error of 5 to 9 %. Our relativistic results (DC-HF) for the ClF molecule are similar to those of Sadlej[140] and Perera and Bartlett[141]. However, for the other molecules significant differences are found and these differences increase for heavier molecules. The smaller relativistic corrections of Sadlej and Perera and Bartlett (table 4.11) are probably due to absence of spin-orbit interaction in the Cowan-Griffin Hamiltonian. Fowler *et al.* [142] included relativistic effects in their calculations on the BrCl molecule using the one-component form of the Douglas-Kroll approximation. Here the spin-orbit coupling is also neglected and the resulting relativistic effects are comparable to those of Sadlej and Perera and Bartlett.

In contrast to the results obtained for the other molecules there are large differences between the DZ and TZ results of μ_z for the iodine containing molecules. This suggests that in comparison with the other atoms the basis sets for the iodine atom lacks the necessary flexibility to reproduce this property well. Our NR-HF results are in close agreement with those of Sadlej[140] and Perera and Bartlett[141]. For the three lightest molecules the results with the basis sets of Sadlej are comparable to our double zeta (DZ) results whereas in the iodine containing molecules they lie closer to the triple zeta (TZ) results. There are discrepancies between our results and those of Straub and McLean[134] and Kucharski *et al.* [132] which are probably caused by basis set deficiencies in these calculations. Fowler *et al.* [142,143] performed calculations on the BrCl molecule and their non-relativistic results are in close agreement with

Table 4.8.a. Calculated dipole moment μ_z (au) for the molecules ClF, BrF and BrCl. The positive sign means polarity X^+Y^-.

	ClF		BrF		BrCl	
Method[a]	apVDZ	apVTZ	apVDZ	apVTZ	apVDZ	apVTZ
NR-HF	0.446	0.438	0.653	0.644	0.197	0.201
DC-HF	0.452	0.444	0.688	0.680	0.230	0.234
NR-SDCI	0.372	0.378	0.561	0.569	0.185	0.194
DC-SDCI	0.377	0.383	0.593	0.601	0.215	0.224
NR-HF[134]	0.355		0.567		0.231	
NR-HF[140]	0.446		0.652		0.205	
CG-HF[140]	0.451		0.679		0.229	
CG-MBPT(4) [140]	0.359		0.556		0.198	
NR-HF[143]					0.206	
NR-HF[132]	0.479		0.715		0.266	
NR-MBPT(4) [132]	0.350		0.550		0.222	
NR-HF[141]	0.446		0.658		0.204	
CG-HF[141]	0.451		0.685		0.228	
CG-CCSD(T) [141]	0.354		0.560		0.199	
NR-HF[142]					0.196	
DK-HF[142]					0.221	
DK-CCSD(T) [142]					0.183	
NF-HF[135]	0.409					
NR-CISD+Q[135]	0.346					
NR-CPF[136]	0.334					
Experiment	0.3494 ± 0.0079[144]		0.559 ± 0.006[146]		0.204 ± 0.002[147]	
	0.346 ± 0.008[145]					

[a]: CG (Cowan-Griffin Hamiltonian used to include relativistic effects), DK (Douglas-Kroll Hamiltonian used to include relativistic effects).

our data. Pettersson *et al.* [135] studied the ClF molecule and their non-relativistically calculated μ_z is significantly lower than our value and that of the other authors.

Our correlation contributions are smaller than those of Sadlej[140] and Kucharski *et al.* [132], both using MBPT(4), and Perera and Bartlett[141], using CCSD(T). Pettersson *et al.* [135] included correlation contributions using CISD for the ClF molecule and their results are similar to our

Table 4.8.b. Calculated dipole moment μ_z (au) for the molecules IF, ICl and IBr. The positive sign means polarity X^+Y^-.

	IF		ICl		IBr	
Method[a]	apVDZ	apVTZ	apVDZ	apVTZ	apVDZ	apVTZ
NR-HF	0.865	0.790	0.488	0.425	0.292	0.243
DC-HF	0.978	0.900	0.616	0.548	0.395	0.340
NR-SDCI	0.776	0.709	0.470	0.405	0.283	0.226
DC-SDCI	0.878	0.810	0.586	0.518	0.373	0.313
NR-HF[134]	0.570				0.254	
NR-HF[140]	0.814		0.442		0.258	
CG-HF[140]	0.891		0.514		0.305	
CG-MBPT(4) [140]	0.753		0.454		0.263	
NR-HF[132]	0.930		0.563		0.334	
NR-MBPT(4) [132]	0.735		0.472		0.274	
NR-HF[141]	0.813		0.442		0.257	
CG-HF[141]	0.890		0.514		0.296	
CG-CCSD(T) [141]	0.756		0.443		0.264	
Experiment	0.766 ± 0.008[148]		0.49 ± 0.01[149]		0.290 ± 0.004[151]	
			0.475 ± 0.001[150]		0.286 ± 0.011[152]	

[a]: CG (Cowan-Griffin Hamiltonian used to include relativistic effects), DK (Douglas-Kroll Hamiltonian used to include relativistic effects).

calculated correlation effects. It is clear that more extensive correlation calculations are required to get closer agreement with the experimental results.

4.4.2 Electric quadrupole moment

We find large relativistic effects for the IF and ICl molecule. In the case of the IF molecule the relativistic effects dominate the magnitude of the Θ_{ZZ} value and at the HF level of theory the sign is even reversed. The Θ_{ZZ} of the two lightest molecules ClF and BrF are within the wide error bars of the experimental data. Our relativistic contributions to the Θ_{ZZ} differ considerably from those calculated by Sadlej[140] for all molecules except the lightest, ClF. Sadlej found small relativistic effects for all molecules except for IBr where our relativistic correction is only half of the correction calculated by Sadlej.
The Θ_{ZZ} shows basis set dependencies for all molecules except for the two lightest molecules ClF and BrF. On the other hand, the relativistic effects do not seem to be basis set dependent.

Table 4.9.a. Calculated quadrupole moment Θ_{zz} (au) for the molecules ClF, BrF and BrCl.

	ClF		BrF		BrCl	
Method[a]	apVDZ	apVTZ	apVDZ	apVTZ	apVDZ	apVTZ
NR-HF	0.901	0.828	0.514	0.382	3.043	2.515
DC-HF	0.911	0.836	0.483	0.349	3.058	2.533
NR-SDCI	0.977	0.912	0.706	0.557	2.974	2.535
DC-SDCI	0.987	0.922	0.688	0.534	2.998	2.560
NR-HF[134]	0.950		0.503		2.617	
NR-HF[140]	0.947		0.519		2.845	
CG-HF[140]	0.958		0.514		2.883	
CG-MBPT(4) [140]	1.102		0.833		2.875	
NR-HF[143,b]					2.797	
Experiment[c]	1.00 ± 0.74		0.68 ± 0.74			
	0.65 ± 0.74		0.91 ± 0.74			

[a]: CG (Cowan-Griffin Hamiltonian used to include relativistic effects).

[b]: Bond length of 2.141 Å is used.

[c]: Ref. 145. Results are for two different isotopes of Cl and Br.

Table 4.9.b. Calculated quadrupole moment Θ_{zz} (au) for the molecules IF, ICl and IBr.

	IF		ICl		IBr	
Method[a]	apVDZ	apVTZ	apVDZ	apVTZ	apVDZ	apVTZ
NR-HF	0.250	0.059	3.026	2.313	4.611	3.696
DC-HF	-0.003	-0.189	2.803	2.123	4.657	3.772
NR-SDCI	0.443	0.255	2.926	2.352	4.485	3.722
DC-SDCI	0.235	0.045	2.749	2.196	4.568	3.815
NR-HF[134]	0.639				3.361	
NR-HF[140]	0.199		2.584		4.165	
CG-HF[140]	0.124		2.597		4.361	
CG-MBPT(4) [140]	0.483		2.635		4.272	

[a]: CG (Cowan-Griffin Hamiltonian used to include relativistic effects).

The NR-HF results of Sadlej[140] for the three lighter systems are comparable to our apVDZ results whereas those for the iodine containing molecules lie closer to the apVTZ results. This trend is similar to the one found for the μ_z. The results of Straub and McLean[134] for the first two molecules ClF and BrF are similar to our double zeta results which is somewhat surprising because of the large discrepancies found for the dipole moments of these molecules. The BrCl and IBr results lie close to, or even below, the apVTZ values whereas the results for IF molecule show large deviations.

Not only the size but also the sign of the correlation corrections change when going from apVDZ to apVTZ quality basis sets. For the molecules BrCl, ICl and IBr, molecules with a large Θ_{zz}, the sign of the corrections changes from negative to positive yielding a larger Θ_{zz} in the triple zeta calculation. The correlation contributions of Sadlej[140] do not show a systematic behaviour either and differ from our corrections as well. More extensive correlated calculations and analysis of the correlation contributions are needed to get a better understanding of the correlation effects on this property.

4.4.3 Dipole polarizability

No experimental values are available for the α_{zz}. Significant relativistic effects are found for the four heaviest molecules BrCl, IF, ICl and IBr with the largest relativistic effects on IBr. Relativity leads to an increase of the α_{zz} except for the IF molecule where a significant decrease is found. Our relativistic effect on the α_{zz} of BrCl is larger than the values obtained by Sadlej[140] and Fowler *et al.* [142] whereas the value of Sadlej for the IF molecule is in close

Table 4.10.a. Calculated dipole polarizability α_{zz} (au) for the molecules ClF, BrF and BrCl.

	ClF		BrF		BrCl	
Method[a]	apVDZ	apVTZ	apVDZ	apVTZ	apVDZ	apVTZ
NR-HF	21.63	22.18	27.72	27.97	50.81	51.55
DC-HF	21.66	22.20	27.72	27.96	51.09	51.82
NR-HF[140]	22.48		27.82		51.50	
CG-HF[140]	22.51		27.80		51.65	
CG-MBPT(4) [140]	22.71		27.44		50.92	
NR-HF[142]					51.76	
DK-HF[142]					51.89	
DK-CCSD(T) [142]					51.23	

[a]: CG (Cowan-Griffin Hamiltonian used to include relativistic effects), DK (Douglas-Kroll Hamiltonian used to include relativistic effects).

Table 4.10.b. Calculated dipole polarizability α_{zz} (au) for the molecules IF, ICl and IBr.

	IF		ICl		IBr	
Method[a]	apVDZ	apVTZ	apVDZ	apVTZ	apVDZ	apVTZ
NR-HF	31.25	36.3	59.34	64.98	74.82	78.85
DC-HF	30.93	35.85	60.06	65.49	76.56	80.38
NR-HF[140]	36.54		65.30		78.96	
CG-HF[140]	36.07		65.30		79.24	
CG-MBPT(4) [140]	37.79		65.26		77.96	

[a]: CG (Cowan-Griffin Hamiltonian used to include relativistic effects), DK (Douglas-Kroll Hamiltonian used to include relativistic effects).

agreement with our result. Large discrepancies in the relativistic effects are found for the heavier molecules ICl and IBr.

Our NR-HF results are in close agreement with the results of Sadlej[140] and Fowler *et al.* [142], as can be seen in table 4.10. We have not performed correlated calculations. The results of Sadlej in table 4.10 give small effects for most of the molecules.

4.5 Additivity

Our results for the spectroscopic properties r_e and ω_e in table 4.8 show that for all practical purposes the relativistic and the correlation effects in the studied interhalogens are additive contributions. Some small combined relativistic-correlation contributions are seen for the ΔD_e. We also find a small combined effect of relativity and correlation for the μ_z of the iodine containing molecules (table 4.11). These effects are similar to those found by Perera and Bartlett[141]. The combined effect of relativity and correlation for the Θ_{zz} is somewhat larger than what we observe in calculations on the μ_z.

4.6 Conclusions

The effect of relativity on the spectroscopic and electric properties of the interhalogens has been studied comparing non-relativistic with relativistic all-electron calculations. The effect of the Gaunt correction, the higher-order two-electron relativistic correction is found to be negligible. The inclusion of relativity leads to a weakening of the bond which results in an increase of the r_e and a decrease of the ω_e. This weaker bond is caused by an increase of the anti-bonding character of the occupied valence spin orbitals. The relativistic effect on the dissociation energy is primarily due to the lowering by spin-orbit splitting of the ^2P atomic asymptote.

Table 4.11. Relativistic effects on electric properties.

		$\Delta\mu_z$ (au)		$\Delta\Theta_{zz}$ (au)		$\Delta\alpha_{zz}$ (au)	
Molecule	Method	apVDZ	apVTZ	apVDZ	apVTZ	apVDZ	apVTZ
ClF	HF	0.006	0.006	0.010	0.009	0.03	0.02
	SDCI	0.005	0.005	0.011	0.010		
	HF[140]	0.005		0.011		0.03	
	HF[141]	0.005					
	CCSD[141]	0.004					
BrF	HF	0.036	0.036	-0.031	-0.033	0.00	-0.01
	SDCI	0.032	0.032	-0.018	-0.023		
	HF[140]	0.028		-0.005		-0.02	
	HF[141]	0.027					
	CCSD[141]	0.023					
BrCl	HF	0.033	0.033	0.015	0.018	0.29	0.27
	SDCI	0.031	0.030	0.024	0.025		
	HF[140]	0.023		0.038		0.15	
	HF[141]	0.023					
	CCSD[141]	0.019					
	HF[142]	0.025					
	CCSD[142]	0.019					
IF	HF	0.113	0.111	-0.253	-0.248	-0.32	-0.46
	SDCI	0.102	0.101	-0.208	-0.210		
	HF[140]	0.077		-0.075		-0.47	
	HF[141]	0.077					
	CCSD[141]	0.065					
ICl	HF	0.127	0.123	-0.224	-0.191	0.71	0.51
	SDCI	0.116	0.112	-0.177	-0.156		
	HF[140]	0.072		0.013		0.00	
	HF[141]	0.072					
	CCSD[141]	0.057					
IBr	HF	0.102	0.097	0.046	0.076	1.74	1.53
	SDCI	0.091	0.087	0.084	0.093		
	HF[140]	0.047		0.196		0.28	
	HF[141]	0.039					
	CCSD[141]	0.033					

Relativistic effects increase the electric dipole moment (μ_z) of the interhalogens. This effect is largest for the iodine containing molecules, where an increase of 10-20% is found. Similar relativistic corrections are found for the Θ_{zz}. The electron correlation contribution decreases the μ_z and is underestimated at the CISD level of theory. The relativistic effects on the electric quadrupole moment (Θ_{zz}) are important but do not show a clear trend. We find that the value of Θ_{zz} in IF is dominated by the relativistic contribution. Our DHF results for the Θ_{zz} are in close agreement with other theoretical predictions, but the correlation contribution is not converged with basis set size and shows an irregular behaviour. Relativistic effects increase the dipole polarizability (α_{zz}), except for the IF molecule where a significant decrease is found. Our non-relativistic results for the α_{zz} are in close agreement with the available theoretical results but considerable differences are found when relativistic effects are included in the calculation.

For all practical purposes the relativistic and correlation effects on the spectroscopic properties yield additive contributions for the molecules studied here. However, the calculations on the electric dipole and quadrupole moment show somewhat larger deviations from additivity.

Chapter 5

The ground, excited and ionized states of iodine

In this chapter the electronic structure, spectroscopic and bonding properties of the ground, excited and ionized states of iodine are studied. The experimentally determined properties of the $^1\Sigma_g^+$ ground state are well reproduced by our results calculated at the CCSD(T) level of theory. Relativistic effects and core-valence correlation need to be included in order to get reliable results but the Gaunt interaction can be neglected. The photoelectron spectrum and the potential energy curves of the ionized and excited states are calculated using relativistic configuration interaction and coupled cluster methods. The calculated properties of the excited states are generally in good agreement with the experimental data as well as with earlier theoretical results of Teichteil and Pelissier. An alternative assignment of some recently measured, low lying, ionized states is proposed.

5.1 Introduction

The spectroscopic properties of the iodine molecule have been the subject of many experiments[153-181] and theoretical studies[182-196] yet our understanding of these properties is still incomplete. Crucial in the understanding of these properties is the effect of relativity. In particular the spin-orbit interaction, which leads to severe mixing of excited states, has profound implications for the interpretation of spectroscopic data. The most important relativistic effect here is the spin-orbit interaction which leads to mixing of the bonding σ_g spinor with the anti-bonding $\pi_{g,1/2}$ and similar to the mixing of the anti-bonding σ_u spinor with the bonding $\pi_{u,1/2}$ (see figure 5.1). This mixing lifts the degeneracy of π spinors and weakens the bond due to mixing in of anti-bonding σ_u character into occupied spinors. The inclusion of spin-orbit interactions also leads to severe mixing between excited states and has profound implications for the interpretation of spectroscopic data.

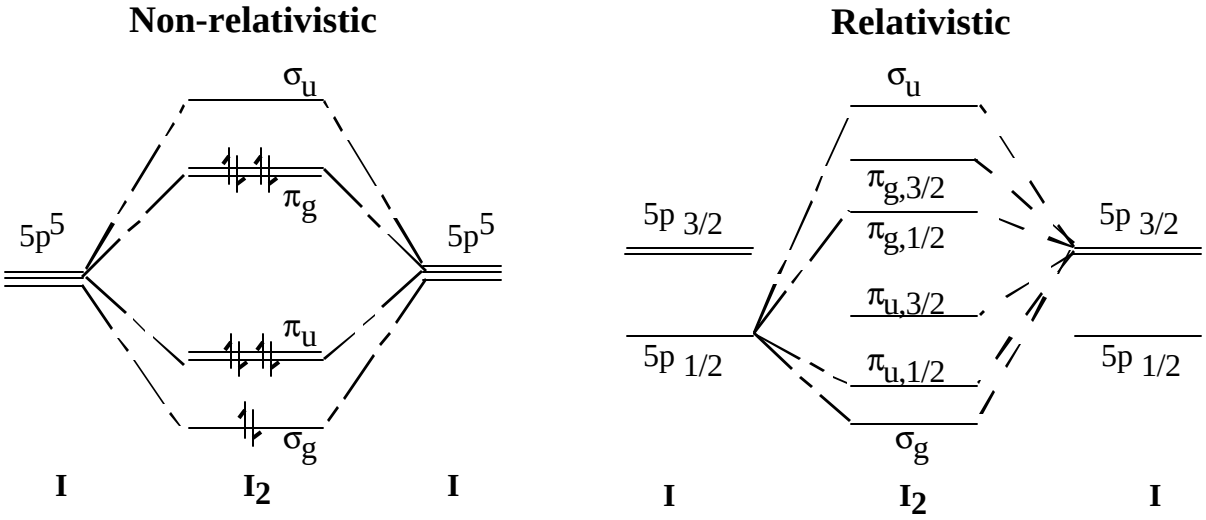

Figure 5.1. Non-relativistic and relativistic bonding schemes for the valence 5p spinors of iodine (For relativistic case the bonding of each type of spinor is shown only once).

The most studied excited state is the B $^3\Pi_u$ (0_u^+), responsible for the visible absorption spectrum, a state that dissociates into $^2P_{3/2}$ + $^2P_{1/2}$ atomic states and thereby crosses repulsive or very weakly bound states originating from $^2P_{3/2}$ + $^2P_{3/2}$ atomic states. These crossings give rise to a number of predissociation effects that have been observed. Predissociation of the B state is now more or less understood[156,157,190]. Other excited states are, however, much less well characterized. Early theoretical work was done by Mulliken[182] who constructed a theoretical spectrum based on one-electron arguments and empirical corrections. Tellinghuisen[160-162,164] constructed potential energy curves on the basis of experimental data. State-of-the-art theoretical calculations can nowadays be used to confirm the form and positions of the proposed curves.

Most of the theoretical work is done on the molecular ground state. The majority of the calculations are valence electron calculations where the core is represented by a relativistic pseudopotential[183,184,186-188,193]. To improve the calculated spectroscopic properties core-valence correlation effects can be included in the pseudopotentials. Another type of calculation applied to the iodine molecule[189] is the Zeroth Order Regular Approximation (ZORA) [48] method, used in combination with density functional theory.

Some calculations were performed on the excited states of the iodine molecule. All these calculations make use of relativistic pseudopotentials. Das and Wahl[187] have determined a few excited states using the MCSCF method with empirical corrections for the relativistic effects. Li and Balasubramanian[193] and Teichteil and Pelissier[183] calculated the excited states by a MCSCF method followed by spin-orbit (SO) CI calculations. The curves obtained by Li and Balasubramanian differ from those calculated by Teichteil and Pelissier leading to two different theoretical pictures for the assignment of the I_2 spectra and the interpretation of spectroscopic phenomena like predissociation.

For the ionized states of iodine there is only a limited amount of experimental[172-176,180] and theoretical data available[193,194]. Li and Balasubramanian[193] calculated potential energy curves and spectroscopic properties for the ionized states of iodine. Given the discrepancies between their work and that of Teichteil and Pelissier for the excited states of the neutral molecule, and in the light of the recent ZEKE experiments on the ionized states[180], another theoretical investigation is of interest.

In this paper the influence of relativity and correlation, including core-valence correlation effects, on the spectroscopic properties of the ground state are studied using the all electron Dirac-Fock method followed by CCSD(T) calculations. All relativistic effects are hence included from the outset.

The potential energy curves for all excited states that dissociate into the ^2P_J + ^2P_J (J = 3/2 or 1/2) atomic states are calculated using the average of configurations Dirac-Hartree-Fock approach[121], followed by a complete active space CI calculation. This approach allows us to assess the influence of spin-orbit coupling on the spectroscopic properties and makes it possible to assign the observed states. In order to obtain information about the accuracy of the calculated spectra additional MRCISD calculations are performed.

Four low lying states of the ionized molecule I_2^+ ($^2\Pi_{g,3/2}$, $^2\Pi_{g,1/2}$, $^2\Pi_{u,3/2}$ and $^2\Pi_{u,1/2}$ respectively) are studied including correlation effects up to the CCSD(T) level of theory. In a second set of calculations the complete spectrum of all ionized states that dissociate into $I + I^+$ is calculated using the same approach as for the curves of the excited states. The assignment of the recently measured "a" state to a $^4\Sigma^-_{u,3/2}$ state by Cockett *et al.* [180] is discussed.

5.2 Computational Model

The molecular spinors of open-shell systems are generated using an average of configurations DHF[121]. Subsequently a full CI is performed in the open-shell spinor space in order to project out the different states that arise from the open-shell manifold. This approach, which is denoted Complete Open Shell Configuration Interaction (COSCI) gives us a balanced description of all states in the manifold and their interaction. Correlation effects are studied at different levels of theory depending on the reference wave function. For the multireference RAS-CI[84] we use the COSCI states as the reference wave functions. For closed shell systems and systems with a single reference determinant the RELCCSD program[86], a relativistic Coupled Cluster Singles Doubles (CCSD) program[40], is used. The next higher order terms, the triple excitations, are included using a non-iterative correction labeled (T) [88].

Table 5.1. Basis set sizes.

	Large Component	Small Component
Non-relativistic	20s16p12d1f / 7s6p4d1f	
Relativistic	21s17p12d1f / 7s8p4d1f	17s33p18d12f1g / 6s11p10d5f1g

For the non-relativistic calculations a point-nucleus model is used whereas for the relativistic calculations the nucleus is represented by a gaussian charge distribution with an exponential value of 0.1845238916E+09. The speed of light is taken to be 137.0359895 atomic units.

The iodine basis is the contracted pVTZ basis taken from Visscher[125]. The primitives are of triple zeta quality in the valence region and the contracted functions are generated using a modified[71,72] version of GRASP[19]. The size of the basis is given in table 5.1.

There are three classes of two-electron repulsion integrals in the DHF calculation, the (LL|LL) class of integrals which are comparable to the non-relativistic integrals, the (LL|SS) class which represents the two-electron spin-orbit interaction and the (SS|SS) class of integrals. This last class of integrals arises from the small component part of the wave function and contributes formally to order α^4 to the electronic energy. Since the small component density is mainly located in regions close to the respective nuclei this contribution has very small effect on the calculated valence properties. In fact it can be shown[100,101] that the interatomic contribution of the (SS|SS) class of integrals can be represented by the Coulomb repulsion between the small component densities of the different atoms in the molecule. In calculating potential energy curves (sections 5.4.1 and 5.5.2) this large class of integrals can therefore be omitted and replaced by a small repulsive (electrostatic) contribution[101] $q_{S1}q_{S2}/R$ at each distance R, where q_{S1} and q_{S2} are the small component densities on atom 1 and 2 respectively. The omission of these integrals in the iterative SCF process has only a small effect on the core-spinors and no significant effect on the valence spinors. For more thorough discussion of this approach we refer to section 2.4.

For the non-relativistic calculations a point-nucleus model is used whereas for the relativistic calculations the nucleus is represented by a gaussian charge distribution[74] with an exponential value of 1.845238916E+09.

The iodine basis is the contracted pVTZ basis taken from Visscher[125]. The primitives are of triple zeta quality in the valence region and the contracted functions are generated using a modified[71,72] version of GRASP[19].

The point groups D_{4h}, O_h and their double groups (D_{4h}^* and O_h^*) are used in the calculations for the I_2 molecule and the I atom respectively.

Equilibrium bond lengths (R_e) and vibration frequencies (ω_e) resulting from the single reference calculations on the ground state and the lowest ionized states are determied by a 4th order polynomial fit to at least 8 points of the potential energy curve. The polynomial obtained is used to calculate the anharmonicity constant with the MOLCAS[197] program VIBROT. The VIBROT program is also used to derive the spectroscopic properties of the potential energy curves of the excited and ionized states calculated with the COSCI approach. The dissociation energy of the ground state is calculated relative to the energy of the $^2P_{3/2}$ atomic state. The latter energy is obtained by optimizing the average energy of the $5p_{1/2})^2\ 5p_{3/2})^3$ configuration.

The notation σ_g, π_u, π_g and σ_u is used for the molecular orbitals that can be formed as linear combinations of the six atomic 5p orbitals. The molecular spinor combinations are labelled by their

dominant character $\sigma_{g,1/2}$, $\pi_{u,1/2}$, $\pi_{u,3/2}$, $\pi_{g,1/2}$, $\pi_{g,3/2}$ or $\sigma_{u,1/2}$. The other filled orbitals are not listed explicitly. In non-relativistic calculations we can assign the molecular states using Λ–Σ coupling. In our relativistic calculations we work with intermediate coupling so only the ω and Ω quantum numbers apply. To connect to previous discussions on the assignment of states, and because the molecular spinors have relatively pure σ or π-character, we have tried to analyze the calculated states in terms of Ω components of Λ–Σ states. This analysis is facilitated by comparing with a non-relativistic calculation in a two-component spinor basis (using the non-relativistic option of MOLFDIR). In this case we obtain pure $\sigma_{g,1/2}$, $\pi_{u,1/2}$, $\pi_{u,3/2}$, $\pi_{g,1/2}$, $\pi_{g,3/2}$ and $\sigma_{u,1/2}$ spinors. We can then analyze which Ω components of the Λ–Σ states contribute to a particular relativistic state by comparing the determinantal compositions of the (non-relativistic) Λ–Σ states, which are also calculated in double group symmetry, with those of the relativistic Ω states. The molecular states are then labelled on the basis of the dominant Λ–Σ state. When the spinors do not have clear σ or π-character this analysis cannot be carried out and only the Ω label is used. When there is no dominant contribution from a particular Λ–Σ state we will label the state only by its Ω quantum number.

5.3 The iodine ground state

In this section results of calculations on the ground state properties of the iodine molecule are shown. The spinors are obtained by DHF calculations on the closed shell configuration $\sigma_g^2\pi_u^4\pi_g^4\sigma_u^0$. Relativistic as well as non-relativistic calculations are performed to study the influence of relativity on the spectroscopic properties of the ground state. Electron correlation is included using the CCSD(T) method and core-valence effects are studied by including excitations from the 4s, 4p, 4d and 5s spinors. A summary of the results is presented in table 5.2. The inclusion of relativistic effects results in a decrease in dissociation energy (D_e), which is mainly due to the spin-orbit splitting of the $^2P + {}^2P$ dissociation asymptote. The spin-orbit interaction is not completely quenched in the molecule, where a Mulliken population analysis gives a mixing of 2% of the anti-bonding

Table 5.2. Overview of calculated spectroscopic properties for the iodine ground state. The calculated results are compared with experimental data and other theoretical work. All calculations have spin-orbit effects included.

Method[a]	CV[b]	R_e (Å)	D_e (eV)	ω_e (cm^{-1})	$\omega_e x_e$ (cm^{-1})
NR-HF	--	2.681	1.03	237	0.39
NR-HF + CCSD(T)	2	2.695	1.91	221	0.49
DHF	--	2.682	0.40	229	0.42
DHF + Gaunt	--	2.683	0.40	229	0.42
DHF + CCSD(T)	1	2.717	1.28	206	0.61
	2	2.699	1.39	210	0.59
	3	2.698	1.39	212	0.58
DHF + CCSD(T) + g-func.[c]	3	2.685	1.53	217	0.58
RECP, HF, MP2[186]		2.733	1.17	202	--
RECP, CASSCF, FOCI[193]		2.770	1.45	210	--
PP, MCSCF[187]		2.699	1.66	230	--
PP, MCSCF, MRCISD[183]		2.769	0.76	185	0.80
PP+CPP, CISD[184]		2.687	1.35	--	--
PP+CPP, CCSD(T) [188]		2.668	1.57	215	--
DFT+GGC, ZORA[189]		2.719	1.58	197	--
Experimental[120]		2.666	1.55	214.5	0.61

a. NR-HF (Non-relativistic Hartree-Fock), DHF (Dirac-Hartree-Fock), RECP (Relativistic effective core potential), PP (Pseudopotential), CPP (Core polarisation potential), DFT+GGC, ZORA (Density functional plus gradient correction using the ZORA method)

b. Active space used in the correlation calculations:

1: 5s core, 5p valence and full virtual space

2: 4d and 5s core, 5p valence and full virtual space

3: 4s, 4p, 4d and 5s core, 5p valence and full virtual space

c. Basis extended with one g-function, see discussion at end of section 5.5.3.

$\sigma_{u,1/2}$ spinor into the occupied bonding $\pi_{u,1/2}$ spinor. The weakened molecular bond is, however, not accompanied by a substantial bond length expansion because scalar relativistic effects contract the spinors and almost cancel the spin-orbit effect on the R_e. The effect of the Gaunt term on the spectroscopic properties is negligible.

Core-valence correlation effects are studied by adding, in a number of stages, core spinors to the CCSD calculation. The inclusion of core spinors in the correlation calculation results in a shortening of the R_e by 0.02 Å and an increase of the D_e by 0.1 eV. Schwerdtfeger *et al.* [184] and Dolg[188] have

performed calculations using relativistic pseudopotentials (PP) in which the core-valence effects are accounted for by a (semi-empirical) core polarization term (CPP). They found effects of 0.03 Å and 0.06 eV and 0.03Å and 0.09 eV respectively upon including core-valence correlation. The size of the core-valence effect calculated in this paper hence is in close agreement with the PP results.

There remains some discrepancy between the experimental and our calculated R_e and D_e. A better agreement with experimental data is obtained in the highly correlated calculations of Dolg[188]. Dolg performed HF and CCSD(T) calculations with a large uncontracted basis set, using a Douglas-Kroll-Hess[43,44] transformed Hamiltonian, where the spin-orbit (SO) term was included afterwards. The HF+SO results from his calculations are in close agreement with the DHF results presented in this paper. His correlated results are better as a result of a larger basis set which includes higher l-functions. Dolg[198] also studied basis set effects by performing a series of PP calculations with an uncontracted basis set where functions with increasing l-values, up to g-functions, were included. In these calculations it was found that the inclusion of g-functions gives a contraction of the R_e by 0.02 Å at the CCSD(T) level. The basis set effects were also discussed by Teichteil and Pelissier[183] and they observed that the inclusion of a g-function has a larger effect than the inclusion of a second f-function. We performed an additional set of calculations where one diffuse g-function, with a judiciously chosen but not optimized exponential value of 0.22, was included. The CCSD(T) results show a reduction of R_e by 0.014 Å. Increases of 0.14 eV and 5 cm^{-1} are found for D_e and ω_e respectively.

We conclude that the small discrepancies with experiment can be resolved by the extension of the basis set and the inclusion of core-valence effects. For the work reported here such an extension of the basis set is impractical at present due to the large number of calculations necessary to obtain the potential energy curves of the excited and ionized states.

5.4 The excited states of iodine

Potential energy curves of all states resulting from the $\sigma_g^k\pi_u^l\pi_g^m\sigma_u^n$ configurations, where k+l+m+n=10, are calculated with the COSCI method using the average of configurations DHF spinors, with 10 electrons in 12 spinors.

The potential energy curves are calculated relativistically as well as non-relativistically, using the non-relativistic option in the MOLFDIR program package. For the non-relativistic case 24 states, of which 12 states dissociate into I^+ and I^-, are calculated. There are 43 states in the relativistic case with 20 states dissociating into ion-pair states. The results are presented and discussed in section 5.4.1. In section 5.4.2 their accuracy is assessed by comparing them with the results of additional MRSDCI calculations, with the COSCI states as references.

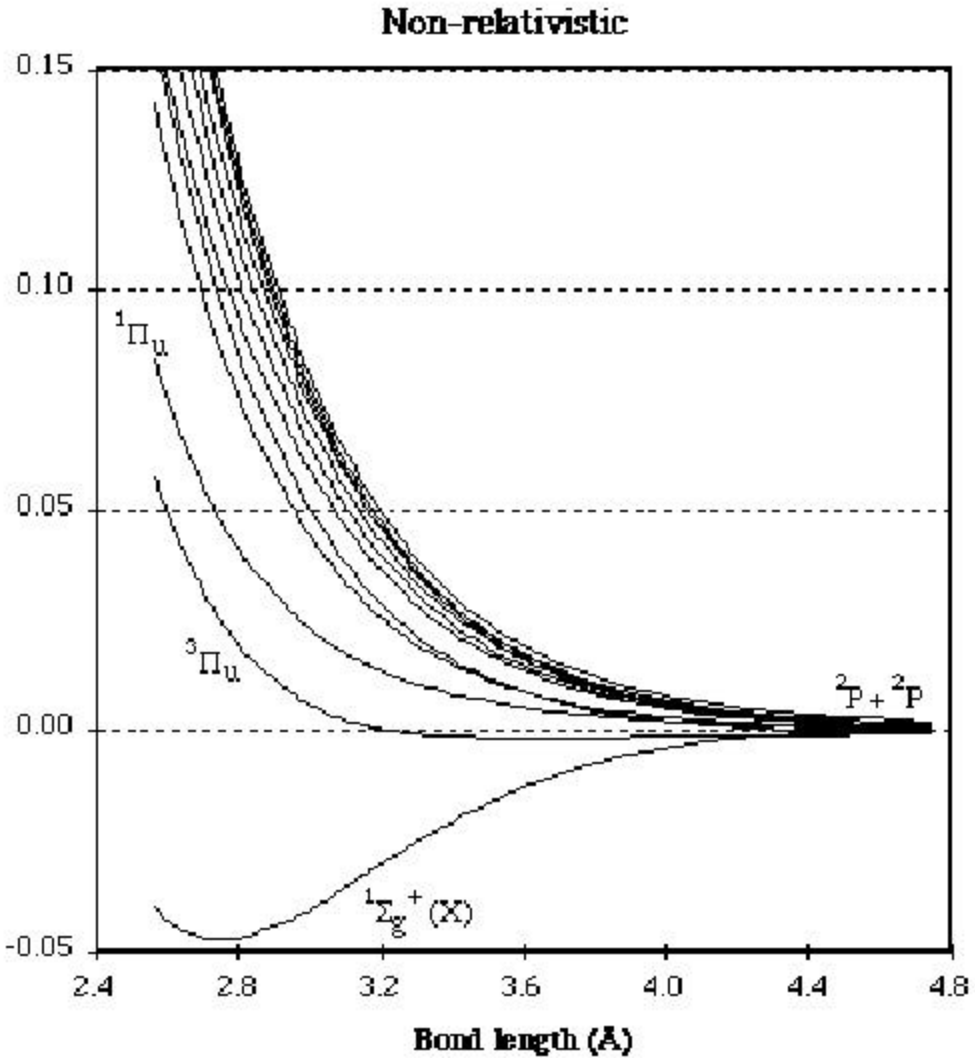

Figure 5.2. Non-relativistic (left page) and relativistic (right page) potential energy curves for the excited states of I_2. (States dissociating in two $5p^5$, ^2P iodine atoms are shown).

5.4.1 Potential energy curves

The potential energy curves of the valence excited states which dissociate into the $^2P_J + ^2P_J$ (J = 3/2 or 1/2) atomic states are derived from COSCI calculations at about 50 different bond distances. The resulting curves are presented in figure 5.2.

The D_e of the ground state (0.71 eV) obtained from the COSCI calculation is too small in comparison to the experimental value (1.55 eV) but larger than the single reference closed shell result (0.40 eV) of section 5.3 because of the interaction with anti-bonding configurational states in the open-shell manifold that assure proper dissociation behaviour. Potential curves of excited states that are known from experiment to be bonding are also found to be less bonding and sometimes even non-bonding. Using COSCI orbitals instead of state optimized orbitals to calculate the D_e for a closed shell wave function of the ground state

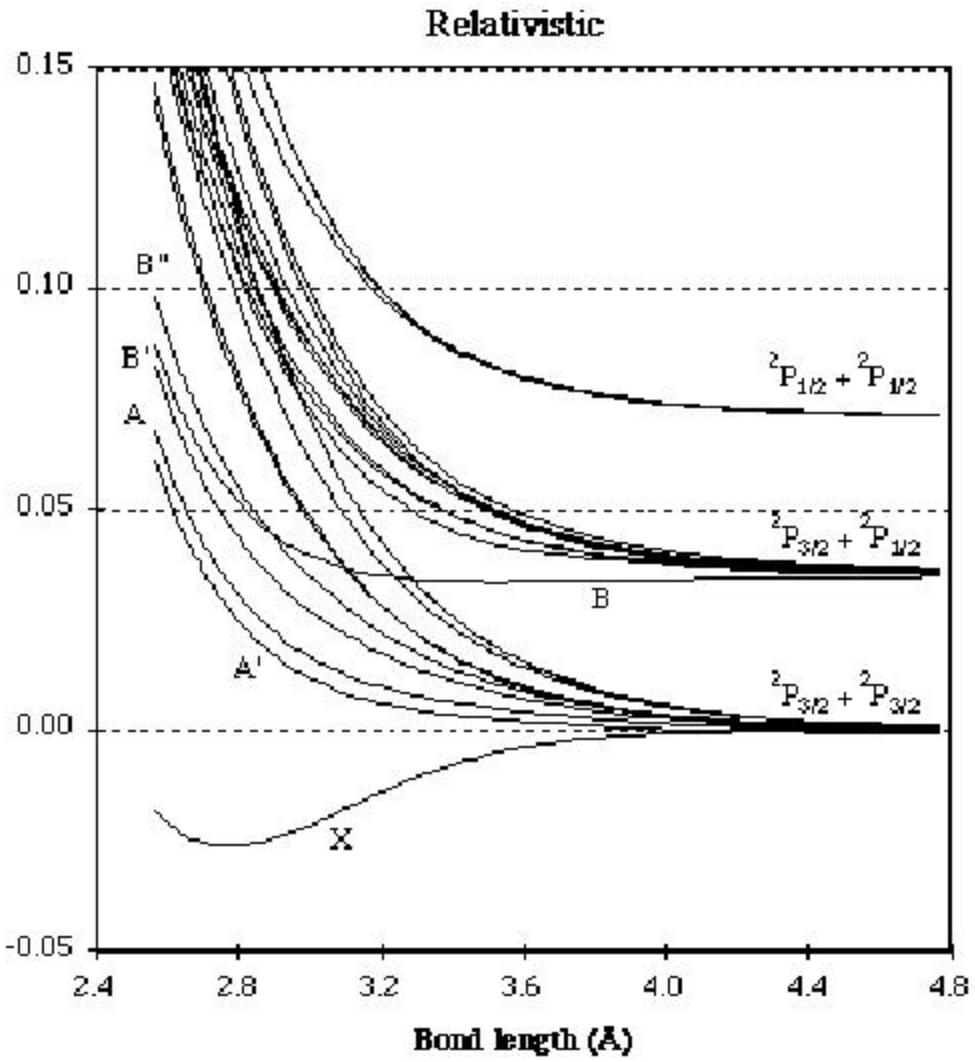

yields results that are very similar to those reported in section 5.3. In line with what is generally observed when anti-bonding configurational states are included in the wave function (non-dynamical correlation) the COSCI bond length of 2.76 Å for the ground state is larger than the single reference bond length of 2.68 Å. Core-valence correlation is probably the main ingredient necessary to shorten the R_e towards the experimental value of 2.66 Å. This is expected to improve the bond distances of the excited states, which are also found 0.1 Å too long, as well.

The splitting of the calculated states due to spin-orbit interaction agrees well with the observed splittings (see table 5.3). The important non-dynamical correlation effects are apparently sufficiently described by a COSCI calculation in the spinor space spanned by the 5p spinors. The relative splitting of the states describing dissociated neutral atoms ($^2P_J + {}^2P_J$ with J = 1/2 or 3/2) is also in good agreement with experimental data.

The calculated potential energy curves and their spectroscopic properties can be compared with two other theoretical calculations in which the relativistic effects are introduced using relativistically optimized pseudopotentials. A two configurations MCSCF approach is employed by Teichteil and Pelissier[183] to calculate the ground state using the configurations $\sigma_g^k\pi_u^4\pi_g^4\sigma_u^n$ with k+n=2. Subsequently they generate one set of orbitals (using improved virtual orbitals) as a basis for an additional MRCI calculation that includes spin-orbit matrix elements between the 23 states that dissociate into neutral atoms. Another route to calculate the potential energy curves and spectroscopic properties is taken by Li and Balasubramanian[193]. Here all states are generated in a CASSCF calculation with partially occupied 5s and 5p orbitals. Dynamical correlation is accounted for by means of additional MRCI calculations. The resulting potential energy curves are finally corrected for the effect of spin-orbit splitting by a limited MRCISD calculation using ground state orbitals.

The main features of the COSCI potential energy curves and their associated properties should be comparable to the results of these two methods discussed above. Especially, differences in the spin-orbit splitting of states should be minor. However, while our relativistic potential energy curves show a close resemblance to the curves generated by Teichteil and Pelissier, they differ from the curves calculated by Li and Balasubramanian.

A possible reason for this is the smaller CI space employed by Li and Balasubramanian. Teichteil and Pelissier perform a CI in a space that contains all states that dissociate into the neutral atoms (23 states). This CI space is identical with that of the COSCI calculations presented in this paper. In the spin-orbit MRCI calculations of Li and Balasubramanian, according to table II of their paper, the configurations $\sigma_g^2\pi_u^3\pi_g^3\sigma_u^2$, $\sigma_g^2\pi_u^2\pi_g^4\sigma_u^2$ and the 1g and 2g components of $\sigma_g^2\pi_u^4\pi_g^2\sigma_u^2$ are not included in the CI reference space. Since some of these configurations give rise to low lying states it may well be that omission of these configurations has a significant effect on the potential energy curves.

5.4.2 Vertical excitation energies

In table 5.3 the calculated, relativistic and non-relativistic, vertical excitation energies are given at the experimental R_e of the ground state. The vertical excitation energies of states dissociating into neutral atoms, third column in table 5.3, are in reasonable agreement with experimental data. The vertical excitation energies of the ion-pair states (not included in table 5.3) are found to be 1.65 eV too high compared to experimental data. This shift is caused by the use of the configurational average DHF approach.

MRCISD calculations were performed to improve the vertical excitation energies and to examine the accuracy of the calculated spectrum. The 5s-like spinors were placed in the RAS1 space to allow for some core-valence correlation. The 12 active spinors were included in the

Table 5.3. Calculated non-relativistic and relativistic vertical excitation energies (eV), at the experimental ground state equilibrium bond length, compared with experimental and other theoretical data. The notation klmn, used for the main configurations, is based on $\sigma_g^k\pi_u^l\pi_g^m\sigma_u^n$.

Non-relativistic		Relativistic				Exp.	Ref. 183	Ref. 182
Λ–Σ states	COSCI	Ω–ω states	COSCI	MR-CISD	Dominant configurations		Teichteil and Pelissier	Mulliken
$^1\Sigma_g^+$	0.00	(1) 0_g^+	0.00	0.00	2440	0.00	0.00	0.00
$^3\Pi_u$	2.25	(1) 2u	1.78	1.75	2431	1.69[a,e]	1.65	1.66
		(1) 1u	1.95	1.91	2431	1.84[a]	1.82	1.79
		(1) 0_u^-	2.34	2.30	2431	2.13[a,e]	2.18	2.34
		(1) 0_u^+	2.50	2.43	2431	2.37[b]	2.34	2.37
$^1\Pi_u$	2.92	(2) 1u	2.72	2.62	2431	2.49[a,f]	2.57	2.38
$^3\Pi_g$	4.17	(1) 2g	3.62	3.59	2341		3.45	3.2
		(1) 1g	3.71	3.69	2341		3.56	3.4
		(2) 0_g^+	4.21	4.17	2341 → 2422 [d]		4.09	4.1
		(1) 0_g^-	4.33	4.25	2341		4.08	4.1
$^1\Pi_g$	4.53	(3) 1g	4.49	4.41	2341		4.27	4.1
$^3\Sigma_u^+$	4.71	(2) 0_u^-	4.64	4.64	1441		4.54	4.5
		(3) 1u	4.71	4.67	1441	4.57[c]	4.58	4.57
$^3\Sigma_g^-$	5.03	(3) 0_g^+	4.36	4.29	2422 → 2341 [d]		4.19	3.9
		(2) 1g	4.84	4.71	2422		4.65	3.8
$^1\Delta_g$	5.30	(2) 2g	5.07	4.98	2422		4.98	4.2
$^1\Sigma_g^+$	5.54	(4) 0_g^+	5.79	5.64	2422 + 2242 [d]		5.65	4.4
$^1\Sigma_u^-$	5.87	(3) 0_u^-	5.02	5.10	2332		4.93	5.4
$^3\Delta_u$	5.95	(1) 3u	5.00	5.11	2332		4.91	4.7
		(2) 2u	5.66	5.73	2332		5.57	5.3
		(4) 1u	6.34	6.38	2332		6.24	5.9
$^3\Sigma_u^+$	6.04	(5) 1u	5.76	5.81	2332		5.64	5.5
		(4) 0_u^-	6.35	6.36	2332		6.25	5.6

[a]: Ref. 161. [b]: Ref. 162. [c]: Ref. 120. [d]: see discussion in section 5.4.2.

[e]: Values estimated by Tellinghuisen.

[f]: The experimental value corresponds to a maximum absorption and is not strictly comparable to our vertical excitation energy.

RAS2 space and the virtuals with energies < 2.5 Hartree were placed in the RAS3 space. This gives a configuration space of 8 million determinants that is reduced to 1 million determinants by using Abelian point group symmetry. The resulting vertical excitation energies are summarized in column 5 of table 5.3. No large differential effects are found in comparison to the DHF results.

In table 5.3 the calculated vertical excitation energies are compared with those of Teichteil and Pelissier[183], Mulliken's[182] predictions and available experimental data. An assignment is given to the states based on their main character at the ground state R_e. The ordering of the states is consistent with the ordering found by Teichteil and Pelissier but differs from the one reported by Li and Balasubramanian[193]. For example, Li *et al.* find a reverse ordering for the 1g and 2g component of the low-lying $^3\Pi_g$, and the 0_u^- component of the $^3\Sigma_u^+$ state (configuration 1441), which is found close to the 1u component of this state, is not present in their results.

There are also some differences in the ordering of the higher excited states when the results, presented here, are compared with those of Mulliken. We agree with Teichteil and Pelissier on the ordering of the states resulting from the 2422 and 1441 configurations and the differences found for the ungerade states could be a result of underestimated interactions between the ω-ω states of the different configurations in the work of Mulliken.

Vertical excitation energies of the states A' 2u ($^3\Pi_u$) and B' 0_u^- ($^3\Pi_u$) were estimated from experimental data by Tellinghuisen[161]. The excitation energy of the A' state is in close agreement with the calculated value but the B' state is found too low in comparison with the results of Teichteil and Pelissier and those presented here. Comparing the differences between our vertical excitation energies and the experimentally estimated ones with those of Teichteil and Pelissier we expect the experimental vertical excitation energy of the B' state to lie in between the value of Teichtel and Pelissier and our result.

The character of the a' (2) 0_g^+ state has been discussed in various studies. We find an avoided crossing between a' (2) 0_g^+ and (3) 0_g^+ at the ground state R_e where the two states interchange $^3\Pi_g$ ($\sigma_g^2\pi_u^3\pi_g^4\sigma_u^1$) and $^3\Sigma_g^-$ ($\sigma_g^2\pi_u^4\pi_g^2\sigma_u^2$) character. This confirms the assignment of Teichteil and Pelissier. At shorter distances the a' (2) 0_g^+ state has mainly $^3\Pi_g$ character and at longer distances it is dominated by the $^3\Sigma_g^-$ state. At the ground state R_e the contribution of both states is found to be 50%.

5.4.3 Improved potential energy curves

The calculated vertical excitation energies of the states dissociating into neutral atoms agree rather well with the experimental data. The deviations are systematic, the calculated transition energies being all about 0.1 eV larger than the measured data. As noted in section 5.4.1, the calculated bond lenghts are also all systematically too large by about 0.1 Å. The D_e and ω_e on the other hand show less regular discrepancies when compared with the experimental data. The CCSD(T) results for the ground state show that extending the COSCI calculations such as to

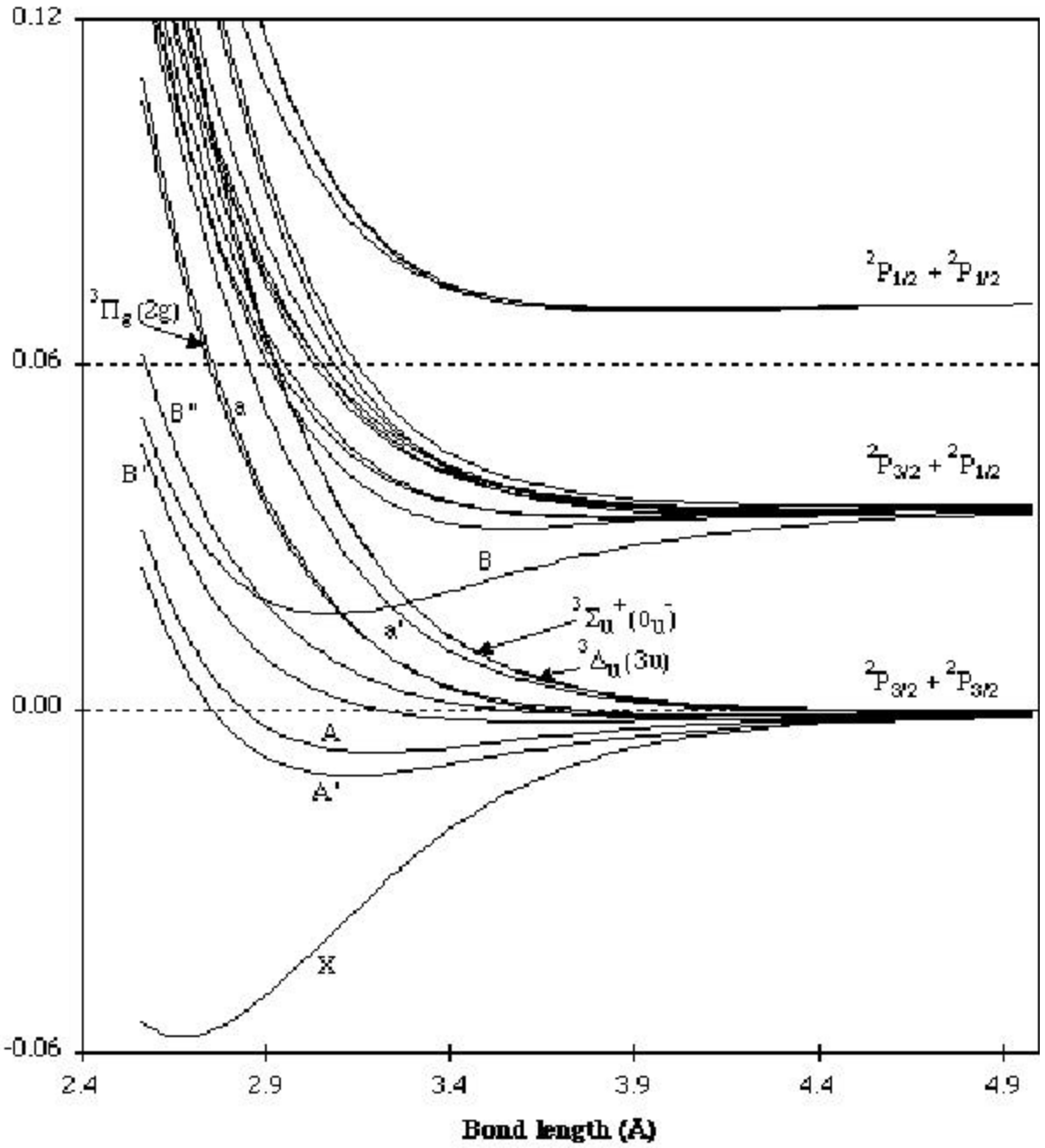

Figure 5.3. Improved relativistic potential energy curves for the excited states of I_2. (States dissociating in two $5p^5\ ^2P_J$ (J = 3/2, 1/2) iodine atoms are shown)

account for dynamical correlation could lead to substantial improvement. Such an extension e.g. by a multi-reference CI method is, however, impractical to carry out for all excited states at all points of their potential energy curves. Following Teichteil[199] improvement can be pragmatically obtained by a simple empirical correction to the ground state potential energy curve. An empirical RKR ground state is constructed[166] and the differences $\Delta E(R)$ between this curve and the calculated one are determined.

Table 5.4. Spectroscopic properties for the excited states of iodine (improved potential energy curves based on COSCI results). Experimental values and their references are given in parenthesis.

State: Ω-ω (Λ-Σ)	Dissociation products	D_e (eV)	T_e (eV)	r_e (Å)	ω_e (cm^{-1})	$\omega_e x_e$ (cm^{-1})
X: 0_g^+ ($^1\Sigma_g^+$)	$^2P_{3/2} + {}^2P_{3/2}$ (ref. 120,166)	1.556	0.000	2.666	214.5	0.65
A': 2u ($^3\Pi_u$)	$^2P_{3/2} + {}^2P_{3/2}$ (ref. 200)	0.316 (0.311)	1.241 (1.245)	3.123 (3.079)	100.9 (108.8)	0.85 (1.28)
A: 1u ($^3\Pi_u$)	$^2P_{3/2} + {}^2P_{3/2}$ (ref. 201)	0.205 (0.203)	1.351 (1.353)	3.190 (3.129)	84.9 (88.3)	1.07 (1.55)
B': 0_u^- ($^3\Pi_u$)	$^2P_{3/2} + {}^2P_{3/2}$ (ref. 159)	0.057 (0.045)	1.499 (1.511)	3.648 (4.2)	30.9 (20.5)	1.20 (0.29)
a: 1g ($^3\Pi_g$)	$^2P_{3/2} + {}^2P_{3/2}$ (ref. 165)	0.045 (0.037)	1.511 (1.505)	4.162 (4.311)	25.2 (23.6)	0.45 (0.48)
B'': 1u ($^1\Pi_u$)	$^2P_{3/2} + {}^2P_{3/2}$ (ref. 164)	0.032 (0.022)	1.525 (1.534)	4.031 (4.2)	21.2 (19.8)	0.35
2g ($^3\Pi_g$)	$^2P_{3/2} + {}^2P_{3/2}$	0.031	1.525	4.226	21.6	0.49
3u ($^3\Delta_u$)	$^2P_{3/2} + {}^2P_{3/2}$	0.013	1.543	4.756	13.9	0.79
a': (2) 0_g^+	$^2P_{3/2} + {}^2P_{3/2}$ (ref. 165)	0.012 (0.017)	1.544 (1.539)	4.681 (4.641)	15.1 (17.7)	0.85 (0.43)
(2) 0_u^-	$^2P_{3/2} + {}^2P_{3/2}$	0.006	1.550	4.803	10.9	0.67
B: 0_u^+ ($^3\Pi_u$)	$^2P_{3/2} + {}^2P_{1/2}$ (ref. 166)	0.517 (0.543)	2.009 (1.955)	3.070 (3.024)	119.3 (125.7)	0.65 (0.76)
(3) 0_g^+	$^2P_{3/2} + {}^2P_{1/2}$ (ref. 202)	0.114 (0.107)	2.412 (2.391)	3.563 (3.645)	72.9 (64.4)	1.02 (1.23)
1g ($^1\Pi_g$)	$^2P_{3/2} + {}^2P_{1/2}$ (ref. 181)	0.070 (0.058)	2.457 (2.441)	3.913 (4.05)	32.1 (29.6)	0.58
0_g^- ($^3\Pi_g$)	$^2P_{3/2} + {}^2P_{1/2}$	0.058	2.468	3.851	32.7	0.60
b': 2u ($^3\Delta_u$)	$^2P_{3/2} + {}^2P_{1/2}$ (ref. 163)	0.040 (0.037)	2.486 (2.461)	4.183 (4.25)	25.7	0.61
1g ($^3\Sigma_g^-$)	$^2P_{3/2} + {}^2P_{1/2}$	0.032	2.495	4.273	22.1	0.54
(3) 0_u^-	$^2P_{3/2} + {}^2P_{1/2}$	0.029	2.497	4.319	20.7	0.48
C: 1u ($^3\Sigma_u^+$)	$^2P_{3/2} + {}^2P_{1/2}$	0.029	2.497	4.322	20.8	0.51
2g ($^1\Delta_g$)	$^2P_{3/2} + {}^2P_{1/2}$	0.022	2.504	4.415	18.3	0.42
1u ($^3\Sigma_u^+$)	$^2P_{3/2} + {}^2P_{1/2}$	0.008	2.518	4.673	12.6	0.93

Table 5.4. Continued from previous page.

State: Ω-ω (Λ-Σ)	Dissociation products	D_e (eV)	T_e (eV)	r_e (Å)	ω_e (cm^{-1})	$\omega_e x_e$ (cm^{-1})
0_g^+ ($^1\Sigma_g^+$)	$^2P_{1/2} + {}^2P_{1/2}$	0.054	3.442	3.928	33.8	0.91
(4) 0_u^-	$^2P_{1/2} + {}^2P_{1/2}$	0.053	3.444	3.918	33.3	0.95
1u ($^3\Delta_u$)	$^2P_{1/2} + {}^2P_{1/2}$	0.045	3.452	3.991	28.2	0.68

The calculated energies at each point R of all excited states are then shifted by $\Delta E(R)$ and again fitted to a curve as described before. The resulting corrected potential energy curves are shown in figure 5.3 together with their assignment.

Table 5.4. displays the spectroscopic properties derived from these curves and it is seen that there is good agreement with the experimental data that is available for some of the states.

Much experimental work concerns the predissociation of the B 0_u^+ state. The potential energy curves of states, responsible for the predissociation processes, should be nearby or crossing the B state. The B' (1) 0_u^- state, which can be assigned as a $^3\Pi_u$, lies below the curve of the B state. States that cross the potential energy curve of the B ($^3\Pi_u$) state, and that can contribute to predissociation of the B state, are the B'' 1u, a 1g, a' 0_g^+ and the (2) 0_u^- respectively. These four states all cross the B curve at low vibrational level. We will now discuss the position, relative to the B state, and the character of these four states. The B'' 1u, which has $^1\Pi_u$ character crosses the inner limb of the B curve around the vibrational quantum numbers $\nu = 4, 5$ which is in agreement with the experimental findings[167]. The potential energy curve of the a 1g ($^3\Pi_g$) state crosses the B state at the outer limb close to the equilibrium distance ($\nu = 0$). The $^3\Pi_g$ (2g) state lies close to the a 1g ($^3\Pi_g$) state and crosses this state below the crossing with the B state. The curves of the a' 0_g^+ and the (2) 0_u^- state cross the outer limb of the B state curve at vibrational numbers around $\nu = 2$ and $\nu = 3, 4$ respectively. The character of the a' 0_g^+ state, which is mainly $^3\Sigma_g^-$ ($\sigma_g{}^2\pi_u{}^4\pi_g{}^2\sigma_u{}^2$) at the crossing point, has been discussed at the end of the previous section. Teichteil and Pelissier discussed the character of the (2) 0_u^- state and the interaction with the (3) 0_u^- and (4) 0_u^- states, resulting from the configurations $\sigma_g{}^2\pi_u{}^3\pi_g{}^3\sigma_u{}^2$ ($^1\Sigma_u^-$, $^3\Sigma_u^+$) and $\sigma_g{}^1\pi_u{}^4\pi_g{}^4\sigma_u{}^1$ ($^3\Sigma_u^+$). At short distances the (2) 0_u^- state has $^3\Sigma_u^+$ ($\sigma_g{}^1\pi_u{}^4\pi_g{}^4\sigma_u{}^1$) character whereas the other two states have $\sigma_g{}^2\pi_u{}^3\pi_g{}^3\sigma_u{}^2$ ($^1\Sigma_u^-$, $^3\Sigma_u^+$) character. Around 2.78 Å an avoided crossing between the (2) 0_u^- state and the (3) 0_u^- state occurs where the two states exchange their character. The (2) 0_u^- state shows mainly $\sigma_g{}^2\pi_u{}^3\pi_g{}^3\sigma_u{}^2$ ($^1\Sigma_u^-$, $^3\Sigma_u^+$) character at the crossing with the B state and at longer distances. These results are comparable with the ones found by Teichteil and Pelissier. An analysis of the singlet or triplet character of the two 0_u^- states resulting from the configuration $\sigma_g{}^2\pi_u{}^3\pi_g{}^3\sigma_u{}^2$,

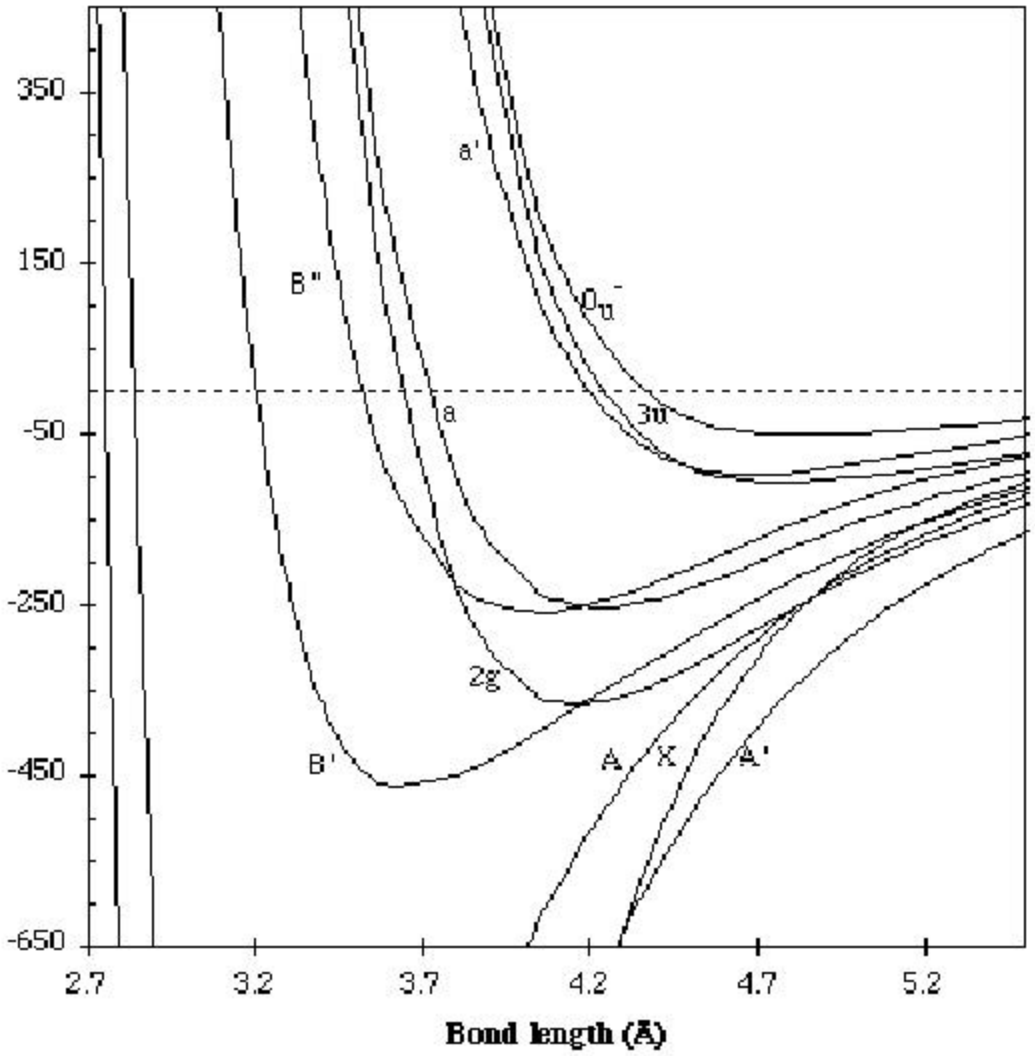

Figure 5.4. Close up of the weakly bound states B" $^1\Pi_u$, a 1g, a' (0_g^+) and (2) 0_u^-.

as was performed by Teichteil and Pelissier, is not straightforward to obtain due to the implicit interaction between the states in a relativistic description.

Tellinghuisen[162] performed experiments on a number of weakly bound states, B' $^3\Pi_u$ (0_u^-), B" $^1\Pi_u$ (1u), a $^3\Pi_g$ (1g) and a' 0_g^+, and generated potential energy curves for the lower parts of these states. Only parts of the curves are known, other parts are estimated by extrapolation. Figure 5.4 shows a magnified picture of our calculated potential energy curves. These curves are in good agreement with the findings of Tellinghuisen. The crossings of the B" 1u state with the a 1g state and the a' 0_g^+ state are found to be around vibrational number $\nu = 5, 6$ and $\nu = 1, 2$ respectively.

Experimental data are available for a number of other states of which the assignment will now be discussed. The assignment of the b' 2u state to a $^3\Delta_u$ by Tellinghuisen[163] is confirmed by the calculations presented here. Ishiwata *et al.* [202] found a weakly bound state which can be assigned to the (3) 0_g^+ state. Its character has been discussed before in combination with the assignment of the a' state.

Viswanathan and Tellinghuisen[159] measured the spectroscopic properties of the B' 0_u^- state ($^3\Pi_u$ character). They used a rough estimate for R_e to fit simulations of the experimental data which differs somewhat from the one calculated in this work. Jewsbury *et al.* [181] determined spectroscopic properties for the c 1g state and also discussed the character of this state. The character of the c 1g state is mainly $^1\Pi_g$ which is in agreement with the experimental findings.

5.5 The ionized states of iodine

Experimental spectroscopic data are available for the three lowest states of I_2^+, the ground states (X) $^2?_g$ (3/2g) and $^2?_g$ (1/2g) and the first excited state (A) $^2?_u$ (3/2u). Assignment and interpretation of experimental data for the higher lying states is found to be more difficult due to the complexity of the spectrum. Of the higher lying states, only the vertical excitation energies of the A state $^2?_u$ (1/2u) and B state $^2?_g^+$ (1/2g) have been identified. Very recently Cockett *et al.* [180] determined the spectroscopic properties of a new state which they assigned to a $^4\Sigma_u^-$ (3/2) on basis of the only set of theoretically calculated potential energy curves available. To date there is only one set of theoretically calculated potential energy curves available[193]. Unfortunately this set shows rather large discrepancies with other experimental data.

We first present spectroscopic data for the lowest states calculated with a single-reference approach. The first four states are described as single determinants with a hole in the $\pi_{g,1/2}$, $\pi_{g,3/2}$, $\pi_{u,1/2}$ or $\pi_{u,3/2}$ molecular spinor respectively, the highest occupied spinors in their corresponding representations. The $^2?_g^+$ (1/2 g) state is obtained by removing an electron from the highest occupied $\sigma_{g,1/2}$ spinor. The spinors resulting from DHF calculations on each of these states are used in subsequent CCSD(T) calculations in order to account for dynamical correlation corrections. The results of these calculations are discussed in section 5.5.1.

Experimental data show that the higher lying states are thoroughly mixed by spin-orbit interaction similar to what we have met in treating the neutral excited states. In section 5.5.2 we therefore use the COSCI approach which allows us to study the mixing of the states in a balanced way. In the average of configurations open-shell DHF all configurations resulting from all possible distributions of 9 electrons over the $\sigma_g^k\pi_u^l\pi_g^m\sigma_u^n$ (where k+l+m+n=9) set of molecular spinors are taken into account. This means that the high-lying states, which dissociate to a double cation (I^{2+}) and an ion (I^-), are included in the calculation. The data from the COSCI calculations are used to generate the potential energy curves of the ionized states. At the ground state equilibrium distance we have also carried out additional MRSDCI calculations, with the states from the COSCI calculation as references.

5.5.1 State-optimized calculations

The potential energy curves for the four $^2\Pi$ states and the $^2\Sigma$ state are obtained by fitting the results of calculations on grids of at least nine points to a fourth-order polynomial. For the correlation calculations a total of 136 spinors is used consisting of 103 virtual spinors (some high-energy solutions were not

included) and 33 occupied spinors representing the 5s and 4d cores and the occupied 5p spinors. All calculations are performed relativistically as well as non-relativistically. The results of calculations on the vertical ionization energy, ω_e and D_e are summarized in table 5.5 where they are compared with the available experimental data and other theoretical work. Correlation has a large effect on properties like the ω_e and the R_e but the effect on the spin-orbit splitting is small.

Table 5.5. Calculated vertical ionization energy (I_v), ω_e and R_e for the four lowest states of I_2^+, compared with experimental and other theoretical data.

Property		$^2?_g$ (3/2)	$^2?_g$ (1/2)	$^2?_u$ (3/2)	$^2?_u$ (1/2)	$^2?_g^+$
I_v (eV)[a]	NR-HF	9.36		11.54		12.12
	DHF	8.94	9.51 (0.57)	11.10 (2.16)	11.85 (2.91)	12.18 (3.24)
	DHF + CCSD(T)	9.13	9.74 (0.62)	10.97 (1.84)	11.65 (2.52)	12.77 (3.64)
	Li *et al.* [193]	8.62	9.38 (0.76)	10.19 (1.57)	10.82 (2.20)	---
	Experiment[176]	9.31	9.95 (0.64)	---	---	---
	Experiment[175]	9.34	9.98 (0.64)	10.96 (1.62)	11.81 (2.47)	12.95 (3.61)
ω_e (cm^{-1})	NR-HF	277		211		124
	DHF	270	233	199	207	174
	DHF + CCSD(T)[b]	238	227	140	156	---
	Li *et al.* [193]	217	208	132	112	72
	Experiment[176,180]	240 (±1)	230 (±2)	138 (±2)	---	---
	Experiment[175]	220 (±8)	214 (±8)	Average 128 (±8)		---
R_e (Å)	NR-HF	2.575		2.805		3.043
	DHF	2.571	2.604	2.820	2.804	2.921
	DHF + CCSD(T)[b]	2.613	2.626	2.949	2.910	---
	Li *et al.* [193]	2.69	2.69	3.09	3.11	3.62
	Experiment[174]	2.58	2.58	2.99	2.98	---

[a]. Relative energies are given in parenthesis.

[b]. Correlated potential energy curve of $^2\Sigma_g^+$ state has large mixing with other states and cannot be studied with the CCSD(T) method. Calculated spectroscopic properties for the four lowest states of I_2^+, compared with experimental and other theoretical data.

We will now discuss our results for the three spectroscopic properties presented and compare them with the available experimental data and other theoretical results. The vertical ionization energies are calculated at the experimental ground state R_e. The spin-orbit splittings of the $^2\Pi_g$ (3/2) and $^2\Pi_g$ (1/2) states agree well with the experimental data. The splitting of the $^2\Pi_u$ states is larger than the splitting of the $^2\Pi_g$ states but smaller than the measured values. This larger spin-orbit splitting of the $^2\Pi_u$ states

was partially explained by Dyke *et al.* [194]. They attribute the difference to the off-diagonal spin-orbit interaction between the $\pi_{1/2}$ and $\sigma_{1/2}$ spinors for gerade and ungerade states, an interaction that is inherently accounted for in a fully relativistic approach. The differences between the calculated and measured spin-orbit splittings must therefore be attributed to multi-reference effects (see end of this section). Li and Balasubramanian[193], using a multi-reference approach, however, find the spin-orbit splitting of the $^2\Pi_u$ states smaller than the splitting of the $^2\Pi_g$ states (0.63 eV and 0.76 eV respectively).

The ω_e calculated for the $^2\Pi_g$ states and the $^2\Pi_u$ (3/2) state compare well with the accurate ZEKE-PFI experiments of Cockett *et al.* [176,180]. No ω_e for the $^2\Pi_u$ (1/2) state is deduced from these experiments. From threshold photoelectron spectroscopy[175] only an averaged frequency for the two $^2\Pi_u$ states is available . The frequencies reported for the gerade states are lower than found in the newer ZEKE-PFI results. Li *et al.* arrive at a frequency for the $^2\Pi_u$ (1/2) state that is 20 cm^{-1} smaller than that of the $^2\Pi_u$ (3/2) state, which is similar to the results of Boerrigter *et al.* [203] for the Br_2^+ molecule.This shift is attributed to the spin-orbit allowed mixing with nearby states, for example the large mixing of the $^2\Pi_u$ (1/2) with a $^2\Sigma_u^+$ (1/2) state. Such mixing cannot be accounted for in single reference CCSD(T).

The calculated R_e are presented in the last part of table 5.5. Based on the bonding character of the orbitals of the neutral molecule the bond lengths of the four Π states are expected to be ordered as $^2\Pi_g$ (3/2g) < $^2\Pi_g$ (1/2g) << $^2\Pi_u$ (1/2u) < $^2\Pi_u$ (3/2u). Through spin-orbit interaction the bonding $\pi_{u,1/2}$ spinor acquires anti-bonding character by mixing in of the $\sigma_{u,1/2}$, whereas the $\pi_{u,3/2}$ remains a pure bonding spinor. Therefore the $^2\Pi_u$ (1/2) will have a shorter R_e then the $^2\Pi_u$ (3/2) state. The anti-bonding $\pi_{g,1/2}$ spinor gets some bonding character from the $\sigma_{g,1/2}$ spinor yielding a longer R_e for the $^2\Pi_g$ (1/2) state compared to the $^2\Pi_g$ (3/2). This ordering is indeed found (see table 5.5) and is in agreement with bond lenghts estimated from experimental data.

We mentioned earlier that the properties of the $^2\Pi_u$ (1/2) state will be affected by non-dynamical correlation in a way similar to that discussed for Br_2^+ by Boerrigter *et al.* [203]. The $^2\Sigma_g^+$ state, which lies even higher in the spectrum, is expected to be heavily influenced by these effects and it has therefore not been discussed as yet. From CCSD correlation calculations information on the growing importance of non-dynamical correlation can be estimated using the T1 diagnostic value[204]. For the two $^2\Pi_g$ states and the $^2\Pi_u$ (3/2) state the diagnostic values are small whereas the values of the $^2\Pi_u$ (1/2) state reaches the critical values proposed in various papers. The T1 diagnostic values of the (B) $^2\Sigma_g^+$ state become very large

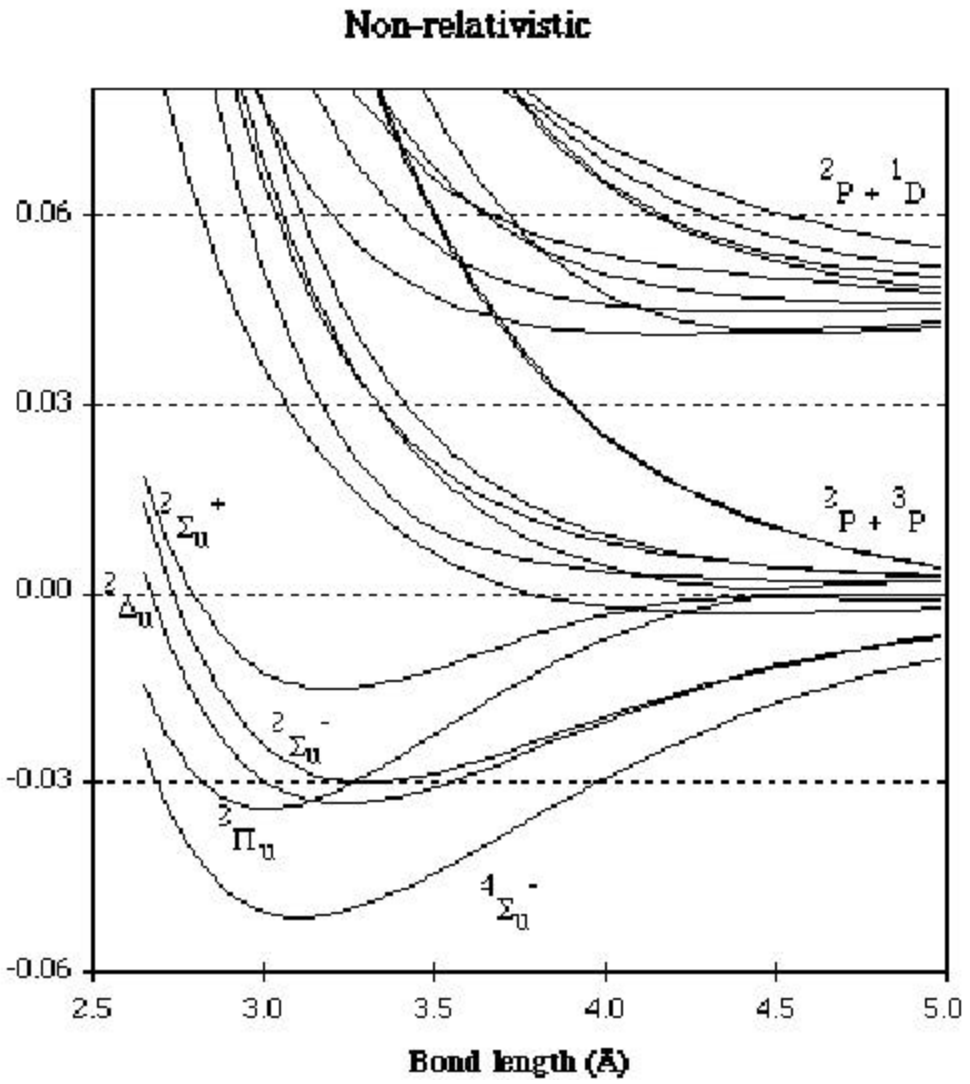

Figure 5.5. Non-relativistic (left page) and relativistic (right page) potential energy curves for the lowest ungerade states of I_2^+. Relativistic dissociation limits: D1 = $^2P_{3/2}$ + $^3P_2$; D2 = $^2P_{3/2}$ + $^3P_0$, $^2P_{3/2}$ + $^3P_1$ and $^2P_{1/2}$ + $^3P_2$; D3 = $^2P_{1/2}$ + $^3P_0$, $^2P_{1/2}$ + $^3P_1$ and $^2P_{3/2}$ + $^1D_2$.

(0.05-0.06) when going to distances longer than the ground state equilibrium distance and the calculated correlated results are hence unreliable. For this reason the correlated results of the relativistically calculated ω_e and R_e are not presented here. When non-dynamical correlation becomes important one requires a multi-reference description from the start. In section 5.5.2 the effects of a multi-reference description will be studied using an average of configuration approach in which all the states are explicitly included in the calculations.

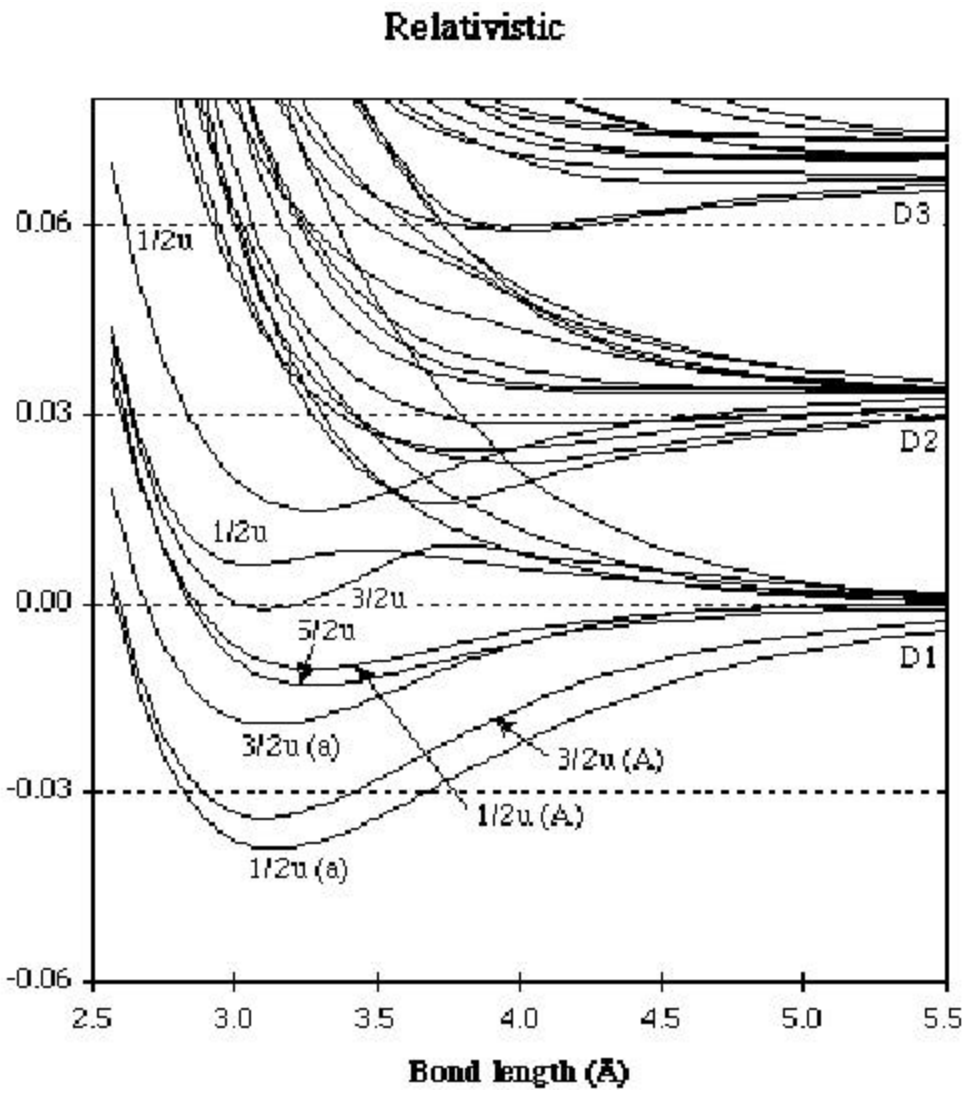

5.5.2 The potential energy curves of ionized iodine

The non-relativistic and relativistic potential energy curves of the states that dissociate into the atom and its cation ($I+I^+$) are obtained from COSCI calculations for about 50 different bond distances. In figures 5.5 and 5.6 the non-relativistic and relativistic potential energy curves for the lowest ionized states are presented, grouped by their parity. Extensive configuration interaction, due to spin-orbit coupling, is found, which makes it difficult to assign Λ-Σ state characters to the potential energy curves. The low lying states can still be identified but the

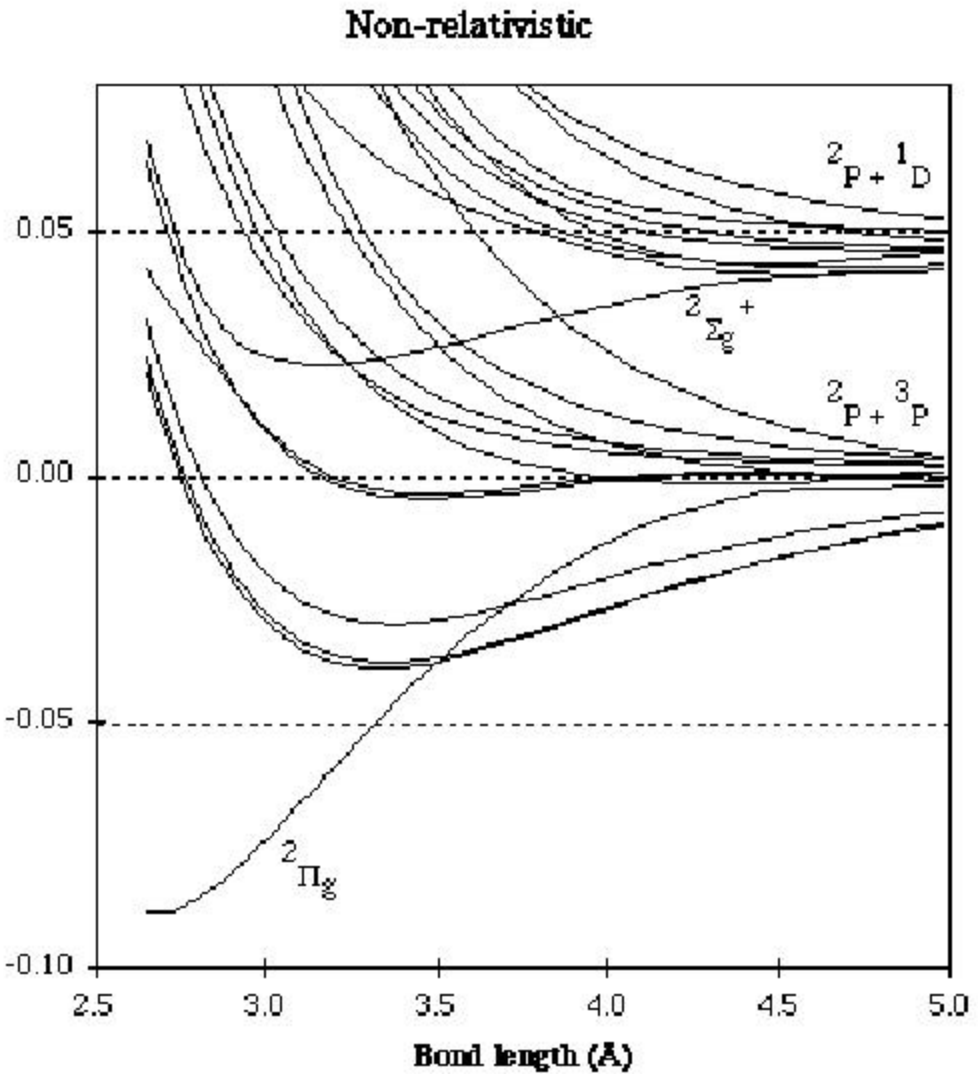

Figure 5.6. Non-relativistic (left page) and relativistic (right page) potential energy curves for the lowest gerade states of I_2^+. Relativistic dissociation limits: D1 = $^2P_{3/2}$ + $^3P_2$; D2 = $^2P_{3/2}$ + $^3P_0$, $^2P_{3/2}$ + $^3P_1$ and $^2P_{1/2}$ + $^3P_2$; D3 = $^2P_{1/2}$ + $^3P_0$, $^2P_{1/2}$ + $^3P_1$ and $^2P_{3/2}$ + $^1D_2$.

complexity increases when one goes to states higher up in the spectrum. Hunds case (c) notation will be used except for those states that have clear Λ-Σ character.

The relative energies of the calculated dissociation limits for the states dissociating into the neutral atom and its cation are in close agreement with numerical atomic calculations (errors less then 0.05 eV). To discuss the assignment of experimentally determined states the spectroscopic properties of the potential energy curves are calculated. These properties show discrepancies from experimental data similar to those discussed for the excited states of the neutral molecule and here too improvement is obtained by applying a simple empirical

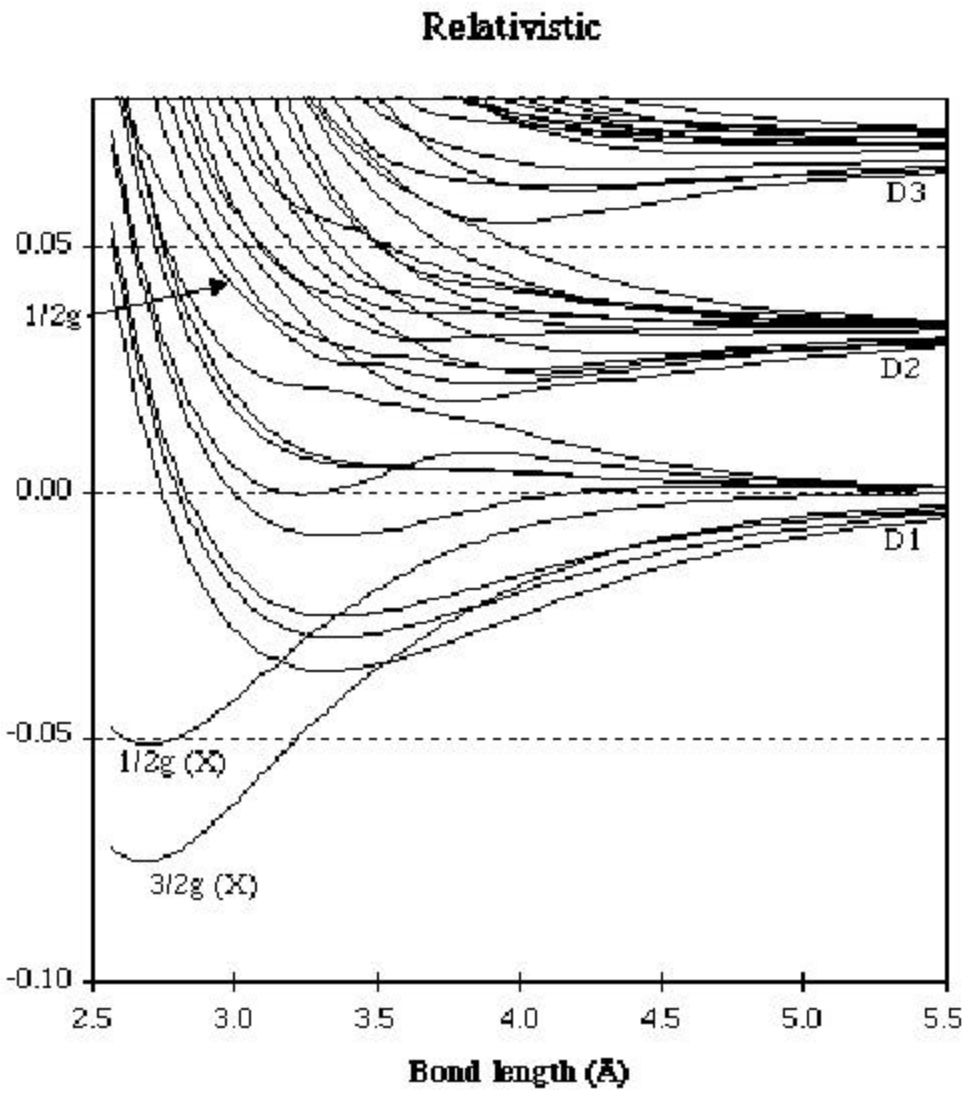

correction to the lowest potential energy curve (see section 5.4.3). No RKR curve is known for the $^2\Pi_g$ (3/2) ionized state and therefore a Morse potential, based on the experimental data of Cockett *et al.* [176,180], is used for the correction. The properties of some of these improved curves, calculated using the VIBROT program of the MOLCAS[197] package, and the vertical excitation energies are collected in table 5.6. These properties are expected to be less accurate than those calculated for the excited states of the neutral molecule because of the simple Morse form used for the correction.

Table 5.6. Relative vertical ionization energies of some selected low lying states of the I_2^+ molecule. For a number of states also other properties are given. The notation klmn, used for the main configurations, is based on $\sigma_g^k\pi_u^l\pi_g^m\sigma_u^n$.

State symm. Ω-ω	Relative vertical ionization energy (eV) COSCI	MRCISD	Exp.[175]	Li *et al.*[193]	D_e (eV)	ω_e (cm^{-1})	$\omega_e x_e$ (cm^{-1})	Main configurations and assignment
3/2g	0.00	0.00	0.00	0.00	2.70	240	0.69	X: 2430 ($^2\Pi_g$)
1/2g	0.65	0.63	0.64	0.76	2.03	230	0.76	X: 2430 ($^2\Pi_g$)
1/2u	1.64	1.68			1.38	137	0.29	a: 2421 ($^4\Sigma_u^-$)
3/2u	1.71	1.68	1.62	1.57	1.26	141	0.32	A: 2340 ($^2\Pi_u$) + 2421 ($^4\Sigma_u^-$)
3/2u	2.09	2.06			0.85	133	0.37	a: 2421 ($^4\Sigma_u^-$) + 2340 ($^2\Pi_u$)
1/2g	2.44	2.50			1.23	242		2331
1/2u	2.55	2.44	2.47	2.22	0.56	117	0.38	A: 2340 ($^2\Pi_u$) + 2421
3/2u	2.57	2.56			0.62	120	0.38	2421 ($^2\Delta_u$)
1/2g	2.68	2.81						2331
1/2g	3.69	3.67						2331
1/2g	3.85	3.88						2331 + 1440 ($^2\Sigma_g^+$)
1/2g	3.97	3.76	3.61	3.46				B: 1440 ($^2\Sigma_g^+$) + 2331

The vertical ionization energies are calculated at the experimental R_e of the ground state. MRCISD calculations are performed to study the effects of dynamical correlation and relaxation on the vertical ionization energies and thereby on the position of the potential energy curves. The CI contains the anti-bonding 5s spinor in RAS1, the 5p spinors in RAS2 (i.e. the states from the COSCI calculation) and 96 virtual spinors in RAS3. The latter number encompasses all virtuals except for those with energies higher than 4 Hartree. Determinants resulting from all single and double excitations between the different spaces are included. This results in a CI space of 9 million determinants which is reduced to 1 million by using Abelian point group symmetry. The calculated vertical ionization energies of the four low lying Π states as well as the spin-orbit splitting are in close agreement with the experimental findings. Only small correlation effects are found for the two (X) $^2\Pi_g$ states and their spectroscopic properties are in close agreement with the single reference results of section 5.5.1. For the (A) $^2\Pi_u$ states considerable admixture of states from different configurations is found. This mixing does not affect the properties of

the $^2\Pi_u$ (3/2) state, which are still close to the results of the single reference calculation of section 5.5.1, but it has a large influence on the ω_e of the $^2\Pi_u$ (1/2) state. This quantity is now 24 cm^{-1} smaller than the value found for the $^2\Pi_u$ (3/2) state which is in better agreement with the multi-reference approach of Li *et al.* [193].

With the calculated data one can now discuss the assignments of these states as they were made by Cockett *et al.* [180] and in the theoretical work of Li and Balasubramanian. We will first discuss the assignment of the ungerade states (A) $^2\Pi_u$ (3/2), (A) $^2\Pi_u$ (1/2) and a $^2\Pi_u$ (1/2) and after that we will consider the gerade states including the ground state. Boerrigter *et al.* [203] attributed the large difference in the ω_e of the two $^2\Pi_u$ states for the Br_2^+ molecule to the difference, induced by spin-orbit coupling, in the configuration interaction with states from the $\sigma_g{}^2\pi_u{}^4\pi_g{}^2\sigma_u{}^1$ configuration i.e. between the $^2\Sigma_u{}^+$ (1/2) and the $^2\Pi_u$ (1/2) states on the one hand and the $^2\Delta_u$ (3/2) and $^2\Pi_u$ (3/2) states on the other. A similarly large difference between the ω_e of the two $^2\Pi_u$ states is found in our calculations on I_2^+ and was also reported by Li *et al.* [193]. However, we find that the properties of the $^2\Pi_u$ (1/2) state are influenced by the $^2\Sigma_u{}^+$ (1/2) state whereas these authors find an interaction with the $^4\Sigma_u{}^-$ (1/2) state. They also find that the $^2\Pi_u$ (3/2) state is unperturbed while our calculations show a strong interaction with the $^4\Sigma_u{}^-$ (3/2) state. This interaction was suggested earlier, based on experimental data, by Jungen[196], Leach[173] and Mason and Tuckett[174]. At larger bond lengths (above 2.9Å) the $^2\Pi_u$ (3/2) state starts to interact with the $^2\Delta_u$ (3/2) state, as found in the Br_2^+ molecule by Boerrigter *et al.*

Cockett *et al.* measured two ungerade states, "a" and "A" with ionization energies that differ only by 0.05eV, which they assigned to $^4\Sigma_u{}^-$ (3/2) and $^2\Pi_u$ (3/2) respectively. We find the lowest ungerade state to be $^4\Sigma_u{}^-$ (1/2) with a state of 3/2u symmetry just 0.07eV above it. A second state of this symmetry is found at 0.38eV above the $^4\Sigma_u{}^-$ (1/2) state. Both states are mixtures of $^2\Pi_u$ (3/2) and $^4\Sigma_u{}^-$ (3/2) at the ground state R_e with the lowest 3/2u state having a somewhat larger $^2\Pi_u$ (3/2) character. The character of the two 3/2u states reverses when going to longer distances, giving a lower state with more $^4\Sigma_u{}^-$ (3/2) character and the higher 3/2u state now also has considerable contributions from the $^2\Delta_u$ (3/2) state.

The calculated D_e and ω_e are in reasonable agreement with the experimental data of Cockett *et al.*, considering the approximations that were made. On the basis of the relative positions of the potential energy curves and the agreement with the calculated spectroscopic properties (table 5.6), we assign the "a" state, measured by Cockett *et al.*, to $^4\Sigma_u{}^-$ (1/2). The measured A state is assigned to a mixed state of $^2\Pi_u$ (3/2) and $^4\Sigma_u{}^-$ (3/2) character.

We will now turn to the three measured states with gerade symmetry, the two (X) $^2\Pi_g$ states and the (B) $^2\Sigma_g{}^+$ state. From the calculated properties of the improved potential energy curves that agree closely with experimental results one can easily assign the $^2\Pi_g$ states. The (B) $^2\Sigma_g{}^+$ state, resulting from the $\sigma_g{}^1\pi_u{}^4\pi_g{}^4$ configuration, non-relativistically (figure 5.6) dissociates into the atomic states $^1D + {}^2P$. In the non-relativistic calculations an avoided crossing with a $^2\Sigma_g{}^+$ state from the $\sigma_g{}^2\pi_u{}^4\pi_g{}^2\sigma_u{}^1$ configuration is found at short distance where these states exchange their character. The potential energy

curve of the B state crosses a large number of states which could interact with this state through spin-orbit coupling. Extensive mixing is indeed found in the relativistic calculations. The vertical excitation energy of the B $^2\Sigma_g^+$ state is 0.35 eV higher than the experimental value. Some improvement is found when a MRCISD calculation is performed on top of the COSCI calculations but the value is still 0.15 eV above the experimental value. Extensive correlation calculations on the whole potential energy curve of the B state, and most of the higher lying ionized states, are required to be able to discuss the detailed form of the potential energy curve presented by Leach. Li *et al.* found a global maximum at longer distances, one of the features of the potential energy curve suggested by Leach. This global maximum is also found in our empirically improved potential energy curve(s) but we cannot exclude that the missing large correlation corrections may considerably influence the form and position of the potential energy curve.

5.6 Conclusions

The spectroscopic properties and potential energy curves of the ground state and the most important excited and ionized states of I_2 are calculated within a 4-component relativistic framework. For the ground state relativity and correlation must be included in order to get results that are in close agreement with experimental data. It is shown that the remaining differences between the experimental and calculated relativistic values can be attributed to basis set effects and core-valence correlation effects. Core-valence correlation, by including excitations from the 4s, 4p, 4d and 5s spinors, results in a bond length contraction of 0.02 Å, comparable to the 0.03 Å that was obtained from semi-empirical corrected pseudopotentials.

The spectroscopic properties of the set of excited states that dissociate into neutral atoms are well described when the calculated potential energy curves are collectively subjected to a simple empirical correction proposed by Teichteil[199]. Our calculated vertical excitation energies agree closely with those of Teichteil and Pelissier[183] but differ from the results of Li and Balasubramanian[193]. We have analyzed the position and character of the states B'' 1_u, a 1_g, a' 0_g^+ and 0_u^- that are responsible for the predissociation of the B state. The character of the a' state at the crossing point is $^3\Pi_g$ but at shorter bond distances this state has $^3\Sigma_g^-$ character due to an avoided crossing. For the (2) 0_u^- state we also find an avoided crossing resulting in $\sigma_g{}^1\pi_u{}^4\pi_g{}^4\sigma_u{}^1$ ($^3\Sigma_u^+$) character at short bond distances and $\sigma_g{}^2\pi_u{}^3\pi_g{}^3\sigma_u{}^2$ ($^1\Sigma_u^-$, $^3\Sigma_u^+$) character at longer distances that include the crossing point with the B state. These results corroborate the findings of Teichteil and Pelissier. The potential energy curves of some weakly bound states are in close agreement with the deductions from experiment of Tellinghuisen[162].

For the ionized states, the spectroscopic properties of the two (X) $^2\Pi_g$ states are well reproduced by our calculations. Non-dynamical correlation effects must be included in order to obtain good results for the properties and the spin-orbit splitting of the two (A) $^2\Pi_u$ states. We find that the $^2\Pi_u$ (3/2) state strongly interacts with the $^4\Sigma_u^-$ (3/2) state arising from the configuration $\sigma_g{}^2\pi_u{}^4\pi_g{}^2\sigma_u{}^1$, whereas the $^2\Pi_u$ (1/2) state mixes with the $^2\Sigma_u^+$ (1/2) state of this configuration. This differs from the analysis of Li

et al. A new state measured by Cockett *et al.* [180] is reassigned to the (unperturbed) $^4\Sigma_u^-$ (1/2) based on the calculated spectroscopic properties. The first "A" state is assigned to a mixed state of $^2\Pi_u$ (3/2) and $^4\Sigma_u^-$ (3/2). Extensive correlation treatment and multi-configuration calculations are required to obtain good potential energy curves for higher ionized states, like the (B) $^2\Sigma_g^+$, of iodine.

Chapter 6

Relativity and the chemistry of UF_6

In this chapter calculations are presented on the electronic structure and bonding of UF_6 and UF_6^-. A stronger bonding but more ionic molecule is found if one compares the relativistic with the non-relativistic results. The first peak in the photo electron spectrum of Karlsson *et al.* is assigned to the $12\gamma_{8u}$ component of the $4t_{1u}$ orbital in agreement with other theoretical and experimental results. Good agreement is found between the experimental and theoretical 5f spectrum of UF_6^-. Some properties, like the dissociation energy and electron affinity, are calculated and the necessity of a fully relativistic framework is shown. The Breit interaction has effect on the core spinors and the spin-orbit splitting of these spinors but the influence on the valence spectrum is negligible.

6.1 Introduction

Properties of actinide elements, like uranium, and of molecules that contain these elements are heavily influenced by relativity. The main effects are due to spin-orbit interaction and mass-velocity and Darwin terms, which result in a substructure and in a contraction or expansion of the electronic shells. This affects the total electronic structure, reactivity and bonding properties of molecules that contain heavy elements from a practical and chemical point of view. Uranium hexafluoride (UF_6) is of great interest for the enrichment process of uranium by for example molecular laser isotope separation[205]. For these reasons the molecule is the subject of a considerable amount of experimental[206-215] and theoretical[216-228] work.

The methods that are used for electronic calculations on UF_6 are various but, except for the Relativistic Effective Core Potential (RECP) plus spin-orbit corrections approach[222,223], no rigorous *ab initio* methods have been used. For the first calculations on UF_6 a non-relativistic Xa scattered wave method has been used[216,217,219,229]. Koelling *et al.* [220] used the Dirac equation as the physical starting point in

their calculations with the Dirac-Slater (DS) discrete variational method. The relativistic effects showed their importance for the properties of the UF_6 molecule and Rosén[221] demonstrated that the relativistic DS method reproduced experimental data better than the non-relativistic methods. Hay *et al.* [222,223] use a non-relativistic *ab initio* approach that is extended with relativistic corrections like the RECP, which will handle the contraction and expansion of the inner shells due to the mass-velocity and Darwin terms, and spin-orbit operators. To date, no attempts were made to use a fully relativistic *ab initio* method, such as a 4-component Dirac-Hartree-Fock (DHF) approach with correlation, on such a molecule. Programs to perform such calculations are hardly available and the computational effort required is considerably larger than that in approaches mentioned above.

In this chapter a study of the relativistic and correlation effects on the electronic structure and the chemical bonding of UF_6 is made using the 4-component DHF plus configuration interaction (CI) method. In section 6.3 results for the uranium atom are presented. Results of the calculation on the ground state of UF_6 are given in section 6.4. The influence of relativity on the chemical bonding of uranium and fluorine is discussed on the basis of a Mulliken population analysis. An assignment of the photo electron spectrum is made on the basis of the calculated results and a comparison is made with other computational results. In section 6.5 results are presented of calculations on the electronic spectrum of UF_6^-. The electron affinity is calculated and compared with other theoretical and experimental data.

6.2 Computational model

The UF_6 molecule has been measured in the gasphase and has octahedral symmetry. Therefore all the calculations, including the atomic calculations and those on the, are performed using the O_h point group symmetry. In the relativistic calculations the 4-component spinors hence span the representations of the octahedral (O_h^*) double-group. In this chapter these representations will be labelled as γ_{6g}, γ_{6u}, γ_{7g}, γ_{7u} for the two-dimensional and γ_{8g}, γ_{8u} for the four-dimensional representations.

The uranium basis was derived from a non-relativistically optimized 24s18p14d12f Gaussian basis[230] with a finite nucleus approximation. This basis was reoptimized under the constraint that the d-exponents form a subset of the s-exponents. The advantage of this constraint is that the primitive basis for the small component p-functions, as obtained by kinetic balance, is already contained in the small component functions that arise from the large component s-exponents which reduces the total number of primitives significantly. The f-exponents were reoptimized with a similar constraint to form a subset of the p-exponents. For the reoptimization the non-relativistic ASCF program[231] was used because a relativistic exponent optimization program was not yet available. It is "expected" that the exponents will get higher values in the core region and that the exponents representing the 5f and 6d would get a more diffuse character in the valence region.

Table 6.1. Basis set sizes.

		Large component		Small component	
		Primitive	Contracted	Primitive	Contracted
U basis	rel.	24s21p16d13f	10s13p11d8f	21s24p21d16f13g	8s17p18d11f8g
	non-rel.	24s21p16d13f	10s8p7d6f		
F basis	rel.	10s6p	5s4p	6s10p6d	4s5p4d
	non-rel.	10s6p	5s4p		

Exponents derived from a non-relativistic optimization give quite reasonable results apart from a deficiency in the basis for the $p_{1/2}$ spinors which need some additional steep basis functions. This deficiency was removed by adding two extra tight p-exponents. These exponents were determined by logarithmic extrapolation of the original set of exponents. No tight s-exponent was needed because a finite nucleus model (a Gaussian charge distribution) was used.

An atomic DHF calculation was done using the uncontracted large component basis and small component basis functions generated from it by kinetic balance. The large component basis was subjected to general contraction using the spinor coefficients from the uncontracted atomic DHF calculation and the small component basis was generated using the atomic balance relation. For both basis sets different contraction coefficients were used for spinor pairs with $j = \ell \pm 1/2$, but an overlap criterion was used to reduce the resulting number of contracted functions. Diffuse functions, three of the s-, p- and d-type and four of the f-type, were added to the large component basis to give more variational freedom in the valence region. These functions were also introduced in the small component basis using kinetic balance.

The exponents for the fluorine basis were taken from recent calculations performed by Visscher[232]. A contracted basis was constructed in a similar way as described above. An overview of the contracted basis sets can be found in table 6.1 and the primitives used are tabulated in Appendix II.

6.3 The uranium atom

The electronic spectrum of the uranium atom is complex due to the large number of states of which the assignment is still difficult. The first six states are assigned to the $5f^3 6d^1 7s^2$ configuration and the next group of lines is assigned to the $5f^3 6d^2 7s^1$ configuration. A J = 6 state is found to be the ground state and is designated as the $^5L_6$ state with odd parity. In section 6.3.1 a comparison is made between the finite basis DHF results and numerical results obtained with the GRASP atomic code[19].

Table 6.2. Total (in parenthesis) and spinor energies (in hartrees) from numerical and finite basis calculations on the $(5f_{5/2}, 5f_{7/2})^3 (6d_{3/2}, 6d_{5/2})^1 7s^2$ configurational average of the uranium atom.

Spinor	Numerical DHF (-28049.696 857)	Finite basis DHF (-28048.979 953)	Finite basis HF
$\varepsilon (1s_{1/2})$	-4278.1195	-4278.1065	-3716.1152
$\varepsilon (2s_{1/2})$	-805.9727	-805.9781	-650.8961
$\varepsilon (2p_{1/2})$	-776.3649	-776.1816	-629.0471
$\varepsilon (2p_{3/2})$	-635.5773	-635.5900	-629.0471
$\varepsilon (3s_{1/2})$	-206.5656	-206.5696	-166.6487
$\varepsilon (3p_{1/2})$	-193.0974	-193.0502	-155.9458
$\varepsilon (3p_{3/2})$	-160.3246	-160.3302	-155.9458
$\varepsilon (3d_{3/2})$	-139.0204	-139.0166	-136.1731
$\varepsilon (3d_{5/2})$	-132.4206	-132.4253	-136.1731
$\varepsilon (4s_{1/2})$	-54.3122	-54.3148	-43.5145
$\varepsilon (4p_{1/2})$	-48.1936	-48.1823	-38.5167
$\varepsilon (4p_{3/2})$	-39.5420	-39.5451	-38.5167
$\varepsilon (4d_{3/2})$	-29.7343	-29.7344	-29.2595
$\varepsilon (4d_{5/2})$	-28.1312	-28.1339	-29.2595
$\varepsilon (4f_{5/2})$	-15.2051	-15.2077	-16.4087
$\varepsilon (4f_{7/2})$	-14.7928	-14.7956	-16.4087
$\varepsilon (5s_{1/2})$	-12.5934	-12.5955	-10.0589
$\varepsilon (5p_{1/2})$	-10.1278	-10.1267	-8.0332
$\varepsilon (5p_{3/2})$	-8.0930	-8.0954	-8.0332
$\varepsilon (5d_{3/2})$	-4.3516	-4.3532	-4.4426
$\varepsilon (5d_{5/2})$	-4.0419	-4.0441	-4.4426
$\varepsilon (6s_{1/2})$	-2.1374	-2.1378	-1.6820
$\varepsilon (6p_{1/2})$	-1.3431	-1.3443	-1.0360
$\varepsilon (6p_{3/2})$	-0.9848	-0.9865	-1.0360
$\varepsilon (5f_{5/2})$	-0.3472	-0.3494	-0.6349
$\varepsilon (5f_{7/2})$	-0.3197	-0.3219	-0.6349
$\varepsilon (6d_{3/2})$	-0.1928	-0.1925	-0.2652
$\varepsilon (6d_{5/2})$	-0.1833	-0.1829	-0.2652
$\varepsilon (7s_{1/2})$	-0.2023	-0.2025	-0.1667

6.3.1 Atomic spinors

In table 6.2 the contracted basis set results for uranium are compared with those from numerical calculations. There is very good agreement in the valence region. A small error is found for the $2p_{1/2}$ spinor which can be resolved by adding an extra tight basis function. It should be pointed out that the core levels, especially the $1s_{1/2}$ and $2p_{1/2}$ spinors, are influenced by the nuclear model that is used. The version of the numerical package, used for these calculations, makes use of a uniformly charged sphere and in the basis set calculations a Gaussian distribution is employed.

In the last column of table 6.2 the non-relativistic HF orbital energies are given. Comparing the DHF and HF results shows that all the shells, except for the $6p_{3/2}$, the 5f and the 6d spinors, go down in energy. For the radial expectation values a contraction is found for the shells from 1s up to the $6p_{1/2}$ spinor whereas the spinors $6p_{3/2}$, the 5f and the 6d get expanded. The upward shift of the 5f spinors is large and has a large influence on the charge distribution in the molecule. The upward shifts can be explained by the larger screening of the nucleus due to the contraction of the inner-shell orbitals.

6.3.2 Atomic spectrum

The first 10 lines of the uranium atomic spectrum arising from the $5f^3 6d^1 7s^2$ configuration are given in table 6.3. These results are compared with the numerical results from GRASP. Again there is good agreement between the numerical and finite basis DHF results showing the adequacy of the basis set.

Table 6.3. Spectrum of the uranium atom. Figures in eV, relative to the J = 6 ground state.

Nr.	J / Parity	Experiment (Ref. 233)		Numerical DHF	Basis set DHF	Basis set DHF + Gaunt	Basis set CI (36 virt.)
1	6^-	$^5L_6$	0.000	0.000	0.000	0.000	0.000
2	5^-	$^5K_5$	0.077	0.129	0.129	0.126	0.116
3	7^-	$^5L_7$	0.471	0.420	0.422	0.409	0.415
4	6^-	$^5K_6$	0.530	0.508	0.510	0.495	0.496
5	8^-			0.858	0.862	0.835	0.849
6	3^-			0.872	0.873	0.871	0.817
7	7^-			0.885	0.888	0.862	0.872
8	5^-			0.906	0.909	0.899	0.873
9	4^-			1.023	1.027	1.018	0.982
10	6^-			1.041	1.043	1.032	1.010

Comparison with the experimental data shows rather poor agreement. The inclusion of the Gaunt interaction has large influences on the core spinors but the influence on the valence spectrum is small as can be seen in table 6.3. A CI-SD calculation allowing excitations from the 5f and 6d spinors (RAS2 space) to 36 virtuals (RAS3 space) yields little improvement.

Experimentalists find a line at 0.480 eV with a label J = 3. Our first transition state with this label is found at 0.873 eV at the DHF level and at 0.817 eV at the CI level. A better description of the spectrum would be found when other important configurations, like $5f^3 7s^1 6d^2$, are introduced. It is difficult to introduce these configurations in the DHF calculation with our average of configurations approach. The only possible average that contains the configurations $5f^3 7s^2 6d^1$ and $5f^3 7s^1 6d^2$ would be $5f^3(7s6d)^3$ but in this way an unwanted high energy configuration $5f^3 7s^0 6d^3$ configuration is also introduced. This difficulty can only be resolved by carrying out state-specific MCSCF calculations.

6.4 Calculations on UF_6

The closed-shell ground state of the neutral UF_6 molecule is calculated and the influence of relativity on the bonding is investigated by Mulliken[234] population analysis. The molecular geometry of UF_6 was assumed to be of O_h symmetry with a U-F bond length of 1.999 Å taken from experiment[206] and the relativistic calculations are performed in the octahedral (O_h^*) double-group symmetry. In an additional CI-SD calculation excitations are allowed from all occupied valence spinors into the virtual spinors dominated by the 5f, 6d and 7s basis spinors.

In 1976 Karlsson *et al.* [210] presented a photo electron spectrum of UF_6. The first peak was assigned to the $12\gamma_{8u}$ component of the t_{1u} orbital. This assigment was confirmed later by more sophisticated calculations. There was a consensus about the assigment until 1983 when Mårtensson *et al.* [213,214] recorded a new spectrum using a higher energy source. They suggested that the first peak in both spectra should be of t_{1g} character notwithstanding the theoretical results. In this section an attempt is made to find the correct assignment for the two spectra and to reconcile the calculated and experimental results.

6.4.1 The UF_6 spinors

A comparison is made between the non-relativistic (HF) and relativistic (DHF) results. The energies of the valence spinors is graphically presented in figure 6.1. The valence spinors obtained from the DHF calculation are analysed by Mulliken population and overlap analyses (table 6.4). The populations found here are comparable with the results obtained by Onoe *et al.* [228].

The $9a_{1g}$ orbital, which was the HOMO in the HF calculation and has 5% $s_{1/2}$ character, shifts down in energy due to the contraction of the uranium $s_{1/2}$ and $p_{1/2}$ shells. In the DHF calculations the HOMO is found to be the four-component spinor of the $10t_{1u}$ orbital. This spinor is also found to be the highest occupied in other calculations.

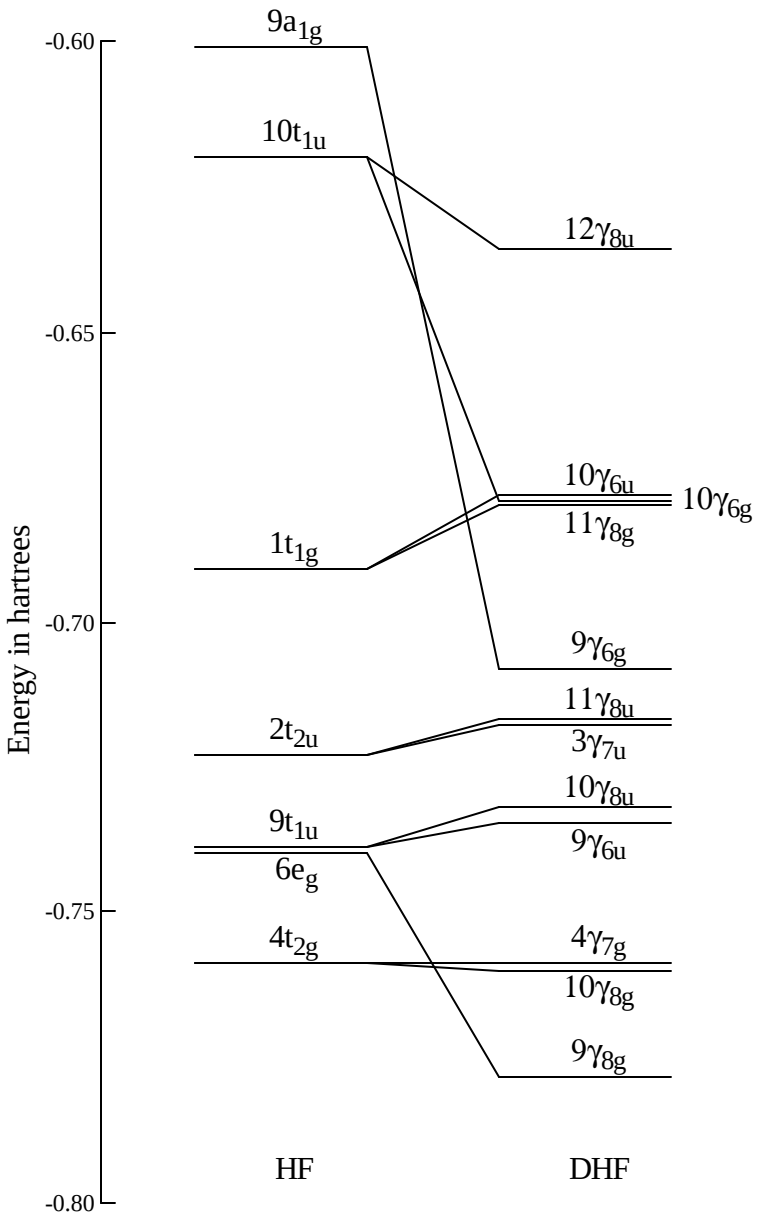

Figure 6.1. Comparison of HF and DHF valence spinors of UF_6.

Another detail that should be noticed is the large spin-orbit splitting of the $10t_{1u}$ orbital. The splitting is important for the assigment of the photo electron spectrum. A more detailed discussion on the assigment of this spectrum can be found in section 6.4.2.

The large splitting of the $10t_{1u}$ orbital into the $10\gamma_{6u}$ and $12\gamma_{8u}$ spinors can be explained. The t_{1u} orbital contains a large amount of U6p character and the U6p orbital has the largest spin-orbit splitting (9.74 eV in the neutral uranium atom) among the valence levels (0.75 eV for U5f and 0.26 eV for U6d). There are more t_{1u} orbitals, besides the one discussed here, that show such a large splitting (see table 6.4).

Table 6.4. Population (left page) and overlap (right page) analyses for UF_6 ([a] HOMO, [b] LUMO). Not listed are the core-spinors, for U up to n=5 shell and for F the 1s.

Spinor Sym.	Energy spinor (hartree)	Population of spinors (in %)					
		U s	U p	U d	U f	F s	F p
$7\gamma_{6g}$	-2.5225	96.3				1.9	1.8
$7\gamma_{6u}$	-1.8016		58.6			38.9	2.5
$8\gamma_{8u}$	-1.6962		13.8			84.3	1.8
$8\gamma_{8g}$	-1.6500			0.8		98.0	1.2
$8\gamma_{6g}$	-1.6249	0.8				98.6	0.7
$8\gamma_{6u}$	-1.5200		38.0			62.0	
$9\gamma_{8u}$	-1.2453		75.1		0.7	16.6	7.7
$9\gamma_{8g}$	-0.7782			14.4		3.2	82.3
$10\gamma_{8g}$	-0.7598			11.9			88.1
$4\gamma_{7g}$	-0.7587			11.2			88.8
$9\gamma_{6u}$	-0.7346				12.8	1.0	86.2
$10\gamma_{8u}$	-0.7318				14.3	0.9	84.8
$3\gamma_{7u}$	-0.7176				8.6		91.4
$11\gamma_{8u}$	-0.7167				8.7		91.3
$9\gamma_{6g}$	-0.7083	6.0				1.4	92.6
$11\gamma_{8g}$	-0.6804						100.0
$10\gamma_{6u}$	-0.6789		6.6		4.2	0.5	88.7
$10\gamma_{6g}$	-0.6781						100.0
$12\gamma_{8u}$[a]	-0.6360		11.2		9.0		79.8
$4\gamma_{7u}$[b]	-0.0891				99.0		1.0
$13\gamma_{8u}$	-0.0685		0.9		89.8		9.4
$5\gamma_{7u}$	-0.0569				96.0		4.0
$14\gamma_{8u}$	-0.0312		1.7		85.9		12.4
$11\gamma_{6u}$	-0.0201		1.4		86.9		11.7
$11\gamma_{6g}$	0.0476	96.8				0.4	2.8
$5\gamma_{7g}$	0.0809			96.4			3.6
$12\gamma_{8g}$	0.0810			96.6			3.4
$13\gamma_{8g}$	0.0849			91.2		0.8	7.9

Spinor	Energy	Overlap populations								
Sym.	spinor (hartree)	5f-2s	5f-2p	6s-2s	6s-2p	6p-2s	6p-2p	6d-2s	6d-2p	U-F
$7\gamma_{6g}$	-2.5225			0.04	0.06					0.10
$7\gamma_{6u}$	-1.8016	-0.01				0.23	0.05			0.27
$8\gamma_{8u}$	-1.6962	-0.04	0.01			0.35	0.06			0.37
$8\gamma_{8g}$	-1.6500							-0.01	0.02	0.01
$8\gamma_{6g}$	-1.6249			-0.19	-0.02					-0.22
$8\gamma_{6u}$	-1.5200					-0.37				-0.37
$9\gamma_{8u}$	-1.2453	0.03				-0.79	0.29			-0.47
$9\gamma_{8g}$	-0.7782							-0.17	0.69	0.51
$10\gamma_{8g}$	-0.7598								0.52	0.52
$4\gamma_{7g}$	-0.7587								0.25	0.25
$9\gamma_{6u}$	-0.7346	-0.03	0.23							0.20
$10\gamma_{8u}$	-0.7318	-0.06	0.47			0.01				0.43
$3\gamma_{7u}$	-0.7176		0.19							0.19
$11\gamma_{8u}$	-0.7167		0.38							0.37
$9\gamma_{6g}$	-0.7083				-0.05					-0.05
$11\gamma_{8g}$	-0.6804									0.00
$10\gamma_{6u}$	-0.6789		0.08				-0.09			0.00
$10\gamma_{6g}$	-0.6781									0.00
$12\gamma_{8u}$[a]	-0.6360		0.19				-0.78			-0.59
$4\gamma_{7u}$[b]	-0.0891		-0.06							-0.06
$13\gamma_{8u}$	-0.0685	-0.06	-0.47			-0.05	-0.11			-0.68
$5\gamma_{7u}$	-0.0569		-0.17							-0.17
$14\gamma_{8u}$	-0.0312	-0.17	-0.52			-0.10	-0.23			-1.01
$11\gamma_{6u}$	-0.0201	-0.10	-0.27			0.02	-0.08			-0.42
$11\gamma_{6g}$	0.0476			-0.11	-0.95					-1.06
$5\gamma_{7g}$	0.0809								-0.35	-0.35
$12\gamma_{8g}$	0.0810								-0.71	-0.71
$13\gamma_{8g}$	0.0849							0.06	-1.18	-1.12

Table 6.5. Comparison of U-F overlap populations.

		Non-relativistic		Relativistic	
		F		F	
		2s	2p	2s	2p
U	5f	-0.09	1.40	-0.12	1.55
	6s	-0.35	-0.63	-0.15	-0.02
	6p	-0.72	-0.47	-0.56	-0.48
	6d	-0.18	1.39	-0.19	1.49
Total U-F bond overlap population		+0.36		+1.53	

If one looks at the total overlap populations in the U-F bond, presented in table 6.5, then it is clear that the bonding gets stronger (from 0.36 to 1.53). On the other hand, from the total populations in table 6.6 one can see that the molecule gets a more ionic character. The dominant contribution in increasing bond strength is the contraction of the U6s orbital. The non-relativistic molecular orbitals that have a large U6s contributions are strongly anti-bonding. Due to the relativistic contraction this U6s orbital will form a non-bonding atomic like U6s spinor and no longer contributes to the molecular bonding. One can use the same arguments for the U6p spinors but here the effects are smaller. The net population of the U6p spinors increases due to the inward shift of the $6p_{1/2}$ and in combination with the reducing overlap an increased gross population is found.

Table 6.6. Total (gross) populations for UF_6 spinors.

		Spinor populations	
	Spinors	Non-relativistic	Relativistic
U	5f	2.94	1.82
	6s	2.00	2.00
	6p	5.63	6.00
	6d	1.18	1.31
	7s	0.02	0.06
U effective charge		2.22	2.72
F	2s	2.00	2.00
	2p	5.34	5.42
F effective charge		-0.37	-0.45

The U5f and U6d get more diffuse, in the relativistic calculation because of the increased screening of the nucleus by the contracted inner-shell orbitals. There is a large energy shift of the U5f spinors and a much smaller one for the U6d (table 6.2). These shifts are reflected in the net populations of the spinors where the population of U6d goes from 0.58 to 053 in the relativistic case and the population of U5f goes from 2.29 to 1.11. A CI-SD calculation was performed allowing the virtual 5f, 6d and 7s spinors to become occupied. The 5f character increases from 1.84 to 2.06 leading to a lower effective charge for the uranium atom. There are no major changes found in the overlap populations and the other gross populations.

Table 6.7. Overview of calculated photo electron spectra.

Spinor	Energies in eV relative to $12\gamma_{8u}$							
Sym.	DHF this work	DHF+G[a] this work	RECP (ref. 222)	DV-DS (ref. 228)	DV-DS (ref. 220)	MS-Xα (ref. 218)	DV-DS[b] (ref. 220)	MS-Xα[b] (ref. 218)
$12\gamma_{8u}$	0.00	0.00	0.00	0.00	0.00	0.00	0.00	0.00
$10\gamma_{6u}$	1.16	1.16	1.23	1.13	1.08	1.10	1.03	1.21
$10\gamma_{6g}$	1.14	1.17	0.69	0.98	1.09	1.07	1.04	1.02
$11\gamma_{8g}$	1.20	1.23	0.67	0.95	1.06	1.04	1.01	0.99
$9\gamma_{6g}$	1.96	1.96	1.85	1.90	1.87	1.77	1.79	1.73
$11\gamma_{8u}$	2.19	2.22	1.77	1.93	1.91	1.84	1.85	1.78
$3\gamma_{7u}$	2.22	2.25	1.75	1.93	1.91	1.83	1.85	1.77
$10\gamma_{8u}$	2.60	2.64	2.21	2.36	2.41	2.33	2.36	2.28
$9\gamma_{6u}$	2.68	2.70	2.28	2.38	2.40	2.45	2.36	2.38
$4\gamma_{7g}$	3.34	3.36	2.67	2.83	2.54	2.42	2.35	2.30
$10\gamma_{8g}$	3.36	3.39	2.71	2.83	2.63	2.48	2.45	2.36
$9\gamma_{8g}$	3.87	3.88	2.86	2.94	3.28	3.51	3.22	3.51
$9\gamma_{8u}$	16.58	16.50	17.32	12.82				12.87
$8\gamma_{6u}$	24.05	23.97	24.07	18.30				18.32
$8\gamma_{6g}$	26.91	26.92	26.62	20.03				19.73
$8\gamma_{8g}$	27.59	27.61	26.83	20.53				20.35
$8\gamma_{8u}$	28.85	28.86	28.16	21.84				21.04
$7\gamma_{6u}$	31.72	31.62	30.68	25.31				23.64
$7\gamma_{6g}$	51.33	51.19	53.04	42.04				

[a]: DHF + Gaunt interaction.

[b]: Transition state procedure.

6.4.2 Photoelectron spectrum of UF_6

An approximate photoelectron spectrum can be obtained from the binding energies of the spinors using Koopmans' theorem or the frozen orbital approximation. The spectrum is presented, relative to the outermost peak, and compared with other theoretical results in table 6.7.

The assignment of the outer most peak to the fourfold degenerate component $12\gamma_{8u}$ of the $4t_{1u}$ is found in all the relativistic calculations. There is agreement in the ordering of the spinors $10\gamma_{8u}$ to $7\gamma_{6g}$ although not in the actual energy values. For the spinors $9\gamma_{6g}$, $11\gamma_{8u}$ and $3\gamma_{7u}$ there are slight differences. In most of the calculations the three spinors are found very close together. The present calculations place the spinor $9\gamma_{6g}$ a little bit lower in energy (0.2 eV) than the other two spinors but the difference is still small.

For the first four spinors there is no agreement on the ordering and interpretation of the spectra. Mårtensson *et al.* [213,214] recorded the photo electron spectrum of UF_6 and they suggested that the ion ground state was of t_{1g} symmetry. One of the main reasons for this assignment was the intensity of the $4t_{1u}$ that was calculated using the population analysis of Hay *et al.* [222] and the atomic photo ionisation cross-sections of Scofield[235]. The population analysis that Hay *et al.* presented was based on a non-relativistic calculation using a relativistic ECP. After the HF step the spin-orbit interaction is introduced in a CI calculation but its effect on the charge distribution is not represented in the population analysis, Mårtensson *et al.* assumed that both components of the non-relativistic t_{1u} orbital, which split 1.23 eV due to spin-orbit interaction, would have the same form and that they could be described using the HF population analyses. The populations analyses presented in table 6.4 show that the two components of the t_{1u} orbital, the spinors $12\gamma_{8u}$ and $10\gamma_{6u}$, are different and this will give the two peaks a different intensity. This is also confirmed by the population analyses of Onoe *et al.* [228]. If one uses the population analyses presented in this chapter for the first four spinors that were calculated by Hay *et al.* then an intensity ratio of approximately 1 : 1 : 3 for the spinors $10\gamma_{6u}$, $10\gamma_{6g}$ together with the $11\gamma_{8g}$ and $10\gamma_{6u}$ respectively is found. A similar structure as that of Hay *et al.* can be obtained if one uses the results of Onoe *et al.*

The results presented in this chapter place the t_{1g} components close together with the twofold component of the t_{1u} orbital which is comparable to the results of Koelling *et al.* [220] and Boring and Wood[218]. This will give only two peaks, as wanted, instead of the three from Hay *et al.* and Onoe *et al.*, but the second peak in the spectrum will get the same intensity as the outer most peak, as suggested by Mårtensson *et al.* When one looks at the differences between the population analysis of the DHF calculation and the additional CI one can see that the 5f contribution changes. These 5f spinors are mainly responsible for the intensity of the first peak. Two different correlation calculations were performed to check the influence of

Table 6.8. Population analysis of the 4 outer most valence spinors of the UF_6 molecule.

Spinor		DHF			SDCI 5f, 6d and 7s as virtuals			SDCI 58 virtuals in E_{1u},E_{2u} and F_u symmetry		
		U 6p	U 5f	F 2p	U 6p	U 5f	F 2p	U 6p	U 5f	F 2p
$4t_{1u}$	γ_{8u}	0.11	0.09	0.80	0.25	0.22	0.53	0.22	0.20	0.58
	γ_{6u}	0.07	0.04	0.89	0.12	0.02	0.86	0.13	0.03	0.81
$1t_{1g}$	γ_{6g}			1.00			1.00			1.00
	γ_{8g}			1.00			1.00			1.00

correlation on the intensity of the peaks. From the resulting natural spinors a population analysis was made (table 6.8).

The numbers in table 6.8 show that the contribution of the 5f-spinors increases from 9% to 20%. The intensity of the outermost peak may therefore increase by more than a factor of two. So if one includes correlation in the calculations one finds two peaks with an intensity ratio varying from 1 : 2 for the large CI to 1 : 2.5 for the small CI where the intensities are calculated as the sum of spinors $10\gamma_{6u}$, $10\gamma_{6g}$ and $11\gamma_{8g}$ and the HOMO $12\gamma_{8u}$ respectively.

Table 6.9. Photo electron spectrum for UF_6 using Koopmans' theorem (eV).

Spinor	Orbital	DHF		DHF + Gaunt		Experimental result[214]
		Calculated	Shifted 3.14 eV	Calculated	Shifted 3.14 eV	
$12\gamma_{8u}$	$4t_{1u}$	17.31	14.17	17.28	14.14	14.14
$10\gamma_{6u}$	$4t_{1u}$	18.47	15.33	18.45	15.31	
$10\gamma_{6g}$	$1t_{1g}$	18.45	15.31	18.45	15.31	15.30
$11\gamma_{8g}$		18.51	15.37	18.51	15.37	
$9\gamma_{6g}$	$3a_{1g}$	19.27	16.13	19.24	16.10	
$11\gamma_{8u}$	$1t_{2u}$	19.50	16.36	19.50	16.36	16.20
$3\gamma_{7u}$		19.53	16.39	19.53	16.39	
$10\gamma_{8u}$	$3t_{1u}$	19.91	16.77	19.92	16.78	16.71
$9\gamma_{6u}$		19.99	16.85	19.98	16.84	
$4\gamma_{7g}$	$1t_{2g}$	20.65	17.51	20.64	17.50	
$10\gamma_{8g}$		20.67	17.53	20.67	17.53	17.36
$9\gamma_{8g}$	$2e_g$	21.18	18.04	21.16	18.02	

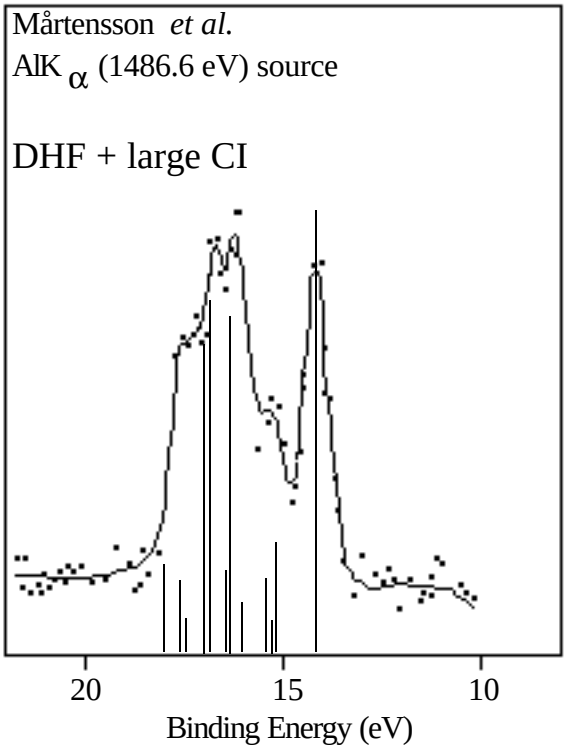

Figure 6.2. Comparison of the experimental[214] and calculated spectrum. Intensities based on spinor populations and photo-ionization cross-sections.

These peaks fit very well to the first two in the experimental spectra. An assignment of the outermost peak to the $12\gamma_{8u}$ component of the t_{1u} orbital can hence be made without difficulty following the reasoning of Mårtensson *et al.*. The next three spinors, $10\gamma_{6u}$, $10\gamma_{6g}$ and $11\gamma_{8g}$, together form the second peak. The next three peaks should then be assigned to the spinors $9\gamma_{6g}$ down to $9\gamma_{8g}$.The intensity of spinor $9\gamma_{6g}$, is very low and will probably not be found in the spectrum. The spinors $11\gamma_{8u}$ and $3\gamma_{7u}$ form the third peak with the right intensity. One can then assign the fourth peak to the spinors $10\gamma_{8u}$ and $9\gamma_{6u}$. The three spinors $4\gamma_{7g}$ to $9\gamma_{8g}$ should be placed in the region around the fifth peak. This peak in the spectrum of Mårtensson *et al.* is very broad. A more detailed spectrum should give better insight. The assigment that is suggested here is presented in table 6.9 and figure 6.2.
It is in reasonable agreement with the various theoretical results and also in good agreement with the experimental data of Karlsson *et al.* [220].
The first ΔSCF ionization potential is found by a DHF calculation on UF_6^+ with the hole placed in the highest occupied $12\gamma_{8u}$ component of the $4t_{1u}$ orbital. An ionization energy of 16.6 eV is obtained which is too large compared to the experimental value of 14.14 eV. The difference can be mainly ascribed to differential correlation effects.

Table 6.10. Comparison of the uranium core level spin-orbit splitting (in eV).

n *l*	DHF UF_6	DHF UF_6 + Gaunt	DHF atom	DHF atom + Gaunt	Experiment	
					UF_6[a]	U metal[b]
2p	3825	3785	3826	3784	--	3782
3p	890	882	890	881	--	878
3d	179	176	179	176	--	176
4p	235	233	235	232	--	229
4d	43.6	42.9	43.6	42.8	42.5	42.1[a]
4f	11.3	10.9	11.2	10.9	10.8	11.1[a]
5p	55.7	55.2	55.3	54.7	--	55.1
5d	8.7	8.6	8.4	8.3	8.9	8.6[a]
6p	--	--	9.7	9.6	--	10.0[a]
5f	--	--	0.75	0.73	--	0.76
6d	--	--	0.26	0.26	--	0.24

[a]: Ref. 214. [b]: Ref. 236.

Some properties of the molecule can be extracted from the calculated results. Spin-orbit splittings are calculated from the core level DHF spinors. They are compared with the splittings found in the atomic calculation and experimental data in table 6.10. The spin-orbit splittings of the uranium core levels are not influenced by the fluorine atoms in the UF_6 molecule. Especially for the deeper core levels, better agreement between the theoretical and experimental data is obtained by taking the Gaunt interaction into account. One has to keep in mind that the description of the $2p_{1/2}$ spinor can be improved by adding an extra tight p function to the basis set. This will then improve the spin-orbit interaction for the 2p and the 3p spinors as well.

Another property is the energy that is needed to let the molecule dissociate into seven atoms.

Table 6.11. Calculated total (hartrees) and atomization (eV) energies.

Calculation	Uranium atom (averaged)	Fluorine atom	UF_6 molecule	Atomization energy
Hartree-Fock	-25662.617823	-99.402999	-26259.365671	9.0
Dirac-Fock	-28048.979953	-99.495166	-28646.799549	23.1
Dirac-Fock + Gaunt interact.	-28006.979389	-99.483255	-28604.714328	22.7

The atomization energies, calculated at the experimental bond length, for the non-relativistic HF, the relativistic DHF and the DHF plus Gaunt interaction are presented in table 6.11. Notice that for the uranium atom the average energy for the $5f^3 6d^1 7s^2$ configuration is used.
The results in table 6.11 indicate that the bonding between the uranium and fluorine atoms gets stronger when relativity is taken into account, because it is not expected that the non-relativistic corrections will be much larger than the relativistic ones. This expectation is substantiated by the fact that the experimental atomization energy is 31.9 eV[237]. An explanation of the stronger bonding can be found in section 6.4.1.

6.4.3 Bond length of UF_6

A bond length optimization was performed on the HF and DHF level. From a 7 point fit a bond length of 1.994 Å is found for the DHF calculation and the HF bond length is found to be 1.995 Å. The experimental bond length is 1.999 (± 0.003) Å[206]. An explanation might be given on the basis of the population analyses but it is hard to do this in a quantitative way.

6.5 UF_6^- calculations

The UF_6^- ion is found in the $CsUF_6$ rhombohedral crystal structure. Reisfeld *et al.* [238] recorded an optical absorption spectrum from this lattice. Their analysis is based on a octahedral ion, although the structure is somewhat distorted, and they find the five states that result from the crystal-field splitting in combination with spin-orbit interaction. Hay *et al.* [222] and Koelling *et al.* [220] performed a calculation using the octahedral UF_6^- ion. In this chapter the same calculation is done using the DHF method and the influence of the Gaunt interaction is examined. The spinors of UF_6^- are generated by putting the extra electron in the unoccupied 5f-like spinors and carrying out an average DHF calculation. The ground state ($^2A_{2u}$) and the four other states in the 5f electronic spectrum are then calculated by a complete open shell CI calculation. An additional CI is performed allowing some relaxation of the 5f-spinors. In the CI calculation single and double excitations are allowed from the fluorine 2p and uranium 6s, 6p to the uranium 5f-, 6d- and 7s-like spinors.

6.5.1 Electronic states of UF_6^-

The electronic 5f spectrum is calculated and the results of the CI calculation are comparable to the RECP plus CI results of Hay *et al.*. There are two major reasons for the difference between the DHF results and experiment. First, an average open-shell calculation is performed on the 5f-spinors which results in an equal occupation of these spinors and allows the higher states to influence the spinor optimization process.

Table 6.12. Electronic 5f spectrum of UF_6^-. Comparison of theoretical and experimental results.

State (J-value)	Excitation energy (eV)					
	Exp. (ref. 238)	DF (this work)	DF+G (this work)	CI (this work)	RECP (ref. 222)	DV-DS (ref. 220)
Γ_{7u} (1/2)	0.00	0.00	0.00	0.00	0.00	0.00
Γ_{8u} (3/2)	0.57	0.74	0.74	0.71	0.67	1.00
Γ_{7u} (1/2)	0.86	0.94	0.91	0.91	0.97	1.13
Γ_{8u} (3/2)	1.58	1.97	1.95	1.90	1.80	2.51
Γ_{6u} (1/2)	1.77	2.16	2.14	2.09	1.95	2.69

Relaxation and introduction of charge-transfer states, by means of a CI calculation, improves the calculated spectrum as can be seen in table 6.12. Second, the spectrum is measured in the $CsUF_6$ lattice which has a rhombohedral structure. This means that the UF_6^- ion is slightly distorted and that the electronic structure of the ion will be influenced by the rest of the crystal. For the calculations presented here an octahedral UF_6^- cluster is used.

6.5.2 Electron affinity of UF_6

The electron affinity is calculated on the Dirac-Hartree-Fock level and a second calculation is performed where the Gaunt interaction is introduced as a perturbation to the DHF spinors. One can see from the DHF and DHF + Gaunt results in table 6.13 that the influence of the Gaunt interaction is small. The introduction of correlation, by means of CI-SD, makes the energy gap smaller. The good agreement between the calculated and experimental electron affinities is probably fortuitous however.

6.6 Conclusions

A basis set was constructed for the uranium atom. The one-electron energies and the valence spectrum calculated with this set show good agreement with the numerical DHF results. When the valence spectrum is compared with experimental data large discrepancies are found. These discrepancies can be ascribed to the fact that a single determinant approach is used instead of a multi determinantal one.

For the spin-orbit splitting, in the atom as well as in the molecule, good agreement is found with experimental results. It is shown that the Gaunt interaction is needed to get good agreement between the experimental and theoretical results for the deeper core levels. The Gaunt interaction has only small effects on the valence spectrum. The spin-orbit splitting of the core p functions can be improved when the basis set is extended with tight p functions and when higher order corrections to the two-electron interaction are introduced.

Table 6.13. Theoretical and experimental electron affinities of UF_6.

Calculation	Total energy (hartree)		Electron affinity
	UF_6 ($^1A_{1g}$)	UF_6^- ($^2A_{2u}$)	
HF	-26259.365671	-26259.692941	8.9 eV
DHF	-28646.799549	-28647.034758	6.4 eV
DHF + Gaunt	-28604.714328	-28604.951897	6.5 eV
CI-SD	-28646.875721	-28647.072045	5.3 eV
Reference	Type of calculation		
Hay *et al.* [222]	RECP + spin-orbit coupling and CI		7.1 eV
Reference	Type of experiment		
R.N.Compton[239]	$Na + UF_6 \rightarrow Na^+ + UF_6^-$		≥ 5.1 eV
J.L.Beauchamp[240]	$BF_3 + UF_6^- \rightarrow BF_4^- + UF_5$		4.9 ± 0.2
	$SF_6 + UF_6^- \rightarrow SF_6^- + UF_6$		8.1

Comparing non-relativistic and relativistic results a much stronger bonding is found when the molecule is studied within a relativistic framework. The stronger bonding can be assigned to the contraction of the inner shells of the uranium atom up to the $6s_{1/2}$ spinor which reduces the anti-bonding properties of the molecule. As a result of the inner-shell contraction the uranium 5f and 6d spinors expand. The contraction and the expansion result in a more ionic charge distribution.

The photo-electron spectrum of Mårtensson *et al.* is assigned and the outer most peak is found to be the $12\gamma_{8u}$ component of the $4t_{1u}$ orbital. The $4t_{1u}$ orbital, that will give one peak if a non-relativistic approach is used, will split in two components in a relativistic framework. This is in agreement with other theoretical results and the experimental data of Karlsson *et al.* Correct intensity ratios can be found when the method of Mårtensson *et al.*, intensities based on population analyses and atomic photo-ionization cross sections, is used. A CI calculation is needed to get good agreement with the experimental results.

The relativistic bond length, that was found in the optimization procedure, lies just below the experimental value. The non-relativistic bond length was found to be only 0.001Å longer. The very small contraction of the bond length in spite of the larger bonding energy found in the relativistic calculation is consistent with the discussion of the bonding properties given in section 6.4.1.

For the UF_6^- ion reasonable agreement with the experimental 5f spectrum is found. The differences between the theoretical and experimental results can be reduced by larger CI calculations. Another thing

that has to be taken into account is the fact that the ion has no octahedral symmetry and that the ion is surrounded by other ions in the crystal structure. The calculated electron affinity is in good agreement with the experimental data.

The Gaunt interaction has only a small influence on the valence properties of the molecule and the ion. This interaction will be more important for core properties as is shown for the spin-orbit interaction in the atom.

Chapter 7

The uranyl ion

In this chapter the bonding of the uranyl ion ($[UO_2]^{2+}$) is studied, non-relativistically as well as relativistically. A bond length expansion is found and the presence of a so-called "U(6p) core-hole" and the U(5f) contribution are hereby found to be important. A different ordering of the valence spinors is found compared to previous work but it is confirmed that the HOMO has σ_u character and has a large U(5f) contribution. The electric field gradient (EFG) at the uranium nucleus is calculated and it is shown that the U(6p) core-hole has also a large influence on the size of the EFG. The non-relativistic EFG value is found to be much larger than the relativistic value. This difference is due to different contributions of the core and U(5f) valence orbitals. The inclusion of a charged environment has a significant effect on the EFG value.

7.1 Introduction

In the past 25 years a considerable amount of theoretical work[226,241-258] has been devoted to understand the structure, bonding and various other properties of the uranyl ion $[UO_2]^{2+}$ on the basis of quantum chemical methods. These calculations were based on approximate relativistic methods or density functional approaches (mainly Xα) but no full four-component Dirac-Hartree-Fock methods have been used to study this molecule. A review concerning the uranyl ion can be found in Ref. 259.

The uranyl ion has a linear O-U-O structure and exists as a free ion in aqueous solutions with pH below 2.7. The ion accepts ligands at higher pH and in crystals. These ligands lie in or close to the equatorial plane through the uranium atom at bond distances that are much larger than the U-O bond lengths in the uranyl ion itself. The U-O bond distance can be tuned from 150 pm to 200 pm by varying type and coordination of the equatorial ligands. Whereas the uranyl has a linear structure, all its isoelectronic counterparts, like ThO_2, are found to have a bent structure. The linearity of the uranyl ion has been the subject of various papers and there are a number of interpretations. Wadt[248] attributes the linearity to

the U($5f_\pi$)-O($2p_\pi$) bonding and finds that the role of the U(6p) orbital is of no importance. On the other hand, Tatsumi and Hoffman[246] find that the interplay between the U($6p_\pi$)-O($2p_\pi$) orbitals and U($5f_\sigma$) orbitals determine the linear structure. This interpretation, generally known as "pushing from below" of the U(6p) [244,246], is supported by various other calculations[226,244,245,250,258]. The origin of the relative short bond length of $[UO_2]^{2+}$ is attributed to strong bonding interactions of the U(5f) orbitals[226,249]. Another question is the symmetry and character of the HOMO and related to this the ordering of the occupied valence orbitals. On the basis of optical absorption spectra, Denning *et al.* [260,261] argue that the HOMO is a σ_u and this is confirmed by most of the theoretical calculations. There is some controversy[251] among experimentalists on the amount of U(5f) character of the HOMO, i.e. to what extend the U(5f) contributes to the molecular bonding. Veal *et al.* [262] found from their XPS data no evidence for U(5f) participation in the bonding whereas Cox[263] comes to the opposite conclusion based on the relative intensities in the spectra of similar experiments. In previous calculations[241,244-246,250,256,257] a significant contribution of the U(5f) to the HOMO is found. The π_u and σ_u orbitals are found close together in theoretical calculations and one can expect that spin-orbit interaction will lead to a HOMO with a mixed π-σ character. The ordering of the orbitals below the HOMO varies from calculation to calculation.

To understand the linearity of the uranyl ion and the character of the HOMO a good description of the valence region of the molecule is needed. The valence configuration of uranium is $6s^2 6p^6 5f^3 6d^1 7s^2$ whereas the oxygen valence shell consists of 2s and 2p orbitals. In a purely ionic picture uranium would have an oxidation state of 6+ and the U(6d) and U(5f) orbitals would not contribute to the bonding. However, theoretical results suggest[241,244-246,250,256,257] that the HOMO will have a significant contribution of the U(5f) orbital. Previous calculations also suggest that the semi-core U(6p) orbitals form bonds with the O(2s) and O(2p) leading to the so-called "U(6p) core hole". There are experimental data from XPS spectra[262] on uranyl compounds that can be interpreted by assuming strong U(6p)-O(2s) mixing. Most of the computational studies are performed within an approximate relativistic framework. In particular, a large number of the calculations neglect spin-orbit coupling. In this chapter we will use a fully relativistic framework to study the uranyl ion.

In this chapter we will also study the electric field gradient (or EFG) at the uranium nucleus. Nuclei with spin > 1/2 have a nuclear quadrupole moment (NQM) which can interact with the EFG generated by the charge distribution of the molecule. The 3 x 3 EFG tensor will have different principal values for molecules with less than tetrahedral symmetry. For such an asymmetric electric field gradient a nucleus with a nuclear quadrupole moment will hence have different energy levels depending on the orientation. These differences can be observed as a hyperfine structure by various experimental techniques, like for example nuclear magnetic resonance spectroscopy. The Hamiltonian for the energy of the interaction between a nuclear quadrupole and an electric field gradient is defined by

$$\hat{H}_{Qq} = \mathbf{eQq_z}\left[\frac{1}{4}\frac{3\hat{I}_z^2 - \hat{\mathbf{I}}^2}{I(2I-1))}\right] \qquad (7.1)$$

where Q is the NQM, q_{zz} the tensor component of the EFG directed along the principal axis of the molecule and I the nuclear spin. In experiments on molecular systems one measures the quantity eQq_{zz}, the so-called nuclear quadrupole coupling constant (NQCC). The q_{zz} can be calculated with *ab initio* methods. The simplest method is to calculate the property as an expectation value which is equivalent to an energy derivative formulation if the Hellmann-Feynman[128,129] theorem is fulfilled. For the uranyl ion, with the uranium atom at the origin, the formula for the q_{zz} at the uranium site is

$$q_{zz}^{U} = \left\langle y \left| \sum_i \frac{\left(3Z_{iU}^2 - R_{iU}^2\right)}{R_{iU}^5} \right| y \right\rangle + \frac{4Z_{Ox}}{R_{U-O}^3} \qquad (7.2)$$

where Z_{iU} is the component along the nuclear axis of the distance R_{iU} between electron i and the uranium nucleus, Z_{Ox} the nuclear charge of the oxygen atom and $R_{U\text{-}O}$ the U-O bond length. The first term is the expectation value for the electronic contribution and the second term describes the contribution of the other nuclei, here the two oxygen atoms. The EFG depends on the electron distribution around a given nucleus. If Q is known from experiments on the respective atom, the fine structure spectra contain information about electron distribution via q_{zz} and visa versa.

The NQCC on the uranium site is measured[264] for the uranyl ion in $[(UO_2)Rb(NO_3)_3]$ and has the value $8.14*10^{18}$ V/cm^2 or 8.4 au., and the NQM is known from experiment[265] to be $10.19*10^{-24}$ cm^2. The structure of this complex is sketched in figure 7.1.

The U-O bond length of the central uranyl ion is 178 pm whereas the next-nearest oxygen's in the nitrate groups lie at a distance of 272 pm from the uranium atom (see Ref. 264 and references therein). Comparison of the experimental value of the EFG with the theoretically calculated one allows us to get some insight in the accuracy of the calculated electronic wave function. Previously Larsson and Pyykkö[226] performed a qualitative analysis of the EFG on uranium and attributed the large value to the occurrence of a U(6p) core-hole, as before. However, they solely attributed the value to this core-hole and did not consider the contributions of the other orbitals. Here we calculate the EFG on uranium in the uranyl ion and analyze the various contributions to it of all occupied molecular orbitals. Another aspect that will be considered is the influence of the charged environment, i.e. the three nitrate groups, on the electron distribution in the valence region of the uranyl ion.

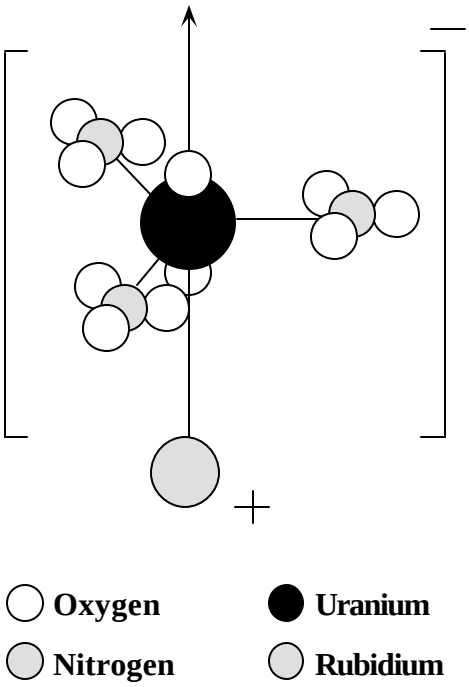

Figure 7.1. Sketched structure of $[(UO_2)Rb(NO_3)_3]$.

7.2 Computational model

The spectroscopic properties and the EFG are studied with the programs MOLFDIR and DIRAC[91]. The EFG integrals defined in (7.2) are calculated by the HERMIT[95] part of the DIRAC program. The molecular calculations in MOLFDIR are done in D_{4h}^* double group symmetry whereas in the DIRAC calculations we use D_{2h}^* double group symmetry. A Gaussian distribution as described in chapter 2.2.2 is used to describe the spatial extent of the nucleus in the non-relativistic as well as in the relativistic calculation. The primitive exponents for uranium are determined by optimizing the relativistic energies of the atomic ground state with an adaptation of the atomic code GRASP[19]. For uranium we use family basis sets, i.e. the d-exponents are a subset of the s-exponents and the f-exponents are a subset of the p-exponents, whereas the exponents of Dunning's cc-pVTZ basis[266] are used for the oxygen atom. The general contracted basis is constructed using the atomic balance procedure (see chapter 2.2.1). Additional diffuse functions are added to the final basis set in order to assure sufficient variational freedom in the valence region. Both the uncontracted and contracted basis sets of uranium differ from the ones used for the UF_6 molecule in chapter 6. The primitive exponents can be found in table A.3 of the appendix and the sizes of the contracted basis sets are given in table 7.1.

Table 7.1. Basis set sizes for uranium and oxygen.

		Large Component		Small Component	
Atom	Type	Primitive	Contracted	Primitive	Contracted
U	Rel.	26s21p17d12f	10s13p11d6f	21s26p21d17f12g	8s15p14d11f6g
	Nonrel.	26s21p17d12f	10s8p7d4f		
O	Rel.	11s7p2d	5s5p2d	7s13p7d2f	4s7p5d2f
	Nonrel.	11s7p2d	5s4p2d		

In our calculations on the spectroscopic properties as well as the EFG we excluded the (SS|SS) class of integrals in order to make the calculations feasible. This was accounted for by Visscher's[101] correction to the total energy, described in chapter 2.4.

The uranyl ion is studied in its closed shell ground state $^1\Sigma_g^+$. In the CCSD(T) calculations 24 electrons are correlated and the virtual space consists of 176 spinors. The spectroscopic properties are obtained by fitting the calculated points of the potential energy curve to a 4th order polynomial in the inter nuclear distance.

We will analyze the wave function at a $R_{U\text{-}O}$=172 pm so that we can compare our results with previous calculations.

The EFG calculations are performed at the DHF level of theory using the contracted basis described above. The experimental[264] $R_{U\text{-}O}$=17 pm of the [$(UO_2)Rb(NO_3)_3$] complex (figure 7.1) is used. The distance to the next-nearest six oxygen's of the equatorial ligands NO_3 is 272 pm. In order to get an estimate of the influence of the charged environment on the electron distribution in the uranyl ion some of the calculations included 4 point charges of -0.75 electrons in the equatorial plane at a distance of 272 pm. By taking four point charges instead of three we can continue working in D_{4h}^* symmetry which has significant computational advantages. We will study the influence of the Gaussian nucleus model on the electron distribution close to the nucleus by performing a similar calculation with a point nucleus. The effect of the neglected (SS|SS) class is calculated by explicitly including them in a direct SCF calculation using the DIRAC program.

7.3 Bonding in the $[UO_2]^{2+}$ molecule

The equilibrium bond length (r_e) and symmetric U-O stretching frequency in $[UO_2]^{2+}$ are studied non-relativistically as well as relativistically at both the uncorrelated and correlated level using CCSD(T). Our results are summarized in table 7.2 where they are compared with other theoretical results.

Table 7.2. Non-relativistic and relativistic bond length and symmetric stretching frequency (ω_e). The relativistic effect Δ is defined as x(relativistic) - x(non-relativistic).

Method[c]	r_e (pm)	ω_e (cm^{-1})
HF contracted	159.9	1368
HF + CCSD(T)	167.5	1015
DHF uncontracted[b]	165.1	1239
DHF contracted[a]	165.0	1240
DHF + CCSD(T)	171.0	974
HFS[250]	167.4	--
HFS + Quasi relativistic effects[250]	170.0	--
HF + R-PP + CCSD[253]	169.7	--
HF + R-PP[254]	162.5	1216
HF + R-PP + MP2[254]	173.2	922
HF+ RECP[252]	166.3	1183
HF+ RECP + MP2[252]	178.3	933
Exp. $Cs_2UO_2Cl_4$[267]	181.0	831
Exp. $[(UO_2)Rb(NO_3)_3]$ [264]	178.0	--
Δ HF	5.2	-128
Δ CCSD(T)	4.1	-41

[a]. Contracted basis with MOLFDIR. [b]. Uncontracted basis with DIRAC.

[c]. HFS (Hartree-Fock-Slater), R-PP (Relativistic Pseudo Potential), RECP (Relativistic effective core potential).

There are no experimental data on the bond length and symmetric stretch for the free uranyl ion. Measurements in molecular systems containing the uranyl ion give a wide range of bond lengths. Two of the molecular systems are given in table 7.2 for comparison. The correlated results are comparable to the experimental data of a uranyl ion in a larger molecular system. Our relativistic results are comparable with the results of other calculations. It is clear that correlation effects have a significant effect on the spectroscopic properties studied here.

A longer bond length and a large decrease of the symmetric stretch is found when relativity is included. A somewhat smaller bond length expansion of 2.6 pm was previously found by Wezenbeek *et al.* [250] We will come back to the origin of the bond lengthening later on in this section.

In figure 7.2 the non-relativistic and relativistic valence orbitals are compared in order to have a clear picture of the relativistic effects. The molecular orbitals presented here include the uranium 5f, 6s, 6p, 6d, 7s orbitals and the oxygen 2s and 2p orbitals. The results of a non-relativistic and relativistic Mulliken population analysis at a bond distance of 172 pm are

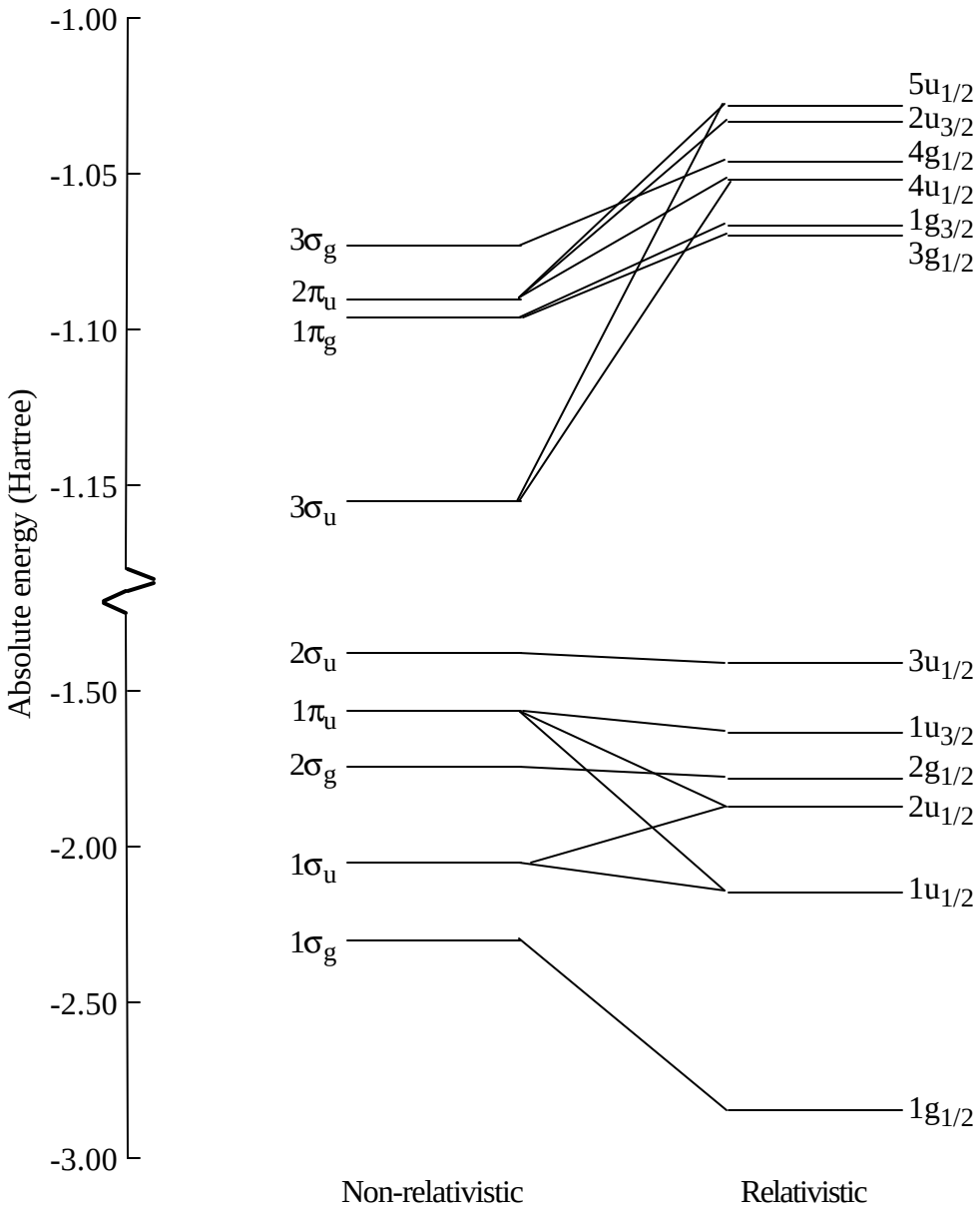

Figure 7.2. Comparison of the occupied non-relativistic and relativistic valence spinors. The uranium orbitals up to 5d and the O(1s) orbitals are not included in the analysis.

summarized in table 7.3 and 7.4. The spinors of the relativistic calculation are denoted with their respective parity and the quantum number ω as a subscript. With the calculated data we will now discuss the issues raised concerning the bonding of the uranyl ion.

Relativistic effects have a large influence on the ordering of the spinors, as can be seen in figure 7.2. The non-relativistic $1\sigma_g$ and $2\sigma_g$ molecular orbitals show some mixing of the U(6s) with the O(2s). Due to relativistic scalar contraction the U(6s) no longer mixes with O(2s) and becomes a non-bonding spinor.

Table 7.3. Mulliken population analysis of the non-relativistic calculation at 172 pm. The uranium orbitals up to 5d and the O(1s) orbitals are not included in the analysis.

Orbital	Energy	Composition of orbital (in %)								
	(hartree)	Us	Upπ	Upσ	Ud	Uf	Os	Opπ	Opσ	Od
$1\sigma_g$	-2.2996	73					22		5	
$1\sigma_u$	-2.0544			20		1	68		10	1
$2\sigma_g$	-1.7463	17			4		79			
$1\pi_u$	-1.5728		95					4		
$2\sigma_u$	-1.3844			35		2	38		25	1
$3\sigma_u$	-1.1549			11		74			15	
$1\pi_g$	-1.0964				16			82		2
$2\pi_u$	-1.0905		3			30		66		
$3\sigma_g$[a]	-1.0736	9			18				73	
Gross population		2.00	3.94	1.33	1.06	2.74	4.11	6.12	2.57	0.13

[a]. HOMO

Table 7.4. Mulliken population analysis of a relativistic calculation at 172 pm. The uranium spinors up to 5d and the O(1s) spinors are not included in the analysis.

Spinor	Energy	Composition of spinor (in %)								
	(hartree)	Us	Upπ	Upσ	Ud	Uf	Os	Opπ	Opσ	Od
$1g_{1/2}$	-2.8448	93					5		2	
$1u_{1/2}$	-2.1523		20	37			33		8	1
$2u_{1/2}$	-1.8736		71	1		1	25	1	2	
$2g_{1/2}$	-1.7844				3		96		1	
$1u_{3/2}$	-1.6425		97					3		
$3u_{1/2}$	-1.4203		7	33		4	45	1	12	
$3g_{1/2}$	-1.0700				19			78	1	2
$1g_{3/2}$	-1.0668				18			80		2
$4u_{1/2}$	-1.0522			3		35		43	17	1
$4g_{1/2}$	-1.0458	5			15		1	1	78	
$2u_{3/2}$	-1.0331		2			22		75		
$5u_{1/2}$[a]	-1.0281		1	7		42		33	17	
Gross population		1.93	3.99	1.60	1.10	2.07	4.16	6.30	2.73	0.12

[a]. HOMO

The large shift downwards of the $1\sigma_g$ is also found in other calculations that include relativistic effects[244,247,250]. This relativistic contraction is also observed in calculations on UF_6 (see chapter 6). In fact the bonding picture seen for the uranyl ion is similar to that of the UF_6 molecule.

The U($6p_\sigma$) is strongly mixed with the ungerade combination of the O(2s) and also has some O(2p) character. We also observe a considerable mixing of the O($2p_\pi$) orbitals with the U(6d) and U(5f). These strong interactions lead to the so-called "U(6p) core-hole" as discussed earlier by Larsson and Pyykkö[226], Pyykkö and Laaksonen[245] and Wezenbeek *et al.* [249,250]. We find that in the non-relativistic calculation 0.7 electrons are squeezed out of the U($6p_\sigma$) due to this mixing, whereas the "hole" is much smaller in the relativistic calculation (0.4 electrons). This can be attributed to the more compact nature of the U($6p_{1/2}$), which gives the largest contribution to the U($6p_\sigma$) in the $1u_{1/2}$ spinor, in the relativistic calculations. Van Wezenbeek *et al.* [249,250] find a "hole" of 0.5 electrons (at a bond distance of 172 pm) but find no decrease when they account for relativistic effects. This is probably caused by the absence of spin-orbit coupling in their calculation. We observe a considerable mixing, due to spin-orbit interaction, between the $1\sigma_u$ and the ω=1/2 component of the $1\pi_u$.

The $3\sigma_u$ orbital, which is dominantly U(5f), shifts up and even becomes the HOMO at the relativistic level of theory. We find that the HOMO is dominantly σ_u with some π_u character due to mixing in of the ω=1/2 component of the $2\pi_u$ with the $3\sigma_u$ orbital as a result of spin-orbit interaction. The HOMO has around 40% U(5f) character which is similar to what is found in other *ab initio* calculations[241,244,250,256,257] but smaller than the 80% suggested by Pyykkö[245,258]. The considerable amount of U(5f) character in the HOMO agrees with the conclusions made by Cox[263] on the basis of experimental XPS spectra. Hence, the large upward shift of the $3\sigma_u$ orbital confirms the idea of "pushing from below" of Tatsumi and Hoffmann[246], DeKock *et al.* [244] and Jørgensen[251].

Table 7.5. Gross populations (per atom) of non-relativistic and relativistic wave functions at 172 pm and 178 pm. The uranium orbitals up to 5d and the O(1s) orbitals are not included in the analysis.

r (pm)	Type	U s	U p	U d	U f	O s	O p	O d	q U	q O
172	Nonrel.	2.00	5.27	1.06	2.74	2.06	4.35	0.06	+2.93	-0.47
	Rel.	1.93	5.59	1.10	2.07	2.08	4.51	0.06	+3.31	-0.65
178	Nonrel.	1.98	5.35	1.05	2.73	2.06	4.32	0.06	+2.89	-0.44
	Rel.	1.93	5.66	1.11	2.03	2.07	4.50	0.06	+3.27	-0.67

Table 7.6. Comparison of the highest six molecular spinors.

Reference	Year	Type[a]	Ordering of spinors
Ref. 242	1975	DS	$4u_{1/2}$ $2u_{3/2}$ $3g_{1/2}$ $1g_{3/2}$ $4g_{1/2}$ $5u_{1/2}$
Ref. 241	1976	DS	$4u_{1/2}$ $2u_{3/2}$ $3g_{1/2}$ $1g_{3/2}$ $4g_{1/2}$ $5u_{1/2}$
Ref. 247	1978	DS	$4u_{1/2}$ $3g_{1/2}$ $2u_{3/2}$ $5u_{1/2}$ $4g_{1/2}$ $1g_{3/2}$
Ref. 256	1981	QR-MS	$3g_{1/2}$ $4u_{1/2}$ $4g_{1/2}$ $2u_{3/2}$ $1g_{3/2}$ $5u_{1/2}$
Ref. 244	1984	RHFS	$3g_{1/2}$ $1g_{3/2}$ $4u_{1/2}$ $2u_{3/2}$ $4g_{1/2}$ $5u_{1/2}$
Ref. 245	1984	REX	$3g_{1/2}$ $1g_{3/2}$ $4g_{1/2}$ $4u_{1/2}$ $2u_{3/2}$ $5u_{1/2}$
Our results	1997	DHF	$3g_{1/2}$ $1g_{3/2}$ $4u_{1/2}$ $4g_{1/2}$ $2u_{3/2}$ $5u_{1/2}$

[a]. DS (Dirac-Slater), QR-MS (Quasi Relativistic Multiple Scattering method), RHFS (Hartree-Fock-Slater + scalar relativistic and spin-orbit effects), REX (Relativistic Extended Hückel), DHF (Dirac-Hartree-Fock).

Inclusion of relativistic effects leads to a more ionic molecule similar to what was found previously for the UF_6 molecule in chapter 6. This increase is due to a smaller U(5f) contribution in the bonding but is partially compensated by the increase of the number of electrons in U(6p), i.e. the "hole" becomes smaller. The ionicity and the size of the "hole" does not vary much with the bond length, as can be seen in table 7.5, but the inclusion of relativity, on the other hand, leads to significant changes.

There is no agreement in the literature on the ordering of the highest four orbitals $3\sigma_g$, $2\pi_u$, $3\sigma_u$, $1\pi_g$ and their six relativistic counterparts. In table 7.6 we compare our results with relativistic calculations that include spin-orbit coupling. Other, more recent, calculations are not directly comparable because they do not include the large spin-orbit effects.

Our calculations give a spinor ordering which again differs from the previous calculations although a closer agreement is found with the more recent calculations. The differences between our results and the older Dirac-Slater calculations are large. There is a general agreement that the HOMO is $5u_{1/2}$. The two components of the $1\pi_g$ are found below the other four spinors and this is similar to what was found in the most recent calculations of Pyykkö *et al.* [245] and DeKock *et al.* [244]. Our ordering of the three remaining spinors differs from the other calculations. However, these spinors lie in a range smaller than 1 eV and the ordering can be affected by the relativistic approach used.

Our calculations show a substantial bond length expansion when relativistic effects are included (table 7.2). Van Wezenbeek *et al.* [250] attribute the expansion to a loss of mass-velocity stabilization due to a decreasing population of the U(6p) core-hole and large off-diagonal mass-velocity matrix elements with the U(6p) and not to the expansion of the U(5f) orbitals. However, they find a depopulation of the U(6p) which is the same for the non-relativistic and the relativistic calculation. Our calculations clearly show a smaller depopulation of the U(6p) when relativity is included. The bonding contribution of the U(5f) decreases significantly when relativity is included. The decrease in the U(5f) occupation was also

observed by van Wezenbeek[249]. Van Wezenbeek[249] attributes the short bond length of the uranyl ion to the strong bonding interaction of the U(5f) and O(2p) which is counteracted by the repulsive interaction of the U(6p) and the O(2s). Other contributions are found to be considerably smaller. This explanation is supported by calculations of Larsson and Pyykkö[226] and Wadt[248]. We agree that the short bond length is caused by these interactions. However, our relativistic calculations show that not only the U(6p) contribution but also the U(5f) contribution change considerably and are therefore both responsible for the bond length expansion.

The last issue that will be discussed in this section is the linearity of the uranyl ion. Tatsumi and Hoffmann[246] attribute the linearity to the strong σ-type U(5f)-O(2p) bonding interaction. Wadt[248] and Pyykkö and Lohr[258] relate the linearity to the strong U($5f_\pi$) contribution to the bonding. Our calculations show a bonding between the π-type orbitals of the U(5f) and O(2p) in the non-relativistic case whereas in the relativistic case also the σ-type orbitals contribute due to spin-orbit interaction. The relativistic approach therefore merges both suggested bonding interactions.

7.4 The electric field gradient on uranium

At a bond length of 178 pm we obtain a value for the EFG of 2.7 au. in a relativistic calculation. This value is much smaller than the experimentally[264] determined value of 8.4 au. Non-relativistically we find a value of 9.3 au. which lies close to the experimental value. The large difference between the relativistic and non-relativistic value shows the impact of relativity on this property.

The results given here are based on calculations on a free uranyl ion. However, the measurements are done on a uranyl ion in the $[(UO_2)Rb(NO_3)_3]$ complex where the uranium atom is surrounded by three NO_3^- groups in the equatorial plane (see figure 7.1). As a first (crude) approximation we have simulated this charged environment by including four point charges of -0.75 electrons in the equatorial plane, keeping D_{4h}^* point group symmetry, at a distance of 272 pm. In addition the nuclear contributions of the nitrate groups and the Rb atom (approximately 0.7 au.) are included. Non-relativistically we find a value for the EFG of 13.8 au. and relativistically we obtain 6.6 au. This brings the relativistic result closer to experiment whereas the non-relativistic value becomes much too large. The large increase of the electronic contribution (relativistic 3.9 au. and non-relativistic 4.5 au.) is a consequence of the additional deformation of the electronic density in the uranyl ion induced by the lower symmetry. Hence, we may assume that the effect will be even larger if we include a more accurate description of the environment.

We will now analyze the EFG contributions in the free uranyl ion. The molecular spinor contributions are summarized in table 7.7. We have grouped the valence orbitals according to their atomic orbital character as defined by the population analysis in table 7.3 and 7.4. The group containing U(6p) is build up from four large contributions which cancel each other. Our calculations are performed in a closed shell molecule which means that the spinors of the same symmetry can arbitrarily rotate among each

other. For these reasons we will from now on use the grouping of the valence orbitals as given in the last column of table 7.7 A more detailed analysis of the core region is presented in figure 7.2.
The largest contribution to the EFG comes from the molecular spinor with U(6p) and O(2s) character. Larsson and Pyykkö[226] analyzed the contribution of the U(6p) in a qualitative way and attributed the EFG to the core-hole arising from the interaction of the U(6p) with the O(2s) and O(2p). However, from table 7.7 and figure 7.3 we can conclude that the contributions of the other valence spinors also have a large effect, i.e. they partially cancel the U(6p) core-hole contribution. For example, the contribution of the U(5f)-O(2p) molecular spinor is half of the U(6p) core-hole contribution.

Table 7.7. Analysis of the molecular orbital contributions to the EFG on uranium at 178 pm. Notation of orbitals and spinors is the same as in section 7.3. The core region includes all uranium orbitals up to U(5d) and O(1s).

Non-relativistic		Relativistic		Character
Orbitals	EFG (au.)	Spinors	EFG (au.)	spinors
Core	1.16		-2.93	--
$1\sigma_g$	-0.05	$1g_{1/2}$	-0.18	U(6s)
$2\sigma_g$	-0.88	$2g_{1/2}$	-1.41	O(2s)
$1\sigma_u$	-25.88	$1u_{1/2}$	-56.06	U(6p)
$1\pi_u$	46.51	$2u_{1/2}$	82.33	+ O(2s)
	46.51	$1u_{3/2}$	70.56	+ O(2p)
$2\sigma_u$	-47.89	$3u_{1/2}$	-76.40	
$1\pi_g$	-0.64	$3g_{1/2}$	-0.98	O(2p)
	-0.64	$1g_{3/2}$	-0.70	+U(6d)
$3\sigma_g$	-2.48	$4g_{1/2}$	-2.82	
$3\sigma_u$	-9.65	$4u_{1/2}$	-9.34	U(5f)
$2\pi_u$	1.22	$5u_{1/2}$	-2.66	+ O(2p)
	1.22	$2u_{3/2}$	2.46	
Sum Valence	+7.33		+4.81	
Core + Valence	+8.49		+1.88	
Nuclear contr.	+0.84		+0.84	
Total EFG	+9.33		+2.72	

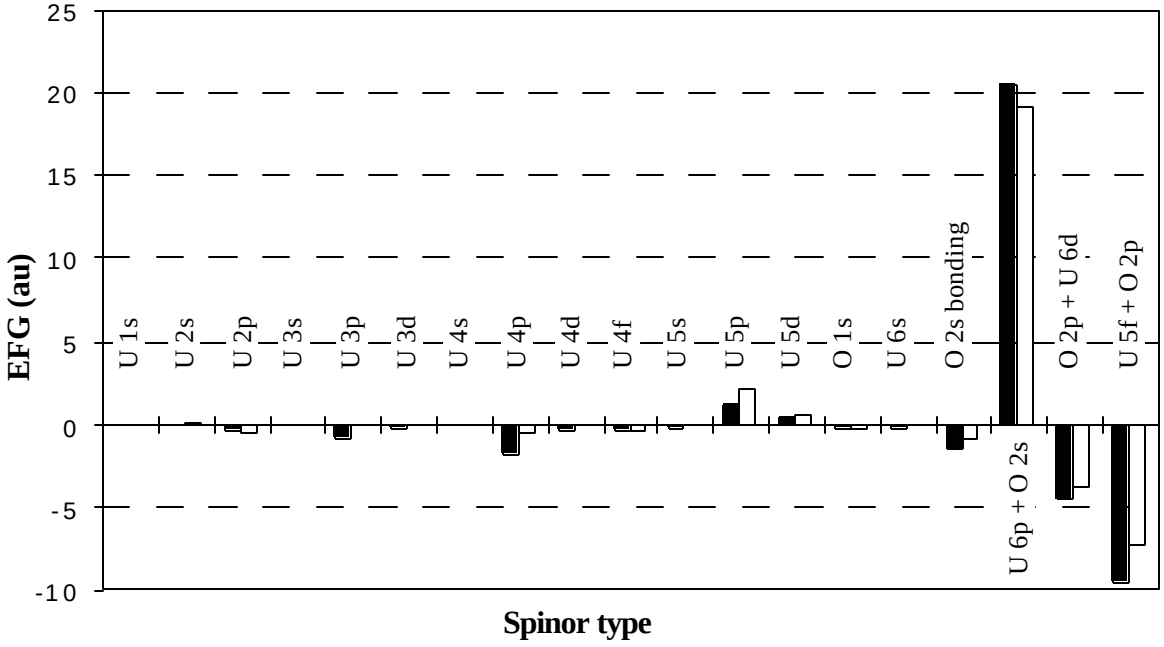

Figure 7.3. Contributions to the electronic part of the EFG for a non-relativistic (white) and a relativistic (black) wave function derived at a bond distance of 178 pm.

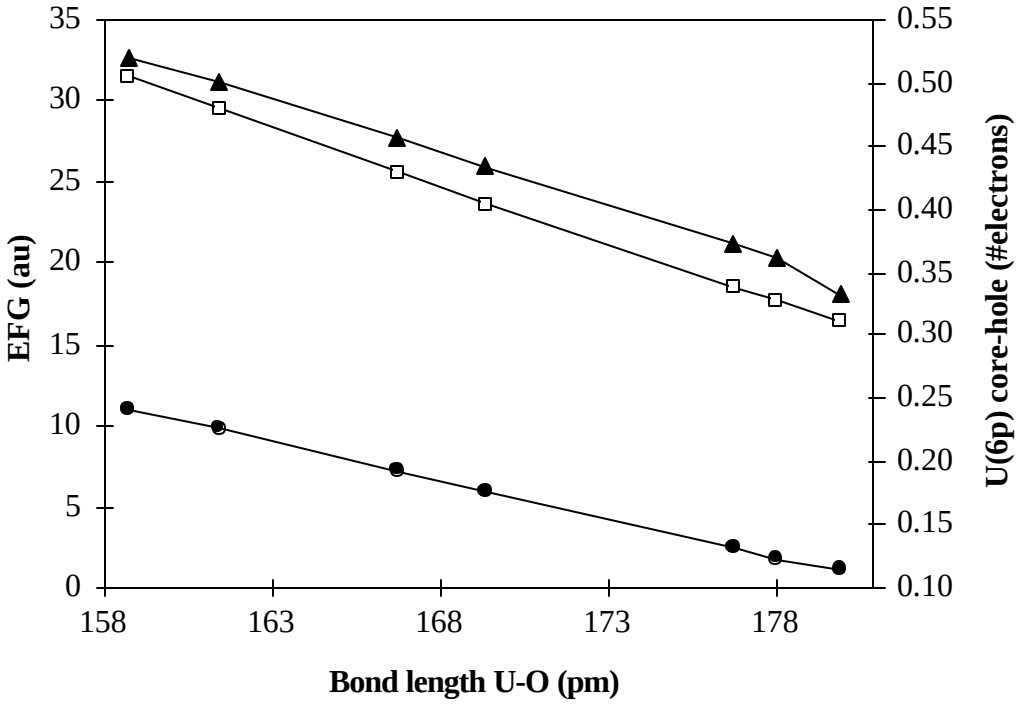

Figure 7.4. Total electronic EFG contribution (—●—), and U(6p) core-hole contribution (—▲—) and U(6p) core-hole size (—□—) versus the U-O bond length. All results come from relativistic calculations.

It is clear that the contribution of the core-region in uranium, i.e. orbitals up to the 5d cannot be neglected. The O(1s) core-orbital screens a part of the nuclear charge of the oxygen atom and its contribution to the EFG (-0.2103 au.) can therefore be modelled by assuming a point charge of -2 at the oxygen position. The total core contribution is found to be much larger than the nuclear contribution arising from the oxygen atoms. In the relativistic case the contribution of the core region is larger than in the non-relativistic case, in fact the sign of the core contribution changes going from a non-relativistic to a relativistic calculation.

Larsson and Pyykkö[226] related the electronic contribution of the EFG to the size of the U(6p) core-hole and the bond length. In figure 7.4 we see a similar relation between the bond length, the U(6p) core-hole and the EFG. The U(6p) core-hole contribution to the EFG value is much larger than the total electronic EFG value itself. Also, the results in table 7.8 suggest that this picture is somewhat misleading because no large core-hole effect is found in the non-relativistic calculation.

The size of the U(6p) core-hole changes only a little when going to longer bond lengths for the non-relativistic as well as the relativistic calculation. On the other hand, table 7.8 shows a large change in the EFG for the relativistic calculation when going to longer bond lengths whereas the slope in non-relativistic calculation is much smaller. In figure 7.5 we compare the distance dependence of the various orbital contributions at two different bond lengths.

Table 7.8. Dependence of EFG on the size of the U(6p) core-hole, a comparison of non-relativistic and relativistic electronic contributions at 159 pm and 178 pm.

	Non-relativistic		Relativistic	
Bond length	U(6p) core-hole	q_{zz} (au)	U(6p) core-hole	q_{zz} (au)
159 pm	0.77	8.9	0.51	11.0
178 pm	0.65	8.5	0.34	1.9

Up to the O(2s) bonding orbital no significant changes are found when changing the bond length. The U(6p)-O(2s) molecular spinor shows in the relativistic case a larger distance dependence than in the non-relativistic case. In the non-relativistic case the contribution of the U(5f)-O(2p) molecular spinors cancels the change in the U(6p)-O(2s) contribution which leads to a similar value for the EFG at both distances. This is not the case for the relativistic calculations where the U(5f)-O(2p) spinors do not show a distance dependence and the change in the EFG value arises entirely from the U(6p) containing molecular spinors. Hence, the distance dependence of the EFG can in the relativistic case indeed be attributed to the U(6p) core-hole, as suggested by Larsson and Pyykkö[226], but in the non-relativistic case the

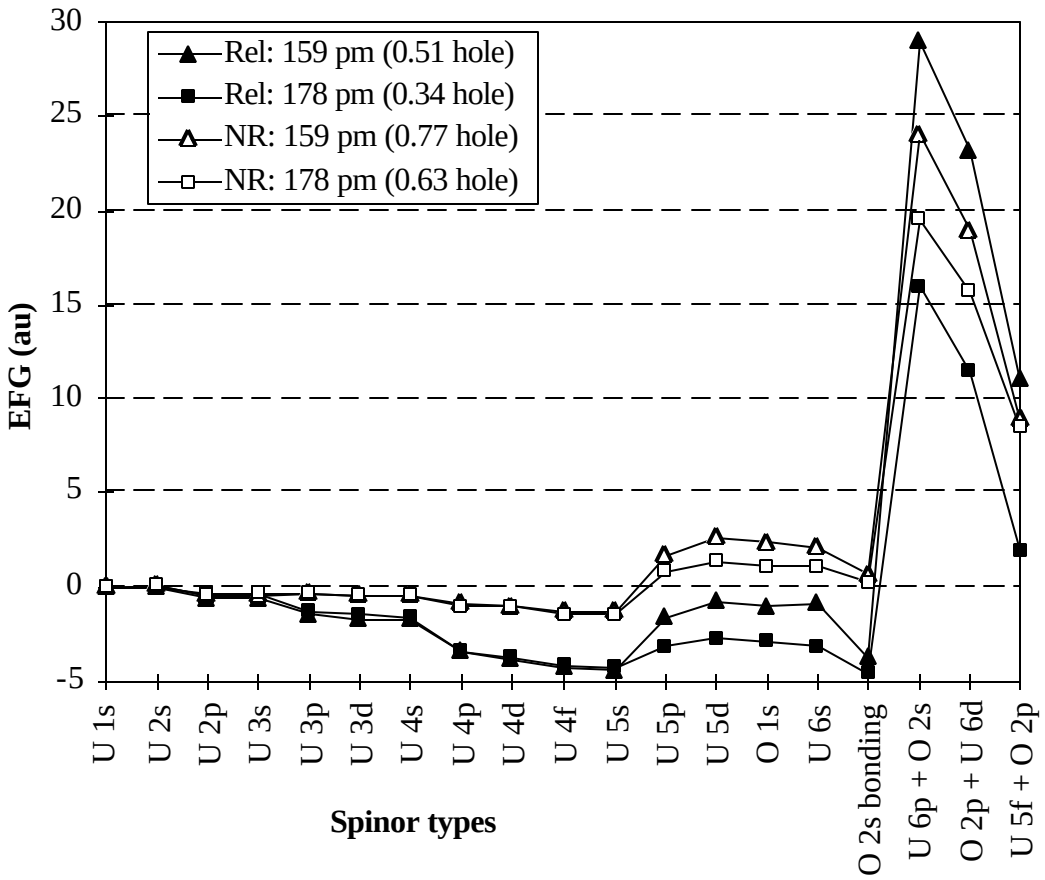

Figure 7.5. Comparison of cumulative contributions to the EFG for non-relativistic (NR) and relativistic (Rel) wave functions at the bond distances 159 pm and 178 pm. U(6p) core-hole is given in parenthesis.

contributions of the other valence spinors also change with the distance and largely cancel the change in the core-hole contribution.

Our calculated value at 178 pm is considerably smaller than the experimental value, even when we take the environment into account. We will now investigate whether this discrepancy is due to computational defects. The results are summarized in table 7.9.

The EFG becomes slightly smaller when we use an uncontracted basis set instead of a contracted basis. Also the inclusion of a polarization function has a minor influence suggesting that this property is not very sensitive to improvements of the basis set used. In our calculations we used a finite nucleus. However, this finite nucleus will affect the form of the wave function close to the nucleus and therefore we have tested the influence by performing a similar calculation using a point nucleus. The effect of a finite nucleus is found to be small. Another approximation made in the calculations presented here is the omission of the (SS|SS) class of integrals but we see that this also has only a small effect.

Table 7.9. Overview of various aspects in the computational model which could affect the EFG on uranium at 178 pm.

Type of contribution	Contribution to EFG (in au.)
Uncontracted instead of contracted basis	-0.33
Adding g-function to large component	-0.07
Using point nucleus instead of Gaussian	-0.11
Including (SS|SS) class of integrals	+0.07

7.5 Conclusions

The bonding properties and the electric field gradient on the uranium site are studied within a fully relativistic framework. The short bond length of the uranyl ion is attributed to a strong U(5f)-O(2p) bonding interaction counteracted by a repulsive interaction of the U(6p) with the O(2s). A bond length expansion is found when relativistic effects are included in the calculation. This expansion can be explained by a relativistic change in the repulsive U(6p) and bonding U(5f) interactions with respect to the non-relativistic situation. A strong mixing between the U(6p), the O(2s) and O(2p) leads to the so-called "U(6p) core-hole". The HOMO has a large U(5f) contribution and is dominantly σ_u. This is in agreement with most of the other (approximate) relativistic calculations. Our ordering of the highest six spinors is slightly different from the most recent calculations of Pyykkö *et al.* [245] and DeKock *et al.* [244]. However, the energetic differences between the orbitals are small and in these calculations the relativistic effects are included in an approximate way. The linearity can be attributed to the strong σ and π bonding interactions between the U(5f) and the O(2p).

We have analyzed the various contributions to the electric field gradient (EFG) at the U nucleus. The bonding of the U(6p) has a profound effect on the size of the EFG, as was suggested by Larsson and Pyykkö. However, the contributions of the other orbitals largely cancel the effect of the U(6p) and therefore cannot be neglected. The contribution of the U(6p) is the same for the non-relativistic and the relativistic EFG value. We find that the differences between the non-relativistic and the relativistic result arise from different contributions of the core region and the other occupied valence orbitals. The inclusion of the environment, which was approximated by including point charges, has a large effect on the size of the EFG and has to be taken into account.

Chapter 8

Summary

Relativity has a significant influence in chemistry. This is not only the case for chemical systems with elements in the lower regions of the periodic system but also for molecules with only elements from the upper regions of the periodic system, as will be shown in this thesis.

In chapter 1 we introduced the reader to the relativistic effects and their influence in chemistry. The main goal of this thesis research was to calculate properties of chemical systems including relativity and to interpret experimental data. We have chosen to study these chemical systems within an *ab initio* relativistic framework with the Dirac Hamiltonian as a starting point. In chapter 2 the many-electron generalization of the Dirac Hamiltonian is introduced and, by gradually allowing more and more well defined standard quantum chemistry approximations, we will arrive at the relativistic quantum chemistry model that was implemented in the MOLFDIR program package. This code was then applied to a variety of molecules.

In chapter 3 we studied the relativistic effects on the so-called ionized and neutral excited states of the copper halide series CuX (with X = Cl, Br, I). The ionized excited states, which are described by states arising from a $Cu^{+}(3d^{9}4s^{1})$ $X^{-}(ns^{2}np^{6})$ configuration, are found to be strongly affected by mixing of the states due to spin-orbit interaction. These spin-orbit effects arise from the copper atom and are similar throughout the whole copper halide series. On the other hand, the spin-orbit effects in the neutral excited states, arising from the $Cu(3d^{10}4s^{1})$ $X(ns^{2}np^{5})$ configuration, are caused by the spin-orbit splitting on the halides and become more important when going to the heavier halides.

MOLFDIR is an ideal tool for relativistic benchmark calculations due to the various correlation methods, available in the program package, and its fully relativistic framework. In chapter 4 we performed benchmark calculations on the spectroscopic properties bond length, harmonic frequency and dissociation energy of the interhalogen series ClF, BrF, BrCl, IF, ICl and IBr. For all molecules studied in this chapter a weakening of the bond was found which was attributed to spin-orbit interaction. We found that for these fairly light systems the relativistic and correlation effects are largely additive. A

huge amount of theoretical work has been done on the calculation of the electric dipole moment of the interhalogens but all with approximate relativistic approaches. We calculated the electric dipole moment and electric quadrupole moment as expectation values. The electric dipole polarizability was studied within the random phase approximation[41]. The relativistic effects were found to have a significant effect on these properties.

The ground, excited and ionized states of the iodine molecule have been studied in chapter 5. Our calculated results for the ground state were found to be in close agreement with experimental data. Core-valence correlation and basis functions with higher angular momenta were found to be important to obtain results in agreement with experiment. The potential energy curves of the excited and low-lying ionized states have been calculated and their respective spectroscopic properties were determined. Relativistic effects, and in particular spin-orbit coupling between states, were found to be extremely important. Our results for the excited states are in close agreement with experiment and with the results of Teichteil and Pelissier[183]. The spectroscopic properties of the low-lying ionized states are in close agreement with experimental data. We have reassigned a recently measured ionized state on the basis of our calculations.

In chapter 6 we studied the uranium hexafluoride (UF_6) molecule. The uranium atom is a heavy element and hence requires a relativistic model in order to understand its properties. We showed that relativity reorders the valence spinors and changes the character of the HOMO which is now in good agreement with experiment. The photoelectron spectrum of UF_6 could be reproduced by our calculations. Calculations on the excited states of the UF_6 cation and the electron affinity also give results that are in agreement with experiment.

The bonding properties of the uranyl ion ($[UO_2]^{2+}$) were studied within a fully relativistic framework and presented in chapter 7. We observed the so-called "U(6p) core-hole" which has a influence on the bonding properties of the molecule. The ordering of the valence spinors differs from previous theoretical predictions but we agree that the HOMO has σ_u character and has a large U(5f) contribution. The electric field gradient (EFG) on the uranium site was evaluated and we showed that the U(6p) core-hole and relativistic effects have a large influence on the size of the EFG. The influence of other effects, in particular that of the environment of the uranyl cluster was found to be significant.

From our fully relativistic *ab initio* quantum chemical calculations on various chemical systems we conclude that relativity often has a significant effect on the calculated properties of the systems studied. For the molecules containing elements from the upper region of the periodic system the most important relativistic effect is the spin-orbit interaction. For the heavier elements also the scalar relativistic effects become important.

Nederlandse samenvatting

In de scheikunde bestudeert men chemische reacties en de chemische en fysische eigenschappen van stoffen op het moleculaire niveau. Stoffen en moleculen worden gevormd uit atomen die op hun beurt weer zijn opgebouwd uit kernen en elektronen die zich om de kernen bewegen. De eigenschappen van stoffen worden bepaald door de interactie tussen de kernen en elektronen en de elektronen onderling. Als we de eigenschappen willen verklaren zullen we een model of theorie moeten gebruiken die deze interacties kan beschrijven. Wanneer we deeltjes met heel kleine afmetingen willen beschrijven moeten we gebruik maken van het kwantummechanische model waarin de deeltjes worden beschreven met een zogenaamde golffunctie. De kwantummechanica is een natuurkundige theorie, die men vorm heeft gegeven in een aantal wiskundige formules. Eén van de belangrijkste kwantum-mechanische formules is de Schrödinger-vergelijking.

Op het eerste gezicht lijkt de kwantummechanica een onbelangrijk iets in onze macroscopische wereld maar de invloed van deze theorie op het alledaagse is bijzonder groot. Zonder de kwantummechanica zijn we niet in staat om eigenschappen als magnetisme en elektrische geleiding echt te begrijpen. Enkele andere tastbare voorbeelden zijn de ontwikkeling van lasers en de elektrische schakelingen (chips). Voor het ontwikkelen van nieuwe materialen, het begrijpen en verbeteren van de werking van medicijnen, snellere elektrische schakelingen, nieuwe en verbeterde reactieprocessen (waaronder katalysatoren), maar ook voor het begrijpen van fenomenen zoals supergeleiding, is een gedegen inzicht nodig in de kwantum-mechanische aspecten van de eigenschappen van stoffen.

Het is niet eenvoudig om de chemie te beschrijven met behulp van alleen een kwantum-mechanisch model. De formules voor het veel-deeltjes probleem dat voortkomt uit de Schrödingervergelijking is moeilijk op te lossen en vereist grootschalige rekenarbeid. Om toch de uitgebreide experimentele kennis te kunnen interpreteren en te kunnen gebruiken in nieuwe technologische ontwikkelingen probeert men op basis van de kwantummechanica gemakkelijkere hanteerbare modellen op te stellen betreffende de opbouw van atomen en moleculen en de samenhang hiervan met allerlei chemische en fysische eigenschappen van materialen. Op basis van experimentele gegevens, bijvoorbeeld spectroscopische technieken, probeert men zo eenvoudig mogelijke kwantummechanische beschrijvingen te vinden voor de gemeten eigenschappen. Men neemt daarvoor bepaalde modelvoorstellingen aan voor de golffuncties waardoor het mogelijk is om bepaalde experimentele grootheden te parameteriseren. Met deze vereenvoudigde modellen kan men proberen om de uitkomsten van nieuwe experimenten te voorspellen en kan men gemeten trends interpreteren. Toch zijn er grenzen aan deze zogenaamde semi-empirische aanpak. Vereenvoudigde modellen werken vaak goed voor bepaalde eigenschappen en

voor bepaalde klassen van materialen. Wanneer men een andere klasse van materialen of andere eigenschappen wil bestuderen moet men vaak het model aanpassen of zelfs uitbreiden. Naast de grenzen van een eenvoudig model zijn er ook grenzen aan wat experimenteel mogelijk is. Men kan hier bijvoorbeeld denken aan het werken met zeer giftige, radioactieve of op een andere manier gevaarlijke stoffen. Het is niet altijd mogelijk om de (zeer kort) levende tussenprodukten in het verloop van een chemisch reactieproces te meten waardoor enkele schakels in de interpretatie ontbreken.

Een andere invalshoek is die van de *ab initio* kwantumchemie, een onderdeel van de theoretische chemie. Deze tak binnen de kwantumchemie houdt zich bezig met het zo exact mogelijk oplossen van de kwantummechanische bewegingsvergelijkingen, de Schrödinger-vergelijking, van de kernen en de elektronen. Met dit model kunnen in principe alle eigenschappen van materialen, individuele moleculen, interacties tussen en reacties van moleculen worden voorspeld door het uitvoeren van berekeningen. In deze tak probeert men zo min mogelijk gebruik te maken van experimentele informatie, de enige experimentele kennis die men gebruikt zijn de fundamentele fysische natuurconstanten. Deze tak van wetenschap begon zich pas echt te ontwikkelen rond 1960 na de ontwikkeling van grootschalige reken- en dataverwerkingsmogelijkheden, het begin van het computertijdperk. Door uit te gaan van alleen een fundamenteel kwantummechanisch model, wordt een beter inzicht verkregen in de basis van de chemie maar kan men ook informatie over chemische systemen verkrijgen die niet (of nog niet) experimenteel beschikbaar zijn, oftewel we kunnen proberen eigenschappen te voorspellen. We zijn (nog) niet in staat om de veel-deeltjes Schrödingervergelijking op te lossen. Dit betekent dat ook binnen de *ab initio* kwantumchemie een aantal (conceptuele) benaderingen moeten worden gemaakt welke in de limiet zullen leiden tot een exacte oplossing van het veel-deeltjes probleem. De formules die overblijven vormen op zichzelf nog steeds een groot rekenprobleem. De huidige beschikbare rekenkracht is op dit moment de beperkende factor wat betreft de chemische probleemstellingen die kunnen worden bestudeerd, we moeten ons veelal beperken tot een klein aantal atomen. Veel eigenschappen van een stof hebben een lokale oorsprong, enkele atomen of een klein cluster van atomen, en kunnen worden beschreven met een klein deel van de stof, al dan niet met een benaderd omgevingsmodel.

We moeten de *ab initio* kwantumchemie zien als één in een lange rij van experimentele technieken. Ze kan worden gebruikt als hulpmiddel voor de verklaring, bevestiging en het modelleren van de interpretatie van experimentele gegevens. Tevens kan de kwantumchemie dienen als numeriek experiment om inzichten te verkrijgen in processen en materialen die niet met experimentele technieken kunnen worden vergaard.

Het oplossen van de (benaderde) Schrödingervergelijking levert in veel gevallen een voldoende nauwkeurige beschrijving van de chemische en fysische eigenschappen van een molecuul. Toch faalt de kwantummechanica op basis van de Schrödingervergelijking wanneer deeltjes die met een zeer hoge snelheid bewegen moet worden beschreven (dit is het geval bij zware elementen zoals uranium). Voor deze snel bewegende deeltjes is een verbeterde versie van de kwantummechanica nodig waarbij

rekening wordt gehouden met een andere natuurkundige theorie, Einstein's speciale relativiteitstheorie. In deze theorie is de lichtsnelheid een fundamentele natuurconstante (snelheid 300000 km/s), dit in tegenstelling tot de Schrödingervergelijking waarin in feite een oneindige lichtsnelheid wordt aangenomen. Dit heeft vooral directe consequenties voor de electronen dicht bij een zware kern welke zich met grote snelheid voortbewegen, maar indirekt ook voor de electronen die zich verder van de kern bevinden. Een model dat rekening houdt met de kwantummechanica en met Einstein's speciale relativiteitstheorie werd in 1928 gepostuleerd door Dirac, de relativistische kwantum-mechanica. Relativiteit heeft een significante invloed op de chemie. De invloed beperkt zich niet alleen tot chemische systemen met elementen uit de onderste regionen van het periodiek systeem, maar strekt zich ook uit tot moleculen met alleen elementen uit de bovenste rijen van het periodiek systeem. Enkele voorbeelden van deze invloed in de chemie zijn de verklaringen voor de kleur van goud en het licht van straatlantaarns.

Het werk dat in dit proefschrift wordt gepresenteerd gaat uit van relativistische kwantum-mechanica zoals die is geformuleerd in de Diracvergelijking. Het rekengereedschap dat hiervoor wordt gebruikt is het MOLFDIR programma pakket dat in onze groep aan de Rijksuniversiteit Groningen is en wordt ontwikkeld. Het proefschrift kan ruwweg in twee secties worden opgedeeld, een theoretische sectie en een sectie met resultaten van berekeningen aan een aantal chemische systemen. In hoofstuk 1 wordt een algemene inleiding gegeven over relativiteit en de relativistische effecten in de chemie. Hoofdstuk 2 behandelt, in het kort, de theorie en zijn implementatie in MOLFDIR.

In het hoofdbestanddeel van het proefschrift, de hoofdstukken 3 t/m 7, wordt de MOLFDIR programmatuur toegepast op een aantal chemische vraagstukken waarbij relativistische effecten van belang zijn of zouden kunnen zijn. We zullen zien dat niet alleen moleculen met zware elementen maar ook moleculen met lichte elementen significant worden beïnvloed door relativiteit. In hoofdstuk 3 worden de relativistische effecten op de zogenaamde geïoniseerde en neutrale aangeslagen toestanden van de koperhalogenen (CuCl, CuBr en CuI) bestudeerd. Het belangrijkste relativistische effect dat deze toestanden sterk beïnvloed is de spin-baan interactie tussen de verschillende toestanden.

Een relativistische berekening aan een bepaald chemisch rekenprobleem is vele malen groter dan wanneer we het rekenprobleem met niet-relativistische methoden bestuderen. Daarom laat men vaak de relativistische effecten weg of probeert men deze te beschrijven met behulp van benaderende modellen. Om de correctheid en nauwkeurigheid van deze modellen te kunnen analyseren is het nodig om volledig relativistische berekeningen uit te voeren. De resultaten van deze berekeningen kunnen dan dienen als referentiekader voor de benaderende methoden. In hoofdstuk 4 worden de resultaten van referentie berekeningen aan interhalogeen moleculen (ClF, BrF, BrCl, IF, ICl en IBr) gepresenteerd. Verschillende spectroscopische en elektrische eigenschappen en het relativistische effect op deze eigenschappen zijn berekend.

In hoofdstuk 5 is naar de spectroscopische eigenschappen van het twee-atomige jodium molecuul gekeken. Naast de grondtoestand zijn ook de geëxciteerde toestanden van het systeem bestudeerd. De resultaten zijn in goede overeenstemming met de experimentele gegevens en de eigenschappen van enkele, nog niet gemeten, toestanden zijn voorspeld. Tenslotte is er gekeken naar de geïoniseerde toestanden van het molecuul. De hier gepresenteerde resultaten hebben geleid tot een andere interpretatie van recente experimentele data en een nieuwe toekenning van een gemeten toestand.
De hoofdstukken 6 en 7 beschrijven de resultaten van berekeningen aan moleculen die uranium bevatten, een element uit de onderste regionen van het periodiek systeem. In hoofdstuk 6 zijn de eigenschappen van het uraniumhexafluoride molecuul bestudeerd. Het ionisatiespectrum, het excitatiespectrum van het kation en de electronenaffiniteit van het molecuul zijn berekend. De rekenresultaten zijn in goede overeenstemming met de beschikbare experimentele gegevens. In hoofdstuk 7 worden resultaten gepresenteerd van berekeningen aan het uranyl ion. De bindingseigenschappen van het molecuul, zoals de korte bindingslengte en de lineariteit van het molecuul, zijn bestudeerd en vergeleken met resultaten van berekeningen op basis van benaderende methoden. Zowel de spin-baan wisselwerking als de scalaire relativistische effecten hebben een grote invloed op de eigenschappen van dit molekuul. Er is ook gekeken naar de gradiënt van het elektrische veld op de uranium positie in het molecuul. De elektrische veld gradiënt wordt gegenereerd door de ladingsverdeling in het molecuul en een combinatie van experimentele en theoretische resultaten levert dus direct informatie op over deze ladingsverdeling en met name die van de electronen. De relativistische effecten zijn belangrijk voor deze eigenschap maar ook de omgevingseffecten leveren een belangrijke bijdrage.
In het algemeen kunnen we concluderen dat de spin-baan wisselwerking het belangrijkste effect is wanneer we kijken naar moleculen bestaande uit lichte elementen. Wanneer we moleculen met zware elementen willen bestuderen moeten ook de scalaire relativistische effecten worden meegenomen om een nauwkeurige beschrijving van het molecuul te krijgen.

Fryske gearfetting

Yn 'e skiekunde wurde gemyske reaksjes en de gemyske en fysyske eigenskippen fan stoffen op it molekulêre nivo bestudearre. Stoffen en molekulen wurde foarme út atomen dy't op har beurt wer opboud binne út kearnen en elektroanen dy't har om 'e kearnen bewege. De eigenskippen fan stoffen wurde bepaald troch de ynteraksje tusken kearnen en elektroanen en de elektroanen ûnderling. As wy dy eigenskippen ferklearje wolle, sil in model (of teory) brûkt wurde moatte dat dy ynteraksje beskriuwe kin. Wannear't wy hiele lytse dieltsjes beskriuwe wolle, moatte wy gebrûk meitsje fan it kwantummeganyske model dêr't de dieltsjes yn beskreaun wurde mei in saneamde weachfunksje. De kwantummeganika is in natuerkundige teory, dy't foarm jûn is yn in tal wiskundige formules. Ien fan de wichtichste kwantummeganyske formules is de Schrödinger-ferliking.

Op it earste each liket de kwantummeganika yn ús makroskopyske wrâld ûnbelangryk, mar de ynfloed derfan op it deistich libben is tige grut. Sûnder de kwantummeganika binne wy net by steat om eigenskippen as magnetisme en elektryske lieding goed te begripen. Oare taastbere foarbylden binne de ûntwikkeling fan lasers en de elektryske skeakelings (chips). Foar it ûntwikkeljen fan nije materialen, it begripen en ferbetterjen fan de wurking fan medisinen, fluggere elektryske skeakelings, nije en ferbettere reaksjeprosessen (b.g. katalysatoaren), mar ek foar it begripen fan ferskynsels lykas superlieding, is in deeglik ynsjoch nedich yn de kwantummeganyske aspekten fan de eigenskippen fan stoffen.

It is net ienfâldich om de gemy te beskriuwen mei help fan allinnich in kwantummeganysk model. De formule foar it hiel wat dieltsjes-probleem dat fuortkomt út de Schrödinger-ferliking is slim op te lossen en freget grutskalich rekkenwurk. Om dochs de wiidweidige eksperimintele kennis ynterpretearje te kinnen en brûke te kinnen yn nije technologyske ûntwikkelings wurdt besocht om op basis fan de kwantummeganika maklik te hantearjen modellen op te stellen oangeande de opbou fan atomen en molekulen en de gearhing dêrfan mei allerhande gemyske en fysyske eigenskippen fan materialen. Op basis fan eksperimintele gegevens, bygelyks spektrokopyske techniken, wurdt besocht om sa ienfâldich mooglike kwantummeganyske beskriuwings te finen foar de eigenskippen dy't fûn wurde. Dêrta wurde foar de weachfunksjes beskate modelfoarstellings nommen en sa is it mooglik om beskate eksperimintele grutheden te parameterisearjen. Mei dy ferienfâldige modellen kin besocht wurde om te sizzen hoe't de útkomsten fan nije eksperiminten wêze sille en kinne trends dy't oantroffen wurde ynterpretearre wurde. Dochs binne der grinzen oan sa'n saneamde semy-empiryske oanpak. Ferienfâldige modellen wurkje faak goed foar beskate eigenskippen en foar beskate klassen fan materialen. Wannear't in oare klasse fan materialen bestudearre wurdt of oare eigenskippen, moat faak

it model oanpast wurde of sels útwreide. Njonken de grinzen fan in ienfâldich model binne der ek grinzen oan wat eksperiminteel mooglik is. Dêrby kin bygelyks tocht wurde oan it wurkjen mei hiel giftige, radio-aktive of oars gefaarlike stoffen. It is net altyd mooglik om de (hiel koart) libjende tuskenprodukten yn it ferrin fan in gemysk reaksjeproses te mjitten. Dêrtroch misse guon skeakels yn 'e ynterpretaasje.

In oare ynfalshoeke is dy fan de *ab initio* kwantumgemy, in part fan de teoretyske gemy. Dy tûke binnen de kwantumgemy hâldt him dwaande mei it sa eksakt mooglik oplossen fan de kwantummeganyske bewegingsferlikings, de Schrödinger-ferliking, fan de kearnen en de elektroanen. Mei dat model kinne yn prinsipe alle eigenskippen fan materialen, yndividuele molekulen, ynteraksjes tusken en reaksjes fan molekulen foarsein wurde troch it dwaan fan berekkenings. Yn dy tûke wurdt besocht om sa min mooglik gebrûk te meitsjen fan eksperimintele ynformaasje. De iennichste eksperimintele kennis dy't brûkt wurdt is dy fan de fûnemintele fysyske natuerkonstanten. Dizze tûke fan wittenskip begûn him earst echt te ûntwikkeljen om 1960 hinne nei de ûntwikkeling fan grutskalige rekken- en dataferwurkingsmooglikheden, it begjin fan it kompjûtertiidrek. Troch út te gean fan allinnich mar in fûneminteel kwantummeganysk model krije wy in better ynsjoch yn 'e basis fan de gemy, mar wy kinne sa ek ynformaasje krije oer gemyske systemen dy't net (of noch net) eksperiminteel beskikber binne, oftewol wy kinne besykje eigenskippen te foarsizzen. Wy binne (noch) net by steat om de withoefolle dieltsjes út 'e Schrödinger-ferliking op te lossen. Dat betsjut dat it ek binnen de *ab initio* kwantumgemy ferskillend (konseptu- eel) oanpakt wurde moatte sil, wat úteinlik liede moatte sil ta in eksakte oplossing fan it hiel wat dieltsjes-probleem. De formules dy't oerbliuwe foarmje op harsels noch hieltyd in grut rekkenprobleem. De hjoeddeiske beskikbere rekkenkrêft is op dit stuit de behinderjende faktor wat de gemyske probleemstellings dy't bestudearre wurde kinne oangiet. Wy moatte ús meastentiids beheine ta in lyts tal atomen. In protte eigenskippen fan in stof hawwe in lokale oarsprong, guon atomen of in lyts kluster fan atomen, en kinne beskreaun wurde mei in lyts part fan de stof, al of net mei in benei kommen omjouwingsmodel.

Wy moatte de *ab initio* kwantumgemy sjen as ien lange rige fan eksperimintele techniken. It kin brûkt wurde as helpmiddel foar it ferklearjen, befestigjen en modellearjen fan de ynterpretaasje fan eksperimintele gegevens. Tagelyk kin de kwantummeganika tsjinje as numeryk eksperimint om ynsjoch te krijen yn prosessen en materialen dy't net mei eksperimintele techniken garre wurde kinne. It oplossen fan de (benei kommen) Schrödinger-ferliking smyt yn in protte gefallen in beskriuwing fan de gemyske en fysyske eigenskippen fan in molekule op dy't sekuer genôch is. Dochs lit de kwantummeganika op basis fan de Schrödinger-ferliking it sitte wan- near't dieltsjes dy't mei gâns faasje bewege beskreaun wurde moatte (dat is it gefal by swiere eleminten sa as uranium). Foar sokke dieltsjes is in ferbettere ferzje fan de kwantummeganika nedich wêrby't rekken hâlden wurdt mei in oare natuerkundige teory, Einstein syn spesjale relativiteitsteory. Yn dy teory is de ljochtsnelheid (300.000 km/s) in fûnemintele natuerkonstante, soks yn tsjinstelling ta de Schrödinger-ferliking dêr't feitliks in

ûneinige ljochtsnelheid yn oannommen wurdt. Dat hat benammen direkte konsekwinsjes foar de elektroanen ticht by in swiere kearn dy't mei gâns faasje foarút geane, mar yndirekt ek foar de elektroanen dy't fierder fan de kearn ôf sitte. In model dat rekken hâldt mei de kwantummeganika en mei Einstein syn spesjale relativiteitsteory waard yn 1928 postulearre troch Dirac: de relativistyske kwantummeganika. Relativiteit hat in sinjifikante ynfloed op 'e gemy. Dy ynfloed beheint him net allinnich ta gemyske systemen út de ûnderste regioanen fan it periodyk systeem, mar omfettet ek molekulen mei allinnich eleminten út de boppeste rigen fan it periodyk systeem. Inkele foarbylden fan dy ynfloed op 'e gemy binne de ferklearrings foar de kleur fan goud en it ljocht fan strjitlantearnen.

Dit proefskrift giet út fan de relativistyske kwantummeganika sa't dy formulearre is yn 'e Dirac-ferliking. It rekkenark dat dêrfoar brûkt is it MOLFDIR programmapakket dat yn ús groep oan de Ryksuniversiteit Grins ûntwikkele is en wurdt. It proefskrift kin rûchwei yn twa seksjes ferdield wurde, in teoretysken-ien en in seksje mei resultaten fan berekkenings fan in tal gemyske systemen. Yn haadstik 1 wurdt in algemiene ynlieding jûn oer relativiteit en de relativistyske effekten yn 'e gemy. Haadstik 2 behannelet yn 't koart de teory en syn ymplemintaasje yn MOLFDIR.

Yn it wichtichste part fan it proefskrift, de haadstikken 3 o/m 7, wurdt de MOLFDIR programmatuer tapast op in tal gemyske fraachstikken dêr't relativistyske effekten by fan belang binne of wêze kinne soene. Wy sille sjen dat net allinnich molekulen mei swiere eleminten, mar ek molekulen mei lichte eleminten sinjifikant beynfloede wurde troch relativiteit. Yn haadstik 3 wurde de relativistyske effekten op de saneamde ionisearre en neutrale oansleine tastannen fan de koperhalogenen (CuCl, CuBr en CuI) bestudearre. It wichtichste relativistyske effekt dat dy tastannen sterk beynfloedet is de spin-baan ynteraksje tusken de ferskillende tastannen.

In relativistyske berekkening fan in beskaat gemysk rekkenprobleem is gâns grutter as wannear't wy it rekkenprobleem mei net-relativistyske metoaden bestudearje.

Dêrom wurde de relativistyske effekten faak weilitten of der wurdt besocht om dy te beskriuwen mei help fan benei kommen modellen. Om de krektens en sekuerens fan dy modellen analisearje te kinnen is it nedich om folslein relativistyske berekkenings út te fieren. De resultaten fan dy berekkenings kinne dan tsjinje as referinsjekader foar de benei kommen metoaden. Yn haadstik 4 wurde de resultaten fan referinsjeberekkenings oan ynterhalogeen molekulen (ClF, BrF, BrCl, IF, ICl en IBr) presintearre. Ferskillende spektroskopyske en elektryske eigenskippen en it relativistyske effekt op dy eigenskippen binne berekkene.

Yn haadstik 5 is nei de spektroskopyske eigenskippen fan de twa-atomige joadium molekule sjoen. Njonken de grûntastân binne ek de eksitearre tastannen fan it systeem bestudearre. De resultaten komme aardich oerien mei de eksperimintele gegevens en de eigenskippen fan guon, noch net metten, tastannen kinne foarsein wurde. By einsluten is sjoen nei de ionisearre tastannen fan de molekule. De resultaten dy't dêr presintearre wurde hawwe laat ta in oare ynterpretaasje fan resinte eksperimintele data en in nije takenning fan in metten tastân. De haadstikken 6 en 7 beskriuwe de resultaten fan

berekkenings oan molekulen dy't uranium befetsje, in elemint út de ûnderste regioanen fan it periodyk systeem. Yn haadstik 6 binne de eigenskippen fan de uraniumheksafluoride molekule bestudearre. It ionisaasjespektrum, it eksitaasjespektrum fan it kation en de elektroane-affiniteit fan 'e molekule binne berekkene. De rekkenresultaten slute moai oan by de beskikbere eksperimintele gegevens. Yn haadstik 7 wurde resultaten presintearre fan berekkenings fan it uranyl ion. De biningseigenskippen fan 'e molekule, sa as de koarte biningslingte en de lineêriteit fan de molekule, binne bestudearre en ferlike mei resultaten fan berekkenings op grûn fan benei kommen metoaden. Sawol de spin-baan wikselwurking as de skalêre relativistyske effekten hawwe in grutte ynfloed op de eigenskippen fan dy molekule. Der is ek sjoen nei de gradiïnt fan it elektryske fjild op de uranium posysje yn 'e molekule. De elektryske fjild-gradiïnt komt fuort út de ladingsferdieling yn 'e molekule en in kombinaasje fan eksperimintele en teoretyske resultaten smyt dus fuortdaliks ynformaasje op oer dy ladingsferdieling en benammen dy fan de elektroanen. De relativistyske effekten binne wichtich foar dy eigenskip, mar de omjouwingseffekten leverje ek in wichtige bydrage.

Oer it generaal kinne wy konkludearje dat de spin-baan wikselwurking it wichtichste effekt is wannear't wy sjogge nei molekulen besteande út lichte eleminten. Wannear't wy molekulen mei swiere eleminten bestudearje wolle, moatte ek de skalêre relativistyske effekten meinommen wurde om in krekte beskriuwing fan 'e molekule te krijen.

List of Publications

1. W. A. de Jong, L. Visscher, O. Visser, P. J. C. Aerts and W. C. Nieuwpoort, "MOLFDIR: A Program Package for Molecular Dirac-Fock-CI Calculations", in "New Challenges in Computational Quantum Chemistry", ed. R. Broer, P. J. C. Aerts and P. Bagus, University of Groningen, 1993.
2. L. Visscher, W. A. de Jong, O. Visser, P. J. C. Aerts, H. Merenga and W. C. Nieuwpoort, "Relativistic Quantum Chemistry. The MOLFDIR Program Package", in "Methods and Techniques in Computational Chemistry: METECC-95", ed. E. Clementi and G. Corongiu, Cagliari, 1995.
3. F. Dijkstra, W. A. de Jong and W. C. Nieuwpoort, "Electron Correlation Effects on the ^{6}P-Manifold of the Eu^{3+} Impurity in Ba_2GdNbO_6", Int. J. Quant. Chem.: Quant. Chem. Symp. **29**, 609 (1995).
4. W. A. de Jong and W. C. Nieuwpoort, "Relativity and the Chemistry of UF_6: A Molecular Dirac-Hartree-Fock-CI Study", Int. J. Quant. Chem. **58**, 203 (1996)
5. C. Sousa, W. A. de Jong, R. Broer and W. C. Nieuwpoort, "Theoretical characterization of low-lying excited states of the CuCl molecule", J. Chem. Phys. **106**, 7162 (1997).
6. C. Sousa, W. A. de Jong, R. Broer and W. C. Nieuwpoort, "Charge Transfer and relativistic effects in the low-lying electronic states of CuCl, CuBr and CuI", Mol. Phys. **92**, 677 (1997).
7. W. A. de Jong, L. Visscher and W. C. Nieuwpoort, "Relativistic and Correlated calculations on the ground, excited and ionized states of iodine", J. Chem. Phys., in press (1997).
8. W. A. de Jong, J. Styszynski, L. Visscher and W. C. Nieuwpoort, "Relativistic and correlation effects on molecular properties. III. The interhalogens ClF, BrF, BrCl, IF, ICl and IBr", J. Chem. Phys., submitted (1997).
9. C. de Graaf, W. A. de Jong, R. Broer and W. C. Nieuwpoort, "Theoretical characterization of the crystal field excitations in CoO", to be published.
10. W.A. de Jong, L. Visscher and W.C. Nieuwpoort, "On the bonding properties and the electric field gradients of the uranyl ion", to be published.

Appendix: Basis sets

Table A.1. Exponents of the primitive gaussian functions of the copper atom used in chapter 3.

copper atom					
s	16975223.97	p	55087.22545	d	298.0572268
s	2229083.124	p	9154.993633	d	88.27690472
s	451233.5370	p	2426.988136	d	33.59803108
s	116016.9513	p	817.6915021	d	14.21976902
s	35105.37331	p	317.9030688	d	6.407230311
s	11965.62551	p	135.8057792	d	2.920998907
s	4468.734581	p	61.92221963	d	1.300012489
s	1794.255638	p	29.41445943	d	0.552561855
s	763.8598886	p	14.37677217	d	0.216248770
s	341.1184458	p	7.042800079	d	0.056551844
s	158.3351783	p	3.368116513		
s	75.13960818	pf	1.554999693		
s	33.35477105	pf	0.679622252		
s	16.62441340	pf	0.173495280		
s	8.269010341	p	0.076901022		
s	3.720272551	p	0.030755227		
s	1.772824927				
s	0.806029497				
s	0.194180439				
s	0.084767799				
s	0.036117812				

Table A.2. Exponents of the primitive gaussian functions of the uranium and fluorine atoms used in chapter 6.

uranium atom				fluorine atom			
s	20937545.7	p	2150385.00	s	18648.5000	p	63.1253000
s	4399173.86	p	509250.000	s	2790.77000	p	14.5012000
s	1188162.75	p	120600.789	s	633.258000	p	4.38233000
s	375430.038	p	28560.6010	s	178.599000	p	1.45355000
s	132390.271	p	9273.75607	s	57.7896000	p	0.46323700
s	50702.2549	p	3625.56475	s	20.4555000	p	0.12657800
s	21550.4994	p	1579.24376	s	7.58796000		
s	9622.86247	pf	731.690718	s	1.99213000		
sd	4244.49864	pf	353.214877	s	0.74985400		
sd	1872.07341	pf	175.883590	s	0.24184500		
sd	843.025290	pf	88.1160134				
sd	378.155889	pf	45.8983269				
sd	180.415319	pf	23.7975245				
sd	88.7130122	pf	12.2465165				
sd	44.6224785	pf	6.29068100				
sd	22.2546744	pf	3.12602146				
sd	11.0982028	pf	1.50427276				
sd	5.44343523	pf	0.68712565				
sd	2.63036288	pf	0.29073227				
sd	1.19652164	pf	0.10975364				
sd	0.41247948	p	0.04200000				
sd	0.12837666						
sd	0.08160996						
sd	0.02473572						

Table A.3. Exponents of the primitive gaussian functions of the uranium and oxygen atoms used in chapter 7.

uranium atom				oxygen atom			
s	53568256.79	p	19827019.11	s	15330.0	p	196.388
s	13449948.46	p	3818229.478	s	2299.00	p	34.4600
s	4189157.736	p	901789.0290	s	522.400	p	7.74900
s	1413577.926	p	242155.6332	s	147.300	p	2.28000
s	510089.7847	p	72353.25334	s	47.5500	p	0.71560
s	193138.3122	p	23663.02464	s	16.7600	p	0.21400
s	76249.72122	p	8424.924339	s	6.20700	p	0.05974
s	31009.78871	p	3254.911046	s	1.75200		
sd	12853.68436	p	1353.809558	s	0.68820		
sd	5422.858883	pf	598.0845752	s	0.23840	d	0.64500
sd	2343.749113	pf	277.0748003	s	0.07376	d	0.21400
sd	1041.930412	pf	132.3495565				
sd	476.4979255	pf	64.93591778				
sd	226.6376008	pf	32.28975663				
sd	111.5168789	pf	16.04994303				
sd	56.45122403	pf	7.882601863				
sd	28.80075360	pf	4.094163512				
sd	14.60559738	pf	1.977573498				
sd	7.430625464	pf	0.883350010				
sd	3.591933346	pf	0.396960407				
sd	1.706811777	pf	0.157279744				
sd	0.754165254						
sd	0.312220229						
sd	0.112264515						
sd	0.038913147						
s	0.009978248						

References

1. P. A. M. Dirac, *Proc. Roy. Soc.* **A123,** 714 (1929).
2. L. Visscher, T. Saue, W. C. Nieuwpoort, K. Faegri, and O. Gropen, *J. Chem. Phys.* **99,** 6704 (1993).
3. P. Pyykkö, *Chem. Rev.* **88,** 563 (1988).
4. H. Partridge, C. W. Bauschlicher, and L. Visscher, *Chem. Phys. Lett.* **246,** 33 (1995).
5. P. A. M. Dirac, *Proc. Roy. Soc.* **A117,** 610 (1928).
6. A. Einstein, *Ann. Phys.* **17,** 173 (1905).
7. P. A. Christiansen, W. C. Ermler, and K. S. Pitzer, *Ann. Rev. Phys. Chem.* **36,** 407 (1985).
8. W. H. E. Schwarz, E. M. van Wezenbeek, E. J. Baerends, and J. G. Snijders, *J. Phys. B* **22,** 1515 (1989).
9. E. J. Baerends, W. H. E. Schwarz, P. Schwerdtfeger, and J. G. Snijders, *J. Phys. B* **23,** 3225 (1990).
10. This picture was made by Jo Asplin, Department of Computer Science at the University of Tromsø (Norway), using electron densities (on a grid) constructed with CALDENS (a module of the MOLFDIR program package).
11. P. Pyykkö and J.-P. Desclaux, *Acc. Chem. Res.* **12,** 276 (1979).
12. P. Pyykkö, *Adv. Quant. Chem.* **2,** 353 (1978).
13. K. S. Pitzer, *Acc. Chem. Res.* **12,** 271 (1979).
14. P. A. M. Dirac, *Proc. Roy. Soc.* **A118,** 351 (1928).
15. G. Breit, *Phys. Rev.* **34,** 553 (1929).
16. M. Born and J. R. Oppenheimer, *Ann. Phys.* **84,** 457 (1927).
17. B. Swirles, *Proc. Roy. Soc.* **A152,** 625 (1935).
18. J. P. Desclaux, *Comp. Phys. Comm.* **9,** 31 (1975).
19. K. G. Dyall, I. P. Grant, C. T. Johnson, E. P. Plummer, and F. Parpia, *Comp. Phys. Comm.* **55,** 425 (1989).
20. T. A. Welton, *Phys. Rev.* **74,** 1157 (1948).
21. Y. S. Lee and A. D. McLean, *J. Chem. Phys.* **76,** 735 (1982).
22. I. P. Grant and H. M. Quiney, *Adv. At. Mol. Phys.* **23,** 37 (1988).
23. I. P. Grant, *Phys. Rev. A* **25,** 1230 (1982).
24. Y. Ishikawa, H. Sekino, and R. C. Binning Jr., *Chem. Phys. Lett.* **165,** 237 (1990).
25. P. J. C. Aerts and W. C. Nieuwpoort, *Chem. Phys. Lett.* **113,** 165 (1985).
26. P. J. C. Aerts, Ph.D. Thesis, Groningen, 1986.
27. L. Visscher, P. J. C. Aerts, O. Visser, and W. C. Nieuwpoort, *Int. J. of Quant. Chem. : Quant. Chem. Symp.* **25,** 131 (1991).

28. L. Visscher, in *The effects of Relativity on Atoms, Molecules, and the Solid State,* edited by I. P. Grant, B. L. Gyorffi, and S. Wilson (Plenum Press, New York, 1991), pp. 197.
29. Y. Watanabe and O. Matsuoka, *Bull. Chem. Soc. Jpn.* **68,** 1915 (1995).
30. G. E. Brown and D. G. Ravenhall, *Proc. Roy. Soc.* **A 208,** 552 (1951).
31. A. D. McLean and Y. S. Lee, *J. Chem. Phys.* **76,** 735 (1982).
32. K. G. Dyall, in *Relativistic and correlation effects in molecules and solids.*, Vol. 318, edited by G. L. Malli (Plenum Press, New York, 1994), pp. 17.
33. A. K. Mohanty and E. Clementi, *Int. J. Quant. Chem.* **39,** 487 (1990).
34. T. Saue, Ph. D., University of Oslo, 1995.
35. L. Pisani and E. Clementi, *J. Comp. Chem*. **15,** 466 (1993).
36. S. Okada and O. Matsuoka, *J. Chem. Phys.* **91,** 4193 (1989).
37. L. Visscher, O. Visser, P. J. C. Aerts, H. Merenga, and W. C. Nieuwpoort, *Comp. Phys. Comm*. **81,** 120 (1994).
38. O. Visser, Ph.D. Thesis, University of Groningen, 1992.
39. L. Visscher, Ph.D. Thesis, Rijks Universiteit Groningen, 1993.
40. L. Visscher, K. G. Dyall, and T. J. Lee, *Int. Journal of Quant. Chem. : Quant. Chem. Symp.* **29,** 411 (1995).
41. L. Visscher, T. Saue, and J. Oddershede, *Chem. Phys. Lett.* **274,** 181 (1996).
42. L. L. Foldy and S. A. Wouthuysen, *Phys. Rev.* **78,** 29 (1950).
43. M. Douglas and N. M. Kroll, *Ann. Phys.* **82,** 89 (1974).
44. B. A. Heß, *Phys. Rev. A* **33,** 3742 (1986).
45. A. Rutkowski, *J. Phys. B* **19,** 149 (1986).
46. W. Kutzelnigg, E. Ottschofski, and R. Franke, *J. Chem. Phys.* **102,** 1740 (1995).
47. C. Chang, M. Pélissier, and P. Durand, *Phys. Scr.* **34,** 394 (1986).
48. E. Van Lenthe, E. J. Baerends, and J. G. Snijders, *J. Chem. Phys.* **99,** 4597 (1993).
49. E. Van Lenthe, E. J. Baerends, and J. G. Snijders, *Chem. Phys. Lett.* **236,** 235 (1995).
50. K. G. Dyall, *J. Chem. Phys.* **100,** 2118 (1994).
51. A. J. Sadlej and J. G. Snijders, *Chem. Phys. Lett.* **229,** 435 (1994).
52. W. Pauli, *Z. Phys.* **43,** 601 (1927).
53. H. H. Grelland, *J. Phys. B* **13,** L389 (1980).
54. W. Buchmüller, *Phys. Rev. A* **18,** 1784 (1978).
55. J. A. Gaunt, *Proc. Roy. Soc.* **A122,** 513 (1929).
56. J. Sucher, *Int. J. Quant. Chem.* **25,** 3 (1984).
57. J. Sucher, *Phys. Rev. A* **22,** 348 (1980).
58. M. H. Mittleman, *Phys. Rev. A* **24,** 1167 (1981).
59. W. Kutzelnigg, *Phys. Scr.* **36,** 416 (1987).
60. W. H. Furry, *Phys. Rev.* **81,** 115 (1951).
61. H. Bethe, *Ann. Phys.* **3,** 133 (1929).

62. C. J. Bradley and A. P. Cracknell, *The mathematical theory of symmetry in solids* (Clarendon Press, 1972).
63. H. A. Kramers, *Proc. Acad. Amsterdam* **33,** 959 (1930).
64. L. Visscher, *Chem. Phys. Lett.* **253,** 20 (1995).
65. G. Malli and J. Oreg, *J. Chem. Phys.* **63,** 830 (1975).
66. L. LaJohn and J. D. Talman, *Chem. Phys. Lett.* **189,** 383 (1992).
67. R. C. Raffenetti, *J. Chem. Phys.* **58,** 4452 (1973).
68. W. H. E. Schwarz and H. Wallmeier, *Mol. Phys.* **46,** 1045 (1982).
69. W. H. E. Schwarz and E. Wechsel-Trakowski, *Chem. Phys. Lett.* **85,** 94 (1982).
70. O. Matsuoka, *Chem. Phys. Lett.* **195,** 184 (1992).
71. Additional modifications were done by T. Saue and L. Visscher to interface the program with MOLFDIR.
72. K. G. Dyall and K. J. Faegri, *Theor. Chim. Acta* **94,** 39 (1996).
73. O. Visser, P. J. C. Aerts, D. Hegarty, and W. C. Nieuwpoort, *Chem. Phys. Lett.* **134,** 34 (1987).
74. L. Visscher and K. G. Dyall, *At. Data Nucl. Data Tab.* in press (1997).
75. http://theochem.chem.rug.nl/~luuk/FiniteNuclei/
76. C. C. J. Roothaan, *Rev. Mod. Phys.* **32,** 179 (1960).
77. O. Visser, L. Visscher, and P. J. C. Aerts, in *The effects of relativity on atoms, molecules, and the solid state*, edited by I. P. Grant, B. L. Gyorffi, and S. Wilson (Plenum Press, New York, 1991).
78. R. McWeeny, *Methods of Molecular Quantum Mechanics*, 2 ed. (Academic Press, Pisa, 1996).
79. L. Visscher, W. A. de Jong, O. Visser, P. J. C. Aerts, H. Merenga, and W. C. Nieuwpoort, in *METECC-95*, edited by E. Clementi and G. Corongiu (STEF, Cagliari, 1995), pp. 169.
80. P. J. C. Aerts and W. C. Nieuwpoort, (Schloss Ringberg (Tegernsee), 1984).
81. K. G. Dyall, K. Faegri Jr., and P. R. Taylor, in *The effects of relativity in atoms, molecules and the solid state*, edited by I. P. Grant, B. L. Gyorffi, and S. Wilson (Plenum, New York, 1991).
82. H. J. A. Jensen, K. G. Dyall, T. Saue, and K. Fægri Jr., *J. Chem. Phys.* in press (1997).
83. E. R. Davidson, *J. Comp. Phys.* **17,** 87 (1975).
84. J. Olsen, B. O. Roos, P. Jørgensen, and H. J. A. Jensen, *J. Chem. Phys.* **89,** 2185 (1988).
85. R. J. Bartlett and G. D. Purvis, *Int. J. Quantum Chem.* **14,** 561 (1978).
86. RELCCSD, L. Visscher, T. J. Lee, and K. G. Dyall, NASA Ames Research Center, Moffett Field, California, United States (1995).
87. L. Visscher, K. G. Dyall, and T. J. Lee, *J. Chem. Phys.* **105,** 8769 (1996).
88. K. Raghavachari, G. W. Trucks, J. A. Pople, and M. Head-Gordon, *Chem. Phys. Lett.* **157,** 479 (1989).

89. M. J. O. Deegan and P. J. Knowles, *Chem. Phys. Lett.* **227,** 321 (1994).
90. M. Urban, J. Noga, S. J. Cole, and R. J. Bartlett, *J. Chem. Phys.* **83,** 4041 (1985).
91. DIRAC. Program for Atomic and Molecular Direct Iterative Relativistic All-electron Calculations, T. Saue.
92. J. Oddershede, P. Jørgensen, and D. L. Yeager, *Comp. Phys. Reports* **2,** 33 (1984).
93. G. Aucar and J. Oddershede, *Int. J. Quantum Chem.* **47,** 425 (1993).
94. J. Olsen, H. J. A. Jensen, and P. Jørgensen, *J. Comp. Phys.* **74,** 265 (1988).
95. HERMIT. A molecular integral program, T. Helgaker, P. R. Taylor, and K. Ruud.
96. MOLFDIR, P. J. C. Aerts, O. Visser, L. Visscher, H. Merenga, W. A. de Jong, and W. C. Nieuwpoort, University of Groningen, The Netherlands (1995).
97. R. S. Mulliken, *J. Chem. Phys.* **23,** 1841 (1955).
98. W. A. de Jong, L. Visscher, O. Visser, P. J. C. Aerts, and W. C. Nieuwpoort, in *New Challenges in Computational Quantum Chemistry*, edited by R. Broer, P. J. C. Aerts, and P. S. Bagus (University of Groningen, Groningen, The Netherlands, 1994), pp. 239.
99. http://theochem.chem.rug.nl/~bert/RelQuant/RelQuant.html
100. This idea was first presented by L. Visscher at the REHE workshop in Tromsø (1995) and is supported by subsequent calculations by T. Saue, Ph. D. Thesis, University of Oslo (1991).
101. L. Visscher, *Theor. Chem. Acc.* in press (1997).
102. M. Cardona, *Phys. Rev.* **129,** 69 (1963).
103. A. Ramírez-Solís, *Phys. Rev. A* **47,** 1510 (1993).
104. C. Sousa, W. A. de Jong, R. Broer, and W. C. Nieuwpoort, *Mol. Phys.* **92**, 677 (1997).
105. C. Sousa, W. A. de Jong, R. Broer, and W. C. Nieuwpoort, *J. Chem. Phys.* **106,** 7162 (1997).
106. F. Ahmed, R. Barrow, A. H. Chojnicki, C. Dufour, and J. Schamps, *J. Phys. B* **8,** L362 (1982).
107. J. M. Delaval, Y. Lefebvre, H. Bocquet, P. Bernage, and P. Niay, *Chem. Phys.* **111,** 129 (1987).
108. C. Dufour, J. Schamps, and R. F. Barrow, *J. Phys. B* **15,** 3819 (1982).
109. R. E. Steele and H. P. Broida, *J. Chem. Phys.* **69,** 2300 (1978).
110. J. M. Delaval, J. Schamps, and Y. Lefebvre, *Chem. Phys. Lett.* **115,** 378 (1985).
111. E. P. F. Lee and A. W. Potts, *Chem. Phys. Lett.* **76,** 532 (1980).
112. M. T. Nguyen, M. A. McGinn, and N. J. Fitzpatrick, *Journal of the Chemical Soc. Faraday Trans. II* **82,** 1427 (1986).
113. A. Ramírez-Solís and J. P. Daudey, *Chem. Phys.* **134,** 111 (1989).
114. L. Seijo, Z. Barandiarán, M. Klobukowski, and S. Huzinaga, *Chem. Phys. Lett.* **117,** 151 (1985).
115. J. M. Delaval, J. Schamps, A. Ramirez-Solis, and J. P. Daudey, *97* **9** (1992).
116. Y. Lefebvre, J. M. Delaval, P. Bernage, and P. Niay, *Chem. Phys. Lett.* **139,** 212 (1987).

117. A. Ramírez-Solís and J. P. Daudey, *J. Phys. B* **23,** 2277 (1990).
118. N. W. Winter and D. L. Huestis, *Chem. Phys. Lett.* **133,** 311 (1987).
119. A. Ramírez Solís, J. P. Daudey, and C. Teichteil, *J. Chem. Phys.* **93,** 7277 (1990).
120. K. P. Huber and G. Herzberg, *Constants of diatomic molecules* (Van Nostrand Reinhold, New York, 1979).
121. O. Visser, L. Visscher, P. J. C. Aerts, and W. C. Nieuwpoort, *J. Chem. Phys.* **96,** 2910 (1992).
122. C. Sousa, personal communication.
123. P. Kowalczyk, I. Hikmet, and N. Sadeghi, *Chem. Phys.* **160,** 73 (1992).
124. I. Hikmet, C. Dufour, and B. Pinchemel, *Chem. Phys.* **172,** 147 (1993).
125. L. Visscher and K. G. Dyall, *J. Chem. Phys.* **104,** 9040 (1995).
126. L. Visscher, J. Styszynski, and W. C. Nieuwpoort, *J. Chem. Phys.* **105,** 1987 (1995).
127. A. H. Wapstra and K. Bos, *At. Data Nucl. Data Tab.* **19,** 177 (1977).
128. H. Hellmann, *Einführung in die Quantenchemie.* (Franz Deutiche, Leipzig, 1937).
129. R. P. Feynman, *Phys. Rev.* **56,** 340 (1939).
130. G. H. F. Diercksen and W. P. Kramer, *Chem. Phys. Lett.* **1** (1981).
131. V. Kellö and A. J. Sadlej, *J. Chem. Phys.* **93,** 8122 (1990).
132. S. A. Kucharski, J. Noga, and R. J. Bartlett, *J. Chem. Phys.* **88,** 1035 (1988).
133. W. A. de Jong, L. Visscher, and W. C. Nieuwpoort, *J. Chem. Phys.* in press (1997).
134. P. A. Straub and A. D. McLean, *Theor. Chim. Acta* **32,** 226 (1974).
135. L. G. M. Pettersson, P. E. M. Siegbahn, and O. Gropen, *Mol. Phys.* **48,** 871 (1983).
136. P. Scharf and R. Ahlrichs, *Chem. Phys.* **100,** 237 (1985).
137. K. Balasubramanian, *Chem. Phys.* **95,** 225 (1985).
138. R. D. Cowan and D. C. Griffin, *J. Opt. Soc. Am.* **66,** 1010 (1976).
139. Numerical atomic calculations give a relativistic decrease of the ionization potential of F: 0.02 eV, Cl: 0.03 eV, Br: 0.09 eV, and I: 0.21 eV.
140. A. J. Sadlej, *J. Chem. Phys.* **96,** 2048 (1992).
141. S. A. Perera and R. J. Bartlett, *Chem. Phys. Lett.* **216,** 606 (1993).
142. P. W. Fowler, S. A. Peebles, A. C. Legon, and A. J. Sadlej, *Chem. Phys. Lett.* **257,** 249 (1996).
143. P. W. Fowler, A. C. Legon, S. A. Peebles, and E. Steiner, *Chem. Phys. Lett.* **238,** 163 (1995).
144. R. E. Davis and J. S. Muenter, *J. Chem. Phys.* **57,** 2836 (1972).
145. J. J. Ewing, H. L. Tigelaar, and W. H. Flygare, *J. Chem. Phys.* **56,** 1957 (1972).
146. K. P. R. Nair, J. Hoeft, and E. Tiemann, *J. Mol. Spec.* **78,** 506 (1979).
147. K. P. R. Nair, J. Hoeft, and E. Tiemann, *Chem. Phys. Lett.* **58,** 153 (1978).
148. K. P. R. Nair, J. Hoeft, and E. Tiemann, *Chem. Phys. Lett.* **60,** 253 (1979).
149. E. Herbst and W. Steinmetz, *J. Chem. Phys.* **56,** 5342 (1972).

150. A. Durand, J. C. Loison, and J. Vigué, *J. Chem. Phys.* **106,** 477 (1997).
151. E. Tiemann and A. Dreyer, *Chem. Phys.* **23,** 231 (1977).
152. K. P. R. Nair and J. Hoeft, *J. Mol. Struct.* **79,** 227 (1982).
153. P. B. Beeken, E. A. Hanson, and G. W. Flynn, *J. Chem. Phys.* **78,** 5892 (1983).
154. F. W. Dalby, C. D. P. Levy, and J. Vanderlinde, *Chem. Phys.* **85,** 23 (1984).
155. B. J. Sullivan and D. A. Dows, *Chem. Phys.* **46,** 231 (1980).
156. J. Vigué, M. Broyer, and J. C. Lehmann, *J. Physique* **42,** 949 (1981).
157. J. Vigué, M. Broyer, and J. C. Lehmann, *J. Physique* **42,** 961 (1981).
158. R. J. LeRoy, *J. Chem. Phys.* **52,** 2678 (1970).
159. K. S. Viswanathan and J. Tellinghuisen, *J. Mol. Spec.* **101,** 285 (1983).
160. J. Tellinghuisen, *J. Chem. Phys.* **57,** 2397 (1972).
161. J. Tellinghuisen, *J. Chem. Phys.* **58,** 2821 (1973).
162. J. Tellinghuisen, *J. Chem. Phys.* **76,** 4736 (1982).
163. J. Tellinghuisen, *J. Phys. Chem.* **87,** 5136 (1983).
164. J. Tellinghuisen, *J. Chem. Phys.* **82,** 4012 (1985).
165. S. Churassy, F. Martin, R. Bacis, J. Vergès, and R. W. Field, *J. Chem. Phys.* **75,** 4863 (1981).
166. F. Martin, R. Bacis, S. Churassy, and J. Vergès, *J. Mol. Spec.* **116,** 71 (1986).
167. G. D. Chapman and P. R. Bunker, *J. Chem. Phys.* **57,** 2951 (1972).
168. K. P. Lawley, T. Ridley, Z. Min, P. J. Wilson, M. S. N. Al-Kahali, and R. J. Donovan, *Chem. Phys.* **197,** 37 (1995).
169. D. C. Frost, C. A. McDowell, and D. A. Vroom, *J. Chem. Phys.* **46,** 4255 (1967).
170. S. Evans and A. F. Orchard, *Inorg. Chim. Acta* **5,** 81 (1970).
171. A. B. Cornford, D. C. Frost, C. A. McDowell, J. L. Ragle, and I. A. Stenhouse, *J. Chem. Phys.* **54,** 2651 (1971).
172. J. H. D. Eland, *J. Chem. Phys.* **70,** 2926 (1979).
173. S. Leach, *J. Phys. Chem.* **92,** 5373 (1988).
174. S. M. Mason and R. P. Tuckett, *Chem. Phys. Lett.* **160,** 575 (1989).
175. A. J. Yencha, M. C. R. Cockett, J. G. Goode, R. J. Donovan, A. Hopkirk, and G. C. King, *Chem. Phys. Lett.* **229,** 347 (1994).
176. M. C. R. Cockett, J. G. Goode, K. P. Lawley, and R. J. Donovan, *J. Chem. Phys.* **102,** 5226 (1995).
177. J. P. Horner and J. H. D. Eland, *Chem. Phys. Lett.* **110,** 29 (1984).
178. H. Van Lonkhuyzen and C. A. De Lange, *Chem. Phys.* **89,** 313 (1984).
179. B. R. Higginson, D. R. LLoyd, and P. J. Roberts, *Chem. Phys. Lett.* **19,** 480 (1973).
180. M. C. R. Cockett, R. J. Donovan, and K. P. Lawley, *J. Chem. Phys.* **105,** 3347 (1996).
181. P. J. Jewsbury, T. Ridley, K. P. Lawley, and R. J. Donovan, *J. Mol. Spec.* **157,** 33 (1993).
182. R. S. Mulliken, *J. Chem. Phys.* **55,** 288 (1971).

183. C. Teichteil and M. Pelissier, *Chem. Phys.* **180,** 1 (1994).
184. P. Schwerdtfeger, L. v. Szentpály, K. Vogel, H. Silberbach, H. Stoll, and H. Preuss, *J. Chem. Phys.* **84,** 1606 (1986).
185. C. Y. Yang, *Chem. Phys. Lett.* **41,** 588 (1976).
186. S. Y. Lee and Y. S. Lee, *Chem. Phys. Lett.* **187,** 302 (1991).
187. G. Das and A. C. Wahl, *J. Chem. Phys.* **69,** 53 (1978).
188. M. Dolg, *Mol. Phys.* **88,** 1645 (1996).
189. E. Van Lenthe, Ph.D. Thesis, Free University of Amsterdam, 1996.
190. J. Vigué, M. Broyer, and J. C. Lehmann, *J. Physique* **42,** 937 (1981).
191. M. N. Glukhovtsev, A. Pross, M. P. McGrath, and L. Radom, *J. Chem. Phys.* **103,** 1878 (1995).
192. M. Saute and M. Aubert-Frécon, *J. Chem. Phys.* **77,** 5639 (1982).
193. Q. Li and K. Balasubramanian, *J. Mol. Spec.* **138,** 162 (1989).
194. J. M. Dyke, G. D. Josland, J. G. Snijders, and P. M. Boerrigter, *Chem. Phys.* **91,** 419 (1984).
195. K. Wittel, *Chem. Phys. Lett.* **15,** 555 (1972).
196. M. Jungen, *Theor. Chim. Acta* **27,** 33 (1972).
197. MOLCAS version 3, K. Andersson, M. R. A. Blomberg, M. P. Fülscher, V. Kellö, R. Lindh, P.-Å. Malmqvist, J. Noga, J. Olsen, B. O. Roos, A. J. Sadlej, P. E. M. Siegbahn, M. Urban, and P.-O. Widmark, University of Lund, Sweden (1994).
198. M. Dolg, personal communication.
199. J. Teichteil, *J. Chim. Phys.* **87,** 963 (1990).
200. J. B. Koffend, A. M. Sibai, and R. Bacis, *J. Phys.* **43,** 1639 (1981).
201. S. Gestenkorn, P. Luc, and J. Vergès, *J. Phys. B* **14,** L193 (1981).
202. T. Ishiwata, H. Ohtoshi, M. Sakaki, and I. Tanaka, *J. Chem. Phys.* **80,** 1411 (1984).
203. P. M. Boerrigter, M. A. Buijse, and J. G. Snijders, *Chem. Phys.* **111,** 47 (1987).
204. T. J. Lee and P. R. Taylor, *Int. J. Quant. Chem.: Quant. Chem. Symp.* **23,** 199 (1989).
205. R. N. Zare, *Sci. Am.* **February,** 86 (1977).
206. H. M. Seip, *Acta Chem. Scand.* **19,** 1955 (1965).
207. G. L. DePoorter and C. K. Rofer-DePoorter, *Spec. Lett.* **8,** 521 (1975).
208. R. McDiarmid, *J. Chem. Phys.* **65,** 168 (1976).
209. W. B. Lewis, L. B. Asprey, L. H. Jones, R. S. McDowell, S. W. Rabideau, A. H. Zeltmann, and R. T. Paine, *J. Chem. Phys.* **65,** 2707 (1976).
210. L. Karlsson, L. Mattsson, R. Jadrny, T. Bergmark, and K. Siegbahn, *Phys. Scr.* **14,** 230 (1976).
211. R. Rianda, R. P. Frueholz, and A. Kuppermann, *J. Chem. Phys.* **70,** 1056 (1979).
212. J. C. Miller, S. W. Allison, and L. Andrews, *J. Chem. Phys.* **70,** 3524 (1979).
213. N. Mårtensson, P.-Å. Malmquist, and S. Svensson, *Chem. Phys. Lett.* **100,** 375 (1983).

214. N. Mårtensson, P.-Å. Malmquist, S. Svensson, and B. Johansson, *J. Chem. Phys.* **80,** 5458 (1984).
215. D. P. Armstrong, D. A. Harkins, R. N. Compton, and D. Ding, *J. Chem. Phys.* **100,** 28 (1994).
216. M. Boring, J. H. Wood, and J. W. Moskowitz, *J. Chem. Phys.* **61,** 3800 (1974).
217. M. Boring and J. W. Moskowitz, *Chem. Phys. Lett.* **38,** 185 (1976).
218. M. Boring and J. H. Wood, *J. Chem. Phys.* **71,** 32 (1979).
219. D. H. Maylotte, R. L. St.Peters, and R. P. Messmer, *Chem. Phys. Lett.* **38,** 181 (1976).
220. D. D. Koelling, D. E. Ellis, and R. J. Bartlett, *J. Chem. Phys.* **65,** 3331 (1976).
221. A. Rosén, *Chem. Phys. Lett.* **55,** 311 (1978).
222. P. J. Hay, W. R. Wadt, L. R. Kahn, R. C. Raffenetti, and D. H. Phillips, *J. Chem. Phys.* **71,** 1767 (1979).
223. P. J. Hay, *J. Chem. Phys.* **79,** 5469 (1983).
224. D. C. Cartwright, S. Trajmar, A. Chutjian, and S. Srivastava, *J. Chem. Phys.* **79,** 5483 (1983).
225. S. Larsson, J. S. Tse, J. L. Esquivel, and A. T. Kai, *Chem. Phys.* **89,** 43 (1984).
226. S. Larsson and P. Pyykkö, *Chem. Phys.* **101,** 355 (1986).
227. J. Onoe, K. Takeuchi, H. Nakamatsu, T. Mukoyama, R. Sekine, and H. Adachi, *Chem. Phys. Lett.* **196,** 636 (1992).
228. J. Onoe, K. Takeuchi, H. Nakamatsu, T. Mukoyama, R. Sekine, B.-I. Kim, and H. Adachi, *J. Chem. Phys.* **99,** 6810 (1993).
229. Z. Bacic and J. C. Light, *Ann. Rev. Phys. Chem.* **40,** 469 (1989).
230. K. Fægri, personal communication.
231. ASCF: Atomic Self Consistent Field code, RUG,
232. L. Visscher and W. C. Nieuwpoort, *Theor. Chim. Acta* **88,** 447 (1994).
233. C. C. Kiess, C. J. Humphreys, and D. D. Laun, *Journal of Research of the National Bureau of Standards* **37,** 57 (1946).
234. R. S. Mulliken, *J. Chem. Phys.* **23,** 1833 (1955).
235. J. H. Scofield, *J. Elec. Spec.* **8,** 129 (1976).
236. J. C. Fuggle and S. F. Alvarado, *Phys. Rev. A* **22,** 1615 (1980).
237. N. P. Galkin and Y. N. Toumanov, *Russ. Chem. Rev.* **40,** 154 (1971).
238. M. J. Reisfeld and G. A. Crosby, *Inorg. Chem.* **4,** 65 (1964).
239. R. N. Compton, *J. Chem. Phys.* **66,** 4478 (1977).
240. J. L. Beauchamp, *J. Chem. Phys.* **64,** 928 (1976).
241. P. F. Walch and D. E. Ellis, *J. Chem. Phys.* **65,** 2387 (1976).
242. D. E. Ellis, A. Rosén, and P. F. Walch, *Int. J. Quant. Chem.: Quant. Chem. Symp.* **9,** 351 (1975).
243. M. Boring, J. H. Wood, and J. W. Moskowitz, *J. Chem. Phys.* **63,** 638 (1975).

244. R. L. DeKock, E. J. Baerends, P. M. Boerrigter, and J. G. Snijders, *Chem. Phys. Lett.* **105,** 308 (1984).
245. P. Pyykkö and L. Laaksonen, *J. Phys. Chem.* **88,** 4892 (1984).
246. K. Tatsumi and R. Hoffmann, *Inorg. Chem.* **19,** 2656 (1980).
247. C. Y. Yang, K. H. Johnson, and J. A. Horsley, *J. Chem. Phys.* **68,** 1001 (1978).
248. W. R. Wadt, *J. Am. Chem. Soc.* **103,** 6053 (1981).
249. E. M. v. Wezenbeek, Ph.D., Free University of Amsterdam, 1992.
250. E. M. v. Wezenbeek, E. J. Baerends, and J. G. Snijders, *Theor. Chim. Acta* **81,** 139 (1991).
251. C. K. Jørgensen, *Chem. Phys. Lett.* **89,** 455 (1982).
252. J. S. Craw, M. A. Vincent, I. H. Hillier, and A. L. Wallwork, *J. Phys. Chem.* **99,** 10181 (1995).
253. H. H. Cornehl, C. Heinemann, J. Marçalo, A. Pires de Matos, and H. Schwartz, *Angew. Chem. Int. Ed. Engl.* **35,** 891 (1996).
254. P. Pyykkö and Y. Zhao, *Inorg. Chem.* **30,** 3787 (1991).
255. P. Pyykkö, J. Li, and N. Runeberg, *J. Phys. Chem.* **98,** 4809 (1994).
256. J. H. Wood, M. Boring, and S. B. Woodruff, *J. Chem. Phys.* **74,** 5225 (1981).
257. M. Boring and J. H. Wood, *J. Chem. Phys.* **71,** 392 (1979).
258. P. Pyykkö and L. L. Lohr Jr., *Inorg. Chem.* **20,** 1950 (1981).
259. M. Pepper and B. E. Bursten, *Chem. Rev.* **91,** 719 (1991).
260. R. G. Denning, T. R. Snellgrove, and D. R. Woodwark, *Mol. Phys.* **32,** 419 (1976).
261. R. G. Denning, T. R. Snellgrove, and D. R. Woodwark, *Mol. Phys.* **37,** 1109 (1979).
262. B. W. Veal, D. J. Lam, W. T. Carnall, and H. R. Hoekstra, *Phys. Rev. B* **12,** 5651 (1975).
263. L. E. Cox, *J. Elec. Spec.* **26,** 167 (1982).
264. J. A. Monard, P. G. Huray, and J. O. Thomson, *Phys. Rev. B* **9,** 2838 (1974).
265. J. L. C. Ford Jr., P. H. Stelson, C. E. Bemis Jr., F. K. McGowan, R. L. Robinson, and W. T. Milner, *Phys. Rev. Lett.* **27,** 1232 (1971).
266. T. H. Dunning Jr., *J. Chem. Phys.* **90,** 1007 (1989).
267. K. Ohwada, *Spectrochim. Acta* **A 31,** 973 (1975).